UNIVERSITÀ DEGLI STUDI DI PADOVA

Dipartimento di Ingegneria industriale

CORSO DI DOTTORATO IN INGEGNERIA INDUSTRIALE

Curricula in Ingegneria dell'Energia Elettrica

XXXII° ciclo

Titolo della tesi:

Innovative magnetic materials for the new applications in electrical machines

Coordinatore: Ch. mo Prof. Paolo Colombo

Supervisore: Ch. mo Prof. Nicola Bianchi

Dottorando: Emir Pošković

A.A 2018/2019

Index

I. ABSTRACT

Permanent magnets play a key role as a component in a wide range of devices utilised by many industries; they are widely used in several electromechanical applications to convert energy, including actuators, motors and sensors, home appliances, office automation equipment, speakers, aerospace, wind generators and more.

Traditionally the adopted PMs were obtained from Rare Earth components, such as NdFeB, with high magnetic performance, but expensive. The research of alternative permanent magnets, in many cases has brought to choose the ferrites, mainly due to their low cost, but sometimes with significant design modifications of the final circuit, and possible increment of the weight.

Permanent magnets can roughly be divided into two categories: sintered (metallic) and bonded, these last representing a valid alternative to the first. Bonded magnets consist of two components: a hard magnetic powder and a non-magnetic binder; the powder may be hard ferrite, NdFeB, SmCo, and is mixed with binders for compression or injection moulding. The benefits lie in the adoption of polymeric binders to prepare the magnetic mixture: the resulting magnetic characteristic can be then "tuned" by adopting different percentages of the plastic binder. Moreover, the realisation process is simpler and cheaper than that of sintered materials, and no special protective treatment is needed.

The majority of the magnetic circuits are made with soft magnetic materials. Commonly laminated steels are adopted but recently the use of Soft Magnetic Composite (SMC) materials has increased representing a new solution to design the electrical machines with respect to traditional electrical steels.

SMC materials are realized with pure Iron grains coated and insulated by means of a layer that should be organic or inorganic. With respect to traditional laminated steel, these materials present different advantages: the capability to lead the magnetic flux in all directions, the volume reduction, the possibility to realize components with new complex shapes and geometries, and the reduction of iron losses, mainly the eddy currents, at medium and high frequency. On the other hand, the mechanical performances, in terms of strength, are in general weak.

Furthermore, a new material typology is introduced: the Hybrid Magnetic Composites (HMC), which are obtained with a combination of soft and hard magnetic materials mixed with a binder. The basic idea is that such materials should reflect the performance of AlNiCo magnets, low coercivity and adequate remanence, typically used in sensors applications.

Prototypes of traditional and unconventional rotating machines, such as assisted reluctance motors, brushless DC motors, axial flux machines and electromechanical frequency converters, have been studied in own laboratories and tested to evaluate the results coming from the adoption of the proposed materials in substitution of the commonly adopted (and expensive) Rare Earth sintered magnets. Different type of electrical machines can adopt innovative magnetic materials with the aim to improve their performance.

Induction motors are very useful and robust machines; on the other hand, such type of machines does not have a high dynamic behaviour. The DC motors can be easily controlled, but the presence of the brushes causes limitations on the efficiency, thermal restrictions and reduced life. The axial flux motors (AFM) have high efficiencies but the construction of the machines is very complex. The synchronous reluctance machines (SRM) have a lower cost compared to brushless ones.

In general, the reluctance electrical machines don't use permanent magnets. In this way, they have a reduction in the costs and allow a high overload capability. On the other hand, the lower power factor and power density, compared to PM synchronous motor (PMSM), are the main disadvantages. The filling of flux barriers with the permanent magnets allows the overcoming of these drawbacks. However, the regular ferrite and NdFeB sintered magnets cannot fill the flux barriers with complex geometries. For this reason, the use of bonded magnets can be a solution for a better utilization and design of flux barriers.

Therefore different prototypes have been prepared and analyzed in our laboratories using SMC materials. Several experiments have been performed using dedicated test benches, where magnetic, energetic and mechanical aspects have been considered.

On the other hand, with regard to HMCs, various magnets have been made in our laboratories, and different properties have been investigated: the effect of Iron content in the material and, also the binder content effect has been analysed.

II. MAGNETIC MATERIALS

Magnetic materials can be divided, as primary division, into hard and soft materials [1]; the first are the so called permanent magnets [2], while the others, soft magnets, can be laminated steels, solid core or Soft Magnetic Composites [3]. The soft magnetic materials are characterized by a very thin hysteresis cycle and lose most of their magnetization with the removal of an external magnetic field. Typical soft magnetic materials are laminated sheets used in the electrical machines [4]; their alternatives are Soft Magnetic Composite materials (SMC), which are basically compacted ferromagnetic powders covered with a layer [5],[6]. Other soft magnetic materials are solid pure Iron, amorphous materials and soft ferrites, the latter mostly used in telecommunication or sensor applications [7],[8].

Hard magnetic materials are permanent magnets (PM), which are magnetic flux generators and don't need a magnetic field to maintain magnetization [9],[10]. Significant developments in PM material production and power electronic drives have been made PM electrical machine the preferred candidate for several applications, from very small electric motors for household appliances to medium/large electrical machines for propulsion and power generation applications [11]. Different types of permanent magnets are adopted in electrical machines and electronic devises applications, a general overview has been described in the following paragraphs.

II.I Permanent Magnets

First of all to understand the typologies of permanent magnets some short hints about magnetic properties are shown. The permanent magnets have various parameters to indicate the magnetic performance. The most significant features describing the performance of a permanent magnet are the remanence, B_r, the intrinsic coercivity, H_{cj}, and the maximum energy product, $(BH)_{max}$. This last can be identified as a key point: magnets with higher $(BH)_{max}$ require less volume to obtain given performance; magnet circuit designers should employ magnets of high $(BH)_{max}$ to reduce the size of their circuits. For instance, to produce 0.1 T on the surface distant of 5 mm from magnets, different hard magnetic materials have been adopted. The variation of magnets dimensions is shown in Fig. 1 with the hard magnetic materials development in the 20th century as the function of maximum magnetic energy $(BH)_{max}$.

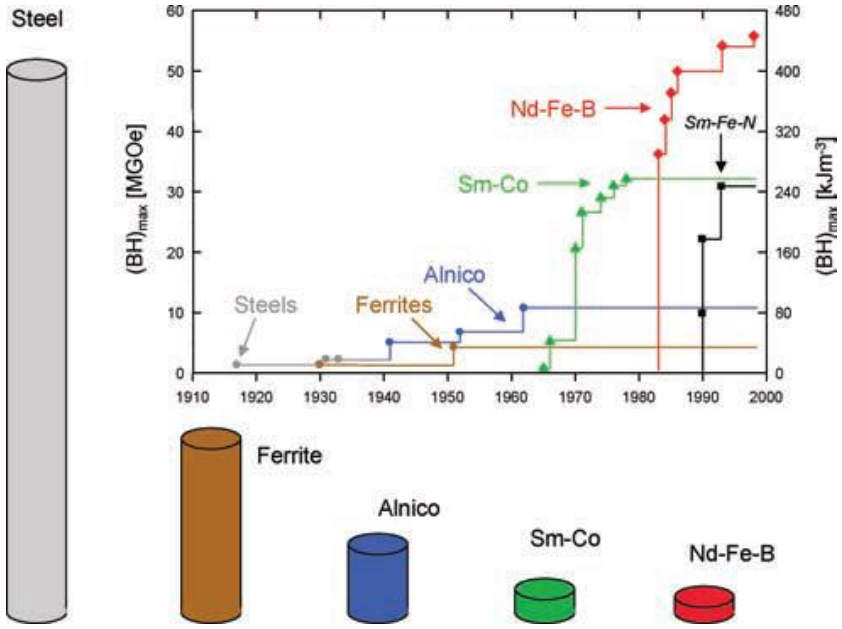

Fig. 1 – Development of hard magnetic materials in the 20th century: dependence of maximum magnetic energy $(BH)_{max}$ [12]

Ferrites are the most common permanent magnets, mostly because of their low cost [13]; on the other hand, the more expensive NdFeB magnets [2],[14],[15] have higher performance. Whatever is the magnet it needs a protective coating against moisture or high temperatures, to avoid oxidation and degradation; SmCo magnets are often used in harsh conditions. In sensor applications, the most frequently adopted magnetic materials are AlNiCo alloys [16],[17], even if expensive, especially for their low coercivity and high remanence. Some considerations about the costs of permanent magnets and their materials are reported in Fig. 2 and Fig. 3. Furthermore, the demagnetization curves of the most popular permanent magnets is shown in Fig. 4.

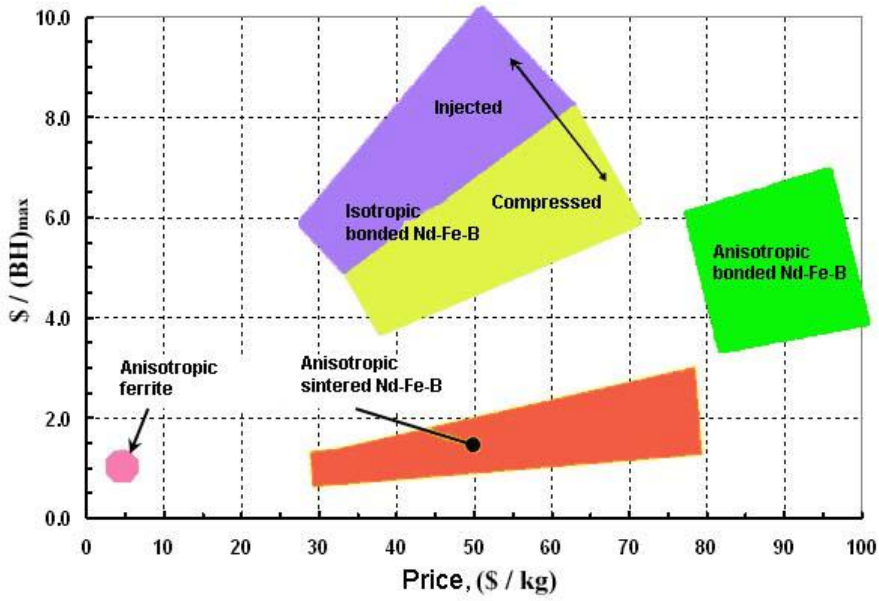

Fig. 2 – Price performance of some permanent magnets[18]

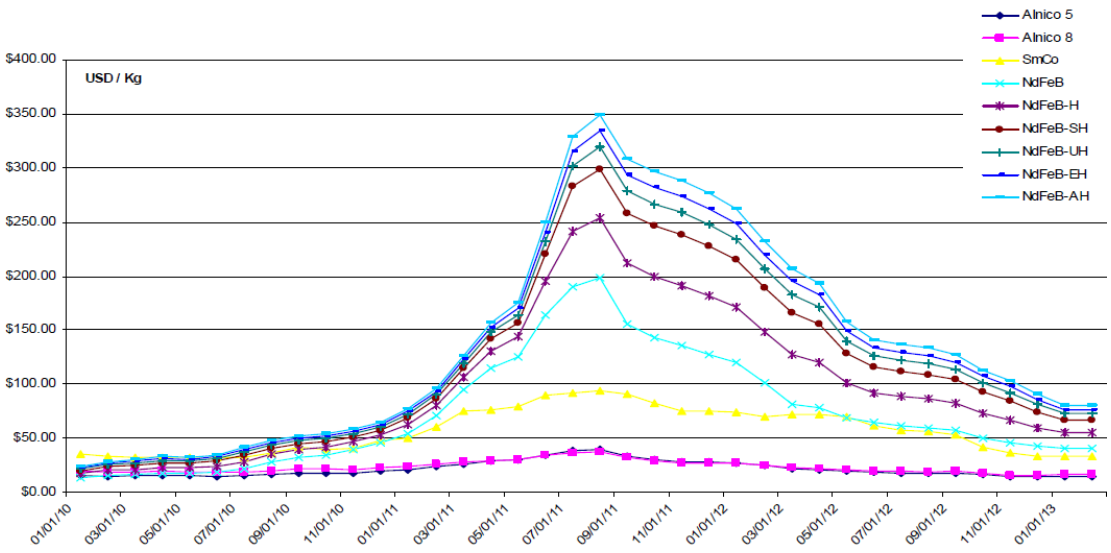

Fig. 3 – Magnetic material price per kg 2010-2013[19]

A further division can be made as "classical" and "modern". The first mentioned magnets have been developed by the 1960s; instead, modern magnets with neodymium alloys are more recent. In the next TABLE I different magnets typologies have been classified in relation to discovery/development and relative trend in nowadays.

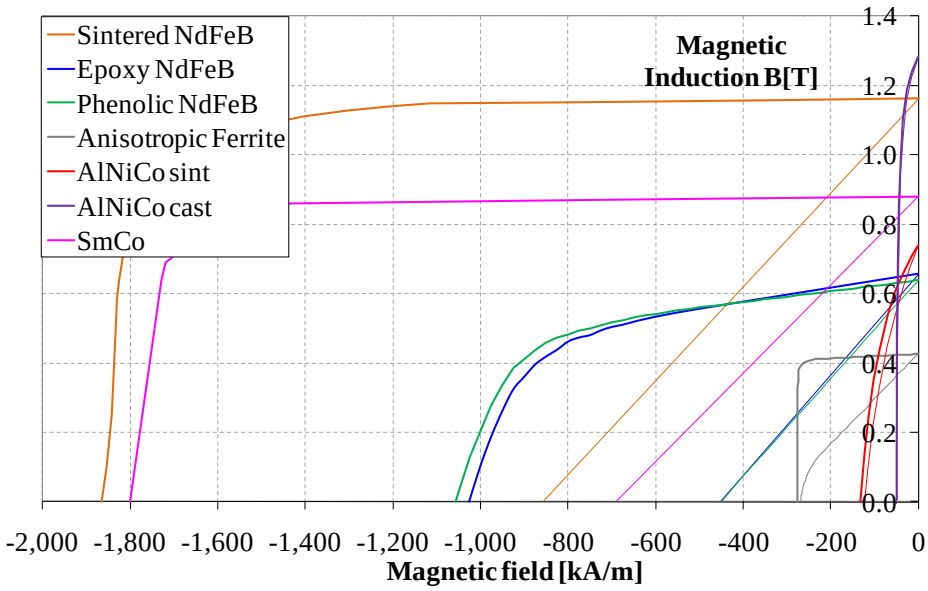

Fig. 4 – Demagnetization curves of the most common permanent magnets; all this magnets have been characterized in the laboratory

TABLE I – Hard magnetic materials: discovery year and trends in applications [20]

Material	Discovery/ development	Present-day importance	Trend
Hard magnetic steels	before 1930	important	
Cu – Ni – Fe	1935 – 1940	unimportant	
Cu – Ni – Co			
Pt – Co	1935 – 1940	minor	decreasing
V – Co – Fe	1940 – 1955	minor	decreasing
Fe – Co (ESD)	1950 – 1960	unimportant	
Cr – Fe – Co	1936 – 1960	minor	unchanged
Mn – Al – C	1958 – 1980	unimportant	
Al – Ni/AlNiCo	1932 – 1960	medium	decreasing
Hard ferrite	1950 – 1970	major	increasing
SmCo 1 : 5	1965 – 1975	major	increasing
SmCo 2 : 17	1975 – 1985	major	increasing
Nd – Fe – B	1983	medium	increasing considerably

II.I.I. AlNiCo

The most important classical hard magnetic materials are represented by the Aluminum, Nickel and Cobalt alloy, more commonly called AlNiCo. They are alloys in which the components vary as a percentage range in weight; such variation of the components will determine a variation in the performance of the magnetic material. On the market there are AlNiCo alloys with the following composition ranges: Aluminum 6-13%; Cobalt 0-32%; Copper 2-6%; Nickel 13-18%; Titanium 0-9%; Niobium 0-3% and the remaining percentage of Iron. Alloys without Cobalt content are called AlNi alloys and have lower magnetic values than the alloys in which Cobalt is present. Usually, the AlNiCo alloys can be made using a casting system or through the sintering process. The latter have finer grains and a more uniform microstructure and allow to have many more advantages compared to casting, such as the production of pieces with smaller volumes and smaller tolerances. In TABLE II and Fig. 5 the values of coercivity, remanence and the demagnetization curves of the AlNiCo alloys available on the market are reported. Depending on the composition of AlNiCo alloys the Curie temperature can vary in the range 760 ÷ 850 °C.

TABLE II – Magnetic properties of differnt AlNiCo magnets [20]

Material designation (DIN)	Composition, wt % Al	Ni	Co	Cu	Ti	'Fe	$(BH)_{max}$, kJ/m^3	Magnetic values Remanence B_r, mT	Coercive force H_{cB}, kA/m	Coercive force H_{cJ}, kA/m	Density ϱ, g/cm^3
Isotropic magnets											
AlNiCo 9/5	13	24	5	7		51	10	550	55	58	6.9
AlNiCo 12/6	11	20	15	4		50	12	600	54	58	7.1
Anisotropic magnets											
AlNiCo 35/5	9	14	24	3		50	40	1250	50	51	7.3
AlNiCo 40/12	8	14	36	3	5	34	44	880	115	120	7.3
AlNiCo 40/15	8	14	40	3	8	27	43	740	150	160	7.3
Columnar crystallized											
AlNiCo 52/6	9	14	24	3		50	62	1240	58	59	7.3
AlNiCo 80/10	8	14	40	3	8	27	80	930	150	155	7.3
Hysteresis materials											
AlNiCo 3/0.6	7	17				76	3	1000	6	6	7.1
AlNiCo 6/1.6	9	17	5			69	6	820	16	16	7.0

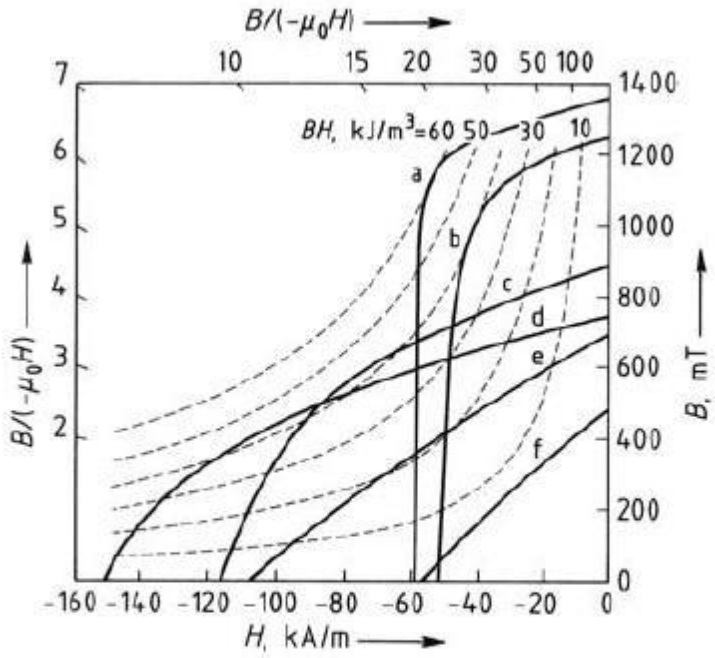

Typical demagnetization curves for isotropic (8/5 and 20/11) and anisotropic AlNiCo magnets a) AlNiCo 52/6; b) AlNiCo 40/5; c) AlNiCo 40/12; d) AlNiCo 40/15; e) AlNiCo 20/11; f) AlNiCo 8/5

Fig. 5 – Demagnetization curves of isotropic and anisotropic AlNiCo magnets [20]

II.I.II. Chromium, Iron, and Cobalt Alloys

The Chromium, Iron, and Cobalt alloys have many similarities with AlNiCo alloys. Also the casting and sintering process has been used to produce magnets. The composition of Cr - Fe - Co hard alloys vary in percentage: the following compositions of elements are available on the market: Chromium 20-30%; Cobalt 3-25%, Silicon 0-3%; Molybdenum 0-3%, Copper 0-3% and the remaining percentage in Iron. The

magnets can be isotropic or anisotropic in analogy with AlNiCo alloys. Typical values of Cr - Fe - Co magnets are shown in Fig. 6 with a comparison of the typical AlNiCo alloy characteristic. These magnets have no importance today in applications due to the fact that the production process of the magnets takes a very long time.

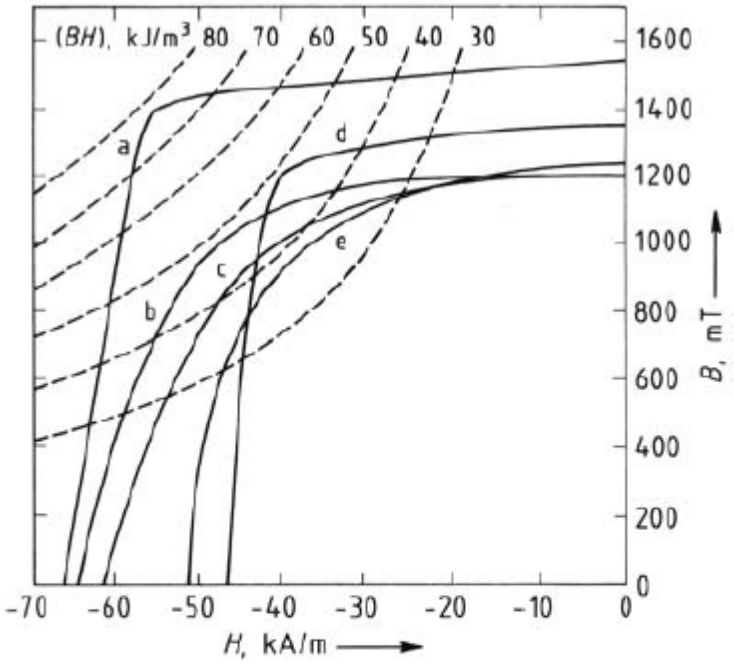

Comparison of the demagnetization curves for the Cr – Fe – Co and Al – Ni – Co alloys (columnar crystallized; magnetically tempered) a) 24 % Cr, 15 % Co, 3 % Mo, remainder Fe (anisotropic through deformation) [29]; b) 33 % Cr, 11.5 % Co, remainder Fe [28]; c) 33 % Cr, 11.5 % Co, 2 % Cu, remainder Fe (magnetic field treatment) [28]; d) 27 % Cr, 9 % Co, remainder Fe [28]; e) AlNiCo 24 % Co, 8 % Al, 14 % Ni, 3 % Cu, remainder Fe

Fig. 6 – Comparison between demagnetization curves of CrFeCo and AlNiCo alloys [20]

II.I.III. Platinum-Cobalt Alloys

Platinum-Cobalt alloys are hard magnetic materials which have 75% by weight of Platinum and the remaining 25% is Cobalt. They were developed in the mid-1930s. They have demagnetizing magnetic energy values around 80 kJ/m^3 and coercive field equal to 50 kA/m. Their use is limited due to the high cost of Platinum and Cobalt, so they are mainly used in medical technology where high corrosion resistance is required.

II.I.IV. Cobalt-Vanadium-Iron Alloys

These alloys are hard magnetic materials that contain 50% by weight of Cobalt, 7-15% by weight of Vanadium and the remaining Iron. In this alloy, 3-5% Vanadium can be

replaced with Chromium and the latter are known as Vicalloy. The high mechanical strength limits its use. The magnetic values are shown in the TABLE III.

TABLE III – Magnetic properties of special hard magnets with minor importance or particular application [20]

Material	Isotropic or anisotropic	B_r, mT	H_{cB}, mA/m	H_{cJ}, mA/m	$(BH)_{max}$, kJ/m^3
Pt – Co	isotropic	600	380	500	70
Co – Fe – V	anisotropic	1200	30	32	20
Cu – Ni – Fe	isotropic	350	30	32	4
Cu – Ni – Fe	anisotropic	550	42	44	12
Co – Fe (ESD)	anisotropic	1050	75	77	50
Mn – Al – C	anisotropic	580	220	250	52

II.I.V. Copper-Nickel-Iron Alloys

The magnetic properties of the Cu - Ni - Fe alloys, with the composition 60% by weight of Cu, 20% by weight of Ni and the remainder of Iron, were discovered in 1930. They are materials that can be obtained in the isotropic and anisotropic form. The magnetic properties are reduced (see TABLE III) so their use in applications is limited.

II.I.VI. ESD magnets and Manganese-Aluminum-Carbone Alloy

The ESD (elongated single domain) magnets are alloys composed of Iron and Cobalt salts in which the elongation of the particles of the single domains obtained by means of a mercury electrode. The powder of other elements is then added, such as tin, antimony, and lead, and pressed into an external oriented magnetic field. ESD magnets were first used and adopted for many years in the United States. Now their use is limited, if not absent. Typical values are shown in TABLE III.

Manganese - Aluminum and Carbon alloys are interesting alloys since these non-ferromagnetic elements joined together give rise to a ferromagnetic material. Their composition range is as follows: 69-75% by weight of Manganese and the remainder of Aluminum. The addition of 0.4-1% by weight of Carbon results in greater stability of the ferromagnetic structure. They have good mechanical and magnetic properties and the Curie temperature is 300 °C. Despite the good magnetic properties (see TABLE III) such materials do not take place in applications due to their difficulties during the production process.

II.I.VII. Hard Ferrites

Hard ferrites are ferromagnetic materials that have high use in industrial applications. Ferrites are ceramic materials based on the following composition: $MFe_{12}O_{19}$ where M can be Barium or Strontium [20]. The ferrites are characterized by high values of the coercive field with respect to abovementioned magnets and may have residual hard induction at 93-95% of the saturation value. They can be made by the sintering process

or with resin or thermoplastic binders. In the sintering process, small amounts of additives, as for instance, SiO_2 and Al_2O_3 are added respectively to control the sintering behavior and to increase the coercive force [21]. The powders that will be compacted are made by grinding in cylindrical or spherical mills and the dimensions of these particles determine the values of coercivity field and residue induction. The magnetic properties strongly depend on the process temperature. The TABLE IV describes the magnetic properties of some common hard ferrites on the market. In Fig. 7 the demagnetization curves of some hard commercial ferrites are shown.

TABLE IV – Magnetic properties of the hard ferrites

Material	Isotropic or anisotropic	B_r, mT	H_{cB}, kA/m	H_{cJ}, kA/m	$(BH)_{max}$, kA/m^3	Density, g/cm^3
Sinter magnets						
Hard ferrite 8/27	isotropic	230	155	290	9	~ 4.9
Hard ferrite 24/35	anisotropic	360	260	350	24	~ 4.9
Hard ferrite 32/25	anisotropic	410	240	250	32	~ 4.9
Hard ferrite 32/17	anisotropic	410	160	165	32	~ 4.9
Injection molded magnets						
Hard ferrite 1/18 P	isotropic	80	60	170	1.0	~ 2.9
Hard ferrite 8/19 P	anisotropic	120	80	200	8.0	~ 3.5
Hard ferrite 12/12 P	anisotropic	250	180	220	12.0	~ 3.5

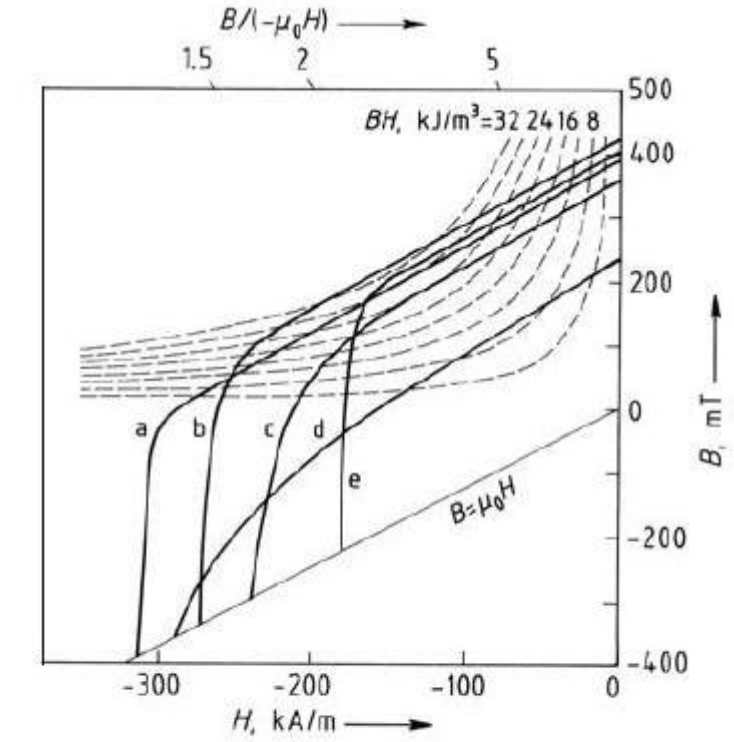

Demagnetization curves for hard ferrites; 8/27 isotropic, remainder anisotropic a) Hard ferrite 26/29; b) Hard ferrite 32/26; c) Hard ferrite 26/29; d) Hard ferrite 8/27; e) Hard ferrite 28/15

Fig. 7 – Demagnetization curves of different hard ferrites

II.I.VIII. Rare Earth Magnets

The development of hard magnetic materials with Rare Earth elements, as essential components, started in the mid-1960s and produced three groups of materials with higher magnetic characteristic than AlNiCo alloys and hard ferrites. The first group of materials is called first-generation and represents the magnets containing Samarium-Cobalt. The $SmCo_5$ is the combination that has the greatest industrial relevance. In the 1970s, another type of material has been developed, named second-generation magnets, which represent the development of first-generation materials. They are characterized by the combination of Samarium-Cobalt with the addition of other materials such as Copper and Iron or Titanium, Zirconium and Hafnium. The most recent group of hard magnetic materials is represented by Neodymium - Iron - Boron (Nd - Fe - B) alloys, which have been developed in Japan and the United States since 1983 and have higher magnetic values with respect to the other known hard magnetic materials. The discovery of more powerful materials can allow the reduction of the size of the magnet as well as the development of new applications. Compared to Samarium, Neodymium is more abundant in the earth's soil, so that a first impact has lower costs for producing magnets. On the other hand, the concentration of Neodymium is 7-16 times greater than Samarium. The production processes of Rare Earth containing magnets are all derived from powder. The grinding to obtain the powders must take place under the inert atmosphere due to the high affinity of the Rare Earth with Oxygen. The Fig. 8 shows the magnetization energy of hard "classic" and "modern" magnetic materials. In the next Fig. 9 the production process of magnets containing Rare Earth is illustrated.

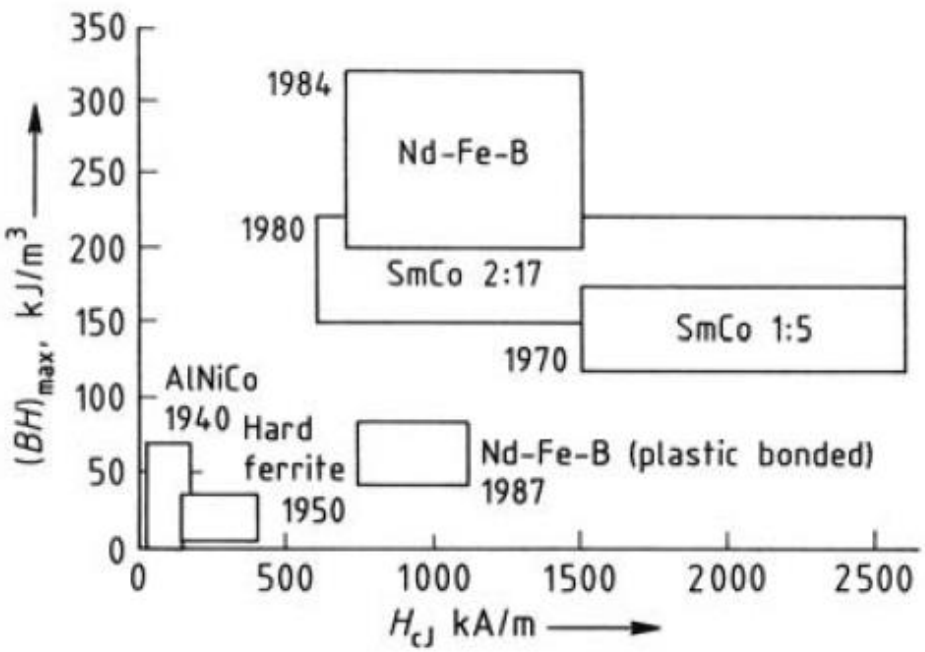

Fig. 8 – Development and magnetic performance of most widespread permanent magnets [20]

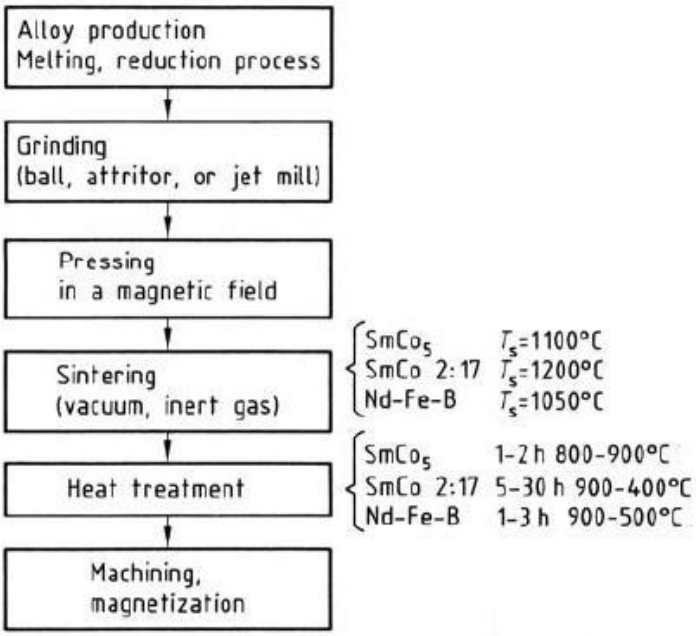

Fig. 9 – Typical production process cycle for magnets with Rare Earth

Alloys formed from Rare Earth and Cobalt can be binary or multi-component alloys. The most used are those that consist of Samarium. They have excellent resistance to corrosion and do not require any protective coating to prevent the magnet oxidation. Samarium - Cobalt magnets have a magnetic flux 5 times greater compared to AlNiCo alloys and hard ferrites. The Samarium-Cobalt magnets have fragile mechanical characteristic, on the other hand, allow to work up to high temperatures, until 300 °C without undergoing significant magnetic characteristic variations. TABLE V shows the magnetic characteristics of the most common Sm-Co alloys.

TABLE V – Magnetic properties of SmCo magnets

	Typical composition, wt%											Typical magnetic values			
Material	Sm	Pr	MM*	Co	Fe	Cu	Zr	Resin				$(BH)_{max}$, kJ/m^3	B_r, mT	H_{cB}, kA/m	H_{cJ}, kA/m
$(Sm_{0.2}MM_{0.8})Co_5$	7		27	66								120	800	580	1000
$(Sm_{0.4}Pr_{0.6})Co_5$	16	18		66								200	1050	720	1200
$Sm(CoCuFe)_5$	34			49	5	12						110	770	290	300
$SmCo_5$	34			66								160	920	680	2500
$Sm(Co, Cu, Fe, Zr)_{6.9}$	24	26		48	50	10	16	5	12	1.5	3	240	1130	540	580
$Sm(Co, Cu, Fe, Zr)_{7.5}$	24	26		48	50	10	16	5	12	1.5	3	210	1080	780	800
$SmCo_5$ (resin bonded)	33		62								2.5	110	760	580	1000

*Misch metal (cerium rich rare earth mixture)

The second most important category of "modern" hard magnetic materials is constituted of alloys with Rare Earth (Neodymium) - Iron and Boron. The composition is (Rare Earth/Nd)$_2$Fe$_{14}$B and have higher saturation values than other materials (about 1.6 T of the Nd compared to 1.02 T of $SmCo_5$ and 1.2 T of Sm_2Co_{17}). Speaking of magnetic energy, that value varies from 26 to 58 MGOe (magnetic energy unit in CGS system). The production process of Nd-Fe-B magnets is similar to that of Samarium-Cobalt

magnets. The process can be divided into two focal types: the traditional one that requires much thinner powders and heat treatments at high temperatures and the modern one using the polymeric binder. In case of sintering process, the powders are reactive with the surrounding environment, then it appears convenient that all the phases of the magnets production takes place in inert environments. In TABLE VI the magnetic characteristics of the most common alloys containing Iron - Boron - Rare Earth are reported.

TABLE VI – Magnetic properties of $(RE)_2Fe_{14}B$

$(RE)_2Fe_{14}B$	J_s, mT	H_A, kA/m	T_c, °C
Ce	1.17	2069	262
Pr	1.56	5970	294
Nd	1.60	5970	317
Dy	0.71		322
Ho	0.81	7320	303

Nd-Fe-B magnets have magnetic characteristics that strongly depend on the operating temperature (Fig. 10). In Fig. 11 it can be noted that at high temperatures the use of other magnets (for example Sm-Co) is privileged because they have more constant energy density values. Nd-Fe-B magnets require surface coating treatments to preserve their magnetic characteristics. Depending on the coating type, different characteristics and coloring of the magnet have been obtained for specific environments, as shown in TABLE VII.

TABLE VII – Different coating types adopted for NdFeB magnets

Available Coatings:				
Surface	**Coating**	**Thickness (μm)**	**Color**	**Resistance**
Passivation		1	Silver Grey	Temporary Protection
Nickel	Ni+Ni	10-20	Bright Silver	Excellent against Humidity
	Ni+Cu+Ni			
Zinc	Zn	8-20	Bright Blue	Good Against Salt Spray
	C-Zn		Shinny Color	Excellent Against Salt Spray
Tin	Ni+Cu+Sn	15-20	Silver	Superior Against Humidity
Gold	Ni+Cu+Au	10-20	Gold	Superior Against Humidity
Copper	Ni+Cu	10-20	Gold	Temporary Protection
Epoxy	Epoxy	15-25	Black, Red, Grey	Excellent Against Humidity & Salt Spray
	Ni+Cu+Epoxy			
	Zn+Epoxy			
Chemical	Ni	10-20	Silver Grey	Excellent Against Humidity
Parylene	Parylene	5-20	Grey	Excellent Against Humidity, Salt Spray. Superior Against Solvents, Gases, Fungi and Bacteria. FDA Approved

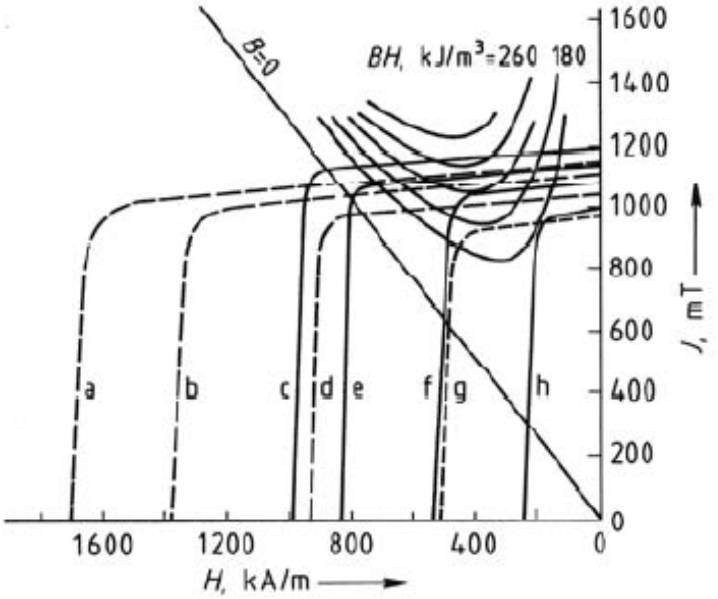

Demagnetization curves of a high- and low-coercitive Nd – Fe – B magnet at varying temperature a) 25 °C; b) 60 °C; c) 25 °C; d) 100 °C; e) 60 °C; f) 100 °C; g) 150 °C; h) 150 °C
– – – high coercivity; —— low coercivity

Fig. 10 – Demagnetization curves of NdFeB as the function of temperature

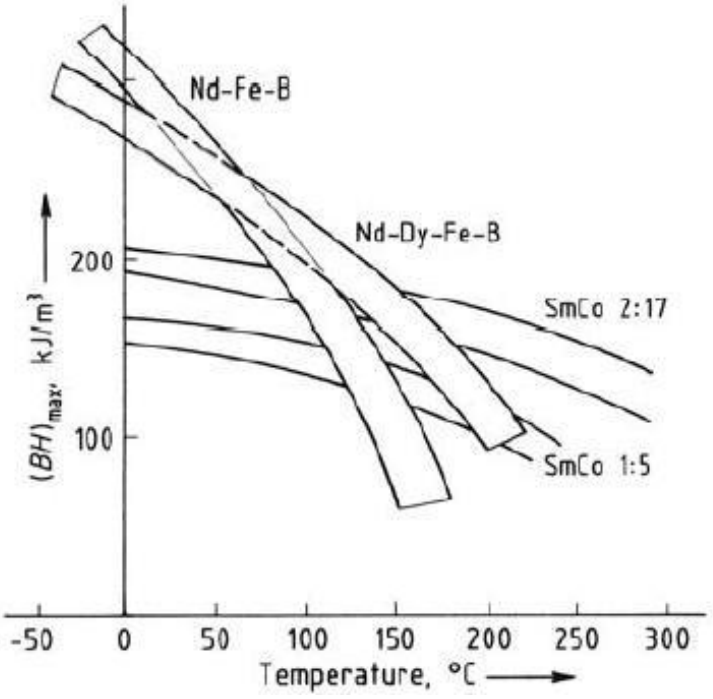

Fig. 11 – Dependence by the temperature of magnetic energy of the Rare Earth magnets

II.II Soft Magnetic Materials

The ferromagnetic soft materials, in general, are prepared to work in the area under the saturation knee as shown in Fig. 12. On the other hand, each material has different BH curve therefore to properly select the material it is necessary to find the combination between magnetization curve and iron losses. Moreover, other parameters affect the soft magnetic materials: operating frequency, manufacturing process, anisotropy, etc.

Soft magnetic materials can also be classified into traditional or modern as a function of the manufacturing process. The traditional ones are defined as the materials that have the aim to maximize the purity through an optimal microstructure obtaining smaller total magnetic energy losses. However, the presence of the impurities inside the ferromagnetic material prevents the formation of large grains and therefore limits the grain size. It should also be remembered that impurities affect the mechanical characteristics compared to pure material. The most common soft magnetic materials are listed in the following paragraphs providing some properties and considerations.

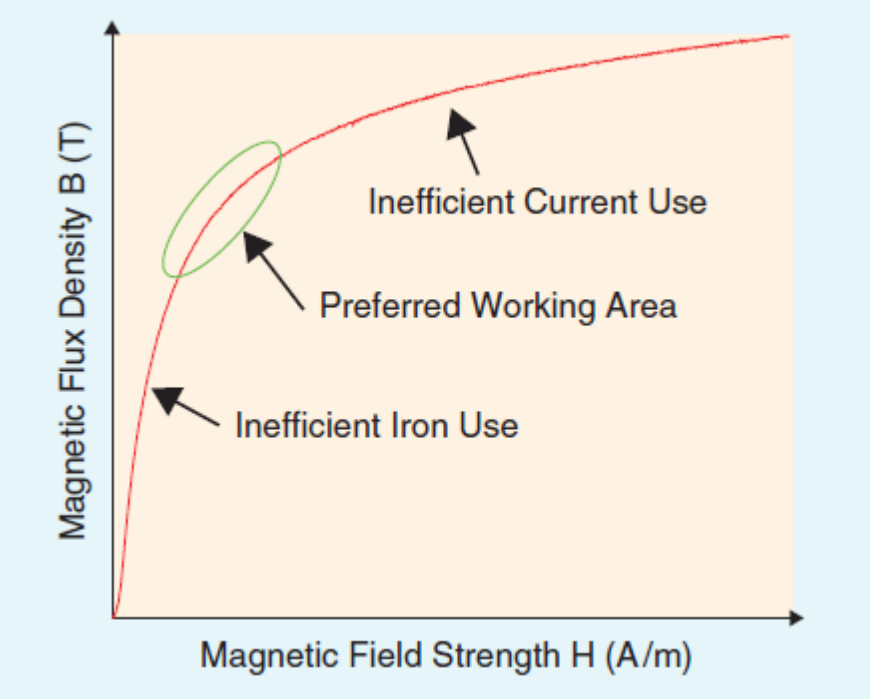

Fig. 12 – The preferable operating area for soft magnetic materials[4]

II.II.I. Iron-Silicon Sheet (FeSi)

The first described material is Iron-Dilicon (Fe-Si), which is the most technologically effective and economical material on the market for reducing iron losses in an electric machine. The pure Iron would be ideal from the magnetic point of view since it allows to have high magnetic performance but has a low value of resistivity which limits its use due to the eddy currents. The addition of Silicon improves the resistivity, but it is better

not to exceed a certain amount because it would consistently reduce the maximum achievable induction as well as the reduction of workability of the metal alloy at room temperature. The limit percentage is 6.5 wt.% of Silicon content inside the metal alloy, the tendency is to work the material also by hot working as they allow to have laminations with thicknesses up to 0.05 mm. Furthermore, electrical sheet can be constituted by structures having non-oriented and oriented grains. The drawbacks in the adoption of this material consist in the operating frequency range; for low frequency it represents the ordinary choice, but for medium and high frequency other soft magnetic materials are adopted.

II.II.II. Nickel-Iron (NiFe)

The next alloy described in this work is the one related to the Iron-Nickel compound. On the market, these alloys are found with an extended Nickel content (30% to 85% by weight of Nickel). It is also part of the category of classic soft magnetic materials. This kind of alloys is divided into 3 subcategories: a low, a medium and a high Nickel content. The Fe-Ni alloys with low Nickel content, i.e. containing about 36 wt.% of Nickel, are the important ones in the realization of soft ferromagnetic materials having high magnetic permeability. By lowering the percentage of Nickel up to 30%, the Fe-Ni alloy magnetic characteristics will strongly depend on the temperature. Alloys with a low Nickel content have values of coercive field and permeability very similar to those of the Fe-Si alloy but with the difference of having far superior resistivity values. They are also characterized by having better mechanical process, in these materials cold workings can be performed. The saturation flux density of Fe-Ni alloys with a low Ni content is 1.3 T, a value that can be considered good. This combination is suitable for medium frequency power applications.

The second type is made by the intermediate Ni content in the Fe-Ni metal alloy. The variation of Ni content is from 45% to 65%, and such alloys have a slight improvement in flux density compared to low Nickel content alloys and high permeability with respect to FeSi alloys. Such materials are suitable for special power transmission applications when small losses are needed. In this type of material, there is the possibility of adding 2% of Molybdenum (Mo) to further increase the resistivity of the Fe-Ni alloy with medium Nickel content. The addition of this material also changes the hysteresis cycle accordingly.

The last category is represented by the Fe-Ni alloy with high Nickel content, with a percentage higher than 70% by weight (Permalloy, mu-metal and Supermalloy). These materials were discovered since 1920 and are important in applications where low magnetic fields are required. This is justified by the fact that they have high initial permeability and low coercive field value having small losses due to hysteresis. In all

Fe-Ni alloys with variable Nickel content, it is necessary to limit the presence of Oxygen and additives inside the alloy in order to maintain the saturation value of the material.

II.II.III. Iron-Cobalt-Vanadium Alloy (Permendur)

The next type of classic soft materials is Iron-Cobalt-Vanadium alloy (Fe-Co-V, normally called Permendur). Alloys composed only of Iron-Cobalt, containing from 27% to 35% of Cobalt, are used only in special high-temperature applications. The performance of the compound $Fe_{49}Co_2V$ is remarkable since it reaches 2.35 T of maximum induction for an external magnetic field about of 10 kA/m. It also has a high Curie temperature (Tc of 950 °C) and high maximum permeability can be reached at high temperatures. Fe-Co alloys are expensive due to their composition and are mainly used for inductive elements in aerospace applications where size and weight savings are important. Alloys composed only of Fe-Co cause machining problems because this structure is fragile. The addition of Vanadium in the Fe-Co alloys generates a messy layer to the structure, which after the annealing phase (below 750 °C), allows performing the hardening of the alloy at room temperature. In this way, sufficient mechanical characteristics have been obtained to be able to carry out mechanical work on the material itself. Furthermore the addition of 0.2% of Niobium or Tantalum instead of Vanadium lead to the same degree of ductility and further improve the magnetic values of the alloy (saturation flux density values equal to 2.45 T).

II.II.IV. Soft Ferrites

The soft ferrites, that were used starting from the end of the 1940s, are distinguished on the basis of their crystalline structure. The magnetic properties depend on the type of structure. The most common structures of soft ferrites are cubic and hexagonal. The first type of structure is made by the following chemical composition *MO*: where M indicates the bivalent metal ion (which can be Fe, Ni, Co, Mn, Mg, Cu, Ti, Cd, and Zn) and O indicates Oxygen. The most common soft ferrites are those consisting of Nickel, Nickel + Zinc and Manganese + Zinc. Such ferrites are suitable for applications with frequencies of the order of MHz. The next structure represents the mixing of the ferrite having a cubic structure with the hexagonal Barium. The resulting material is a ceramic, so at room temperature, a greater resistivity is obtained. These soft ferrites are used in particularly super-high frequency inductive components without drastic losses in the material. The disadvantages of soft ferrites are the brittleness and very small saturation flux density. At numerical level, ferrites are characterized by coercive forces that vary in a range of 10 ÷ 1000 A/m and have a saturation flux density of 0.5 T. Furthermore, they can also reach values of maximum initial permeability equal to 40000 (reached in the Mn-Zn ferrites at few kHz). Lower initial permeability, of the order of a few

thousand, is given by the Ni-Zn ferrites; in order to allow the use of such material in the specific range frequency of MHz. The production process consists of compacting ferromagnetic materials ground and cooked below the temperature of material melting (Fig. 13). Compared to the traditional casting process, the sintering method of ferromagnetic materials allows the smaller tolerances.

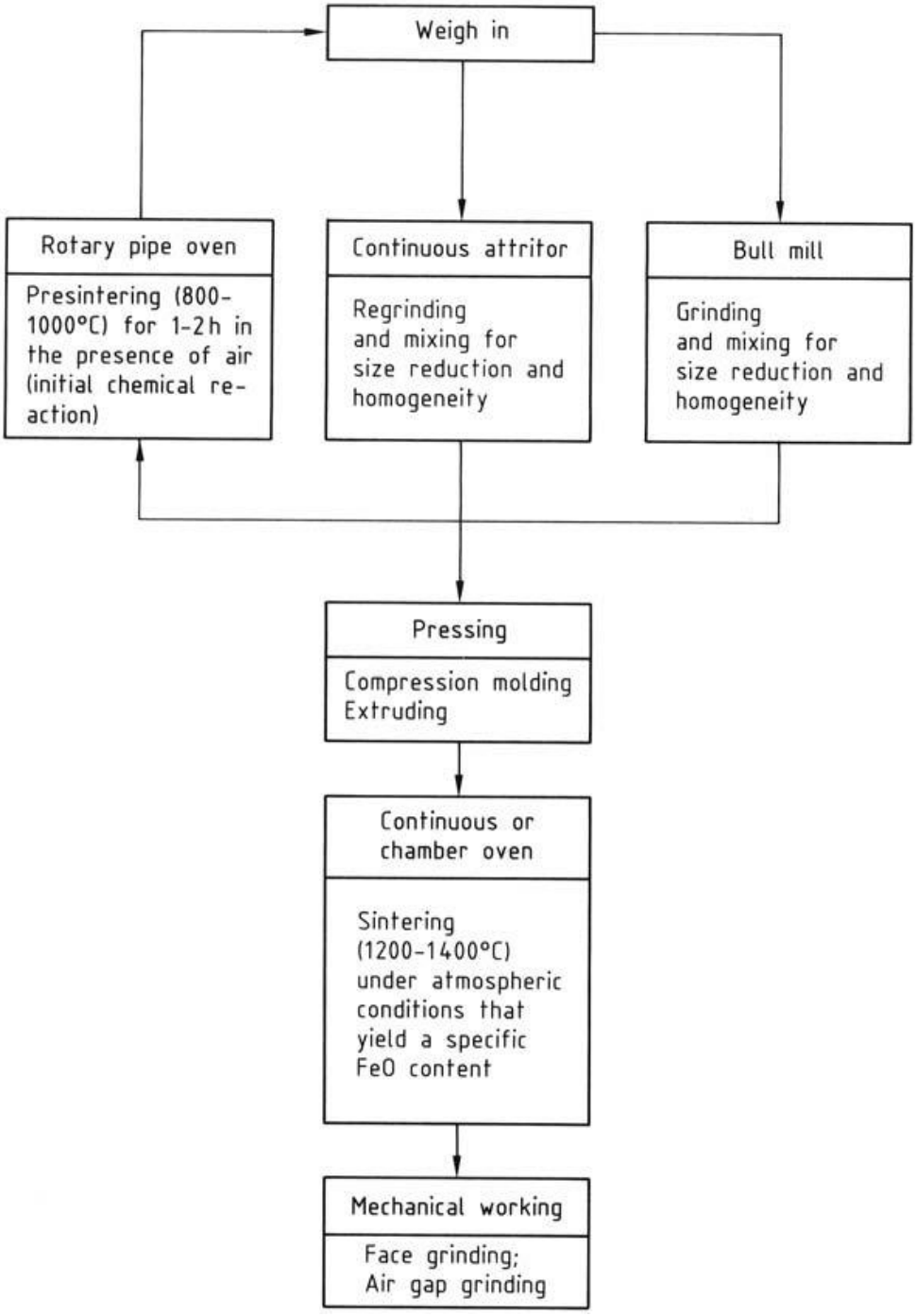

Fig. 13 – Production process of soft ferrites [20]

II.II.V. Amorphous Magnetic Materials

Amorphous materials (also called metallic glass) are considered "modern" soft materials and they are prepared by means of rapidly hardened in order to have the amorphous structure at room temperature, thus blocking the crystallization process of the material during its normal cooling speed. Such materials are characterized by high mechanical hardness. Compared to crystalline materials, the amorphous ones have a resistivity three times greater and the yield strength is 5-10 times greater. Also, amorphous materials are characterized by a better dependence of the magnetic properties as function of temperature and have higher values of flux density, so it follows that these materials are important in those applications where the dimensions of the inductive components must be contained. In amorphous soft materials, there are three important subdivisions that are related to the main element. The most significant are those based on Iron, Cobalt, and Fe-Ni.

Iron-based amorphous alloys are composed of Iron, Silicon, Boron and/or Carbon. The most famous alloys are those given by $Fe_{78}B_{19}Si_3$ and $Fe_{81}B_{13}Si_4C_2$. They are interesting alloys with iron reduced losses comparable to crystalline oriented grain materials and are mainly used in the United States in the ferromagnetic cores of transformers with power less than/equal to 500 kVA. In Europe, this application is not so much of interest since it presents problems of mechanical processing. The second amorphous alloy consists of a Cobalt base and has slightly lower flux density values than Iron-based amorphous alloys one. There are small deformations during the magnetization of the material and they depend on the composition of the Cobalt-base amorphous alloy. For deformations, less than 10^-7 m, the maximum coercive field and relative magnetic permeability are obtained. At low operating frequencies, the magnetic properties are comparable and/or better than those of permalloys (Fe-Ni alloys). Such alloys, in a range of a few kHz, have better magnetic characteristics than ferrites. The main disadvantage is the high costs for high Cobalt content. The third category of amorphous materials is based on Fe-Ni (about 40%) and the remaining components are Silicon and Boron. The addition of Molybdenum included the thermal stability of the amorphous alloy. The magnetostriction values are slightly greater than in the case of the Cobalt-base amorphous alloy and are about 10^-6 m. The magnetic properties of the amorphous Fe-Ni alloy are the compromise between the Iron-base alloys and Cobalt-base ones.

II.II.VI. Nanocrystalline Magnetic Materials

The nanocrystalline magnetic materials were developed in Japan starting in the 1980s and have an extremely fine grain structure. This new structure was produced by rapid cooling and subsequent controlled heating phase above the crystallization temperature of Iron-based alloys (containing mainly Silicon, Copper, Boron and Niobium). In that

way, the metal structure becomes a homogeneous and extremely fine structure with a grain diameter of 10÷20 nm. The Curie temperature value increases using the annealing process in a range of 320÷600 °C maintaining the same flux density. These materials are innovative and combine the advantages of Iron-based and Cobalt-based amorphous alloys.

II.II.VII. Powder Composite Materials

The composite powders are electrically insulated particles from each other. The production of these materials is made by means of metal powders (such as Fe), through the mixing of several elementary powders (such as Fe, Si, Ni, Co) or through alloy powders (such as Fe-Si, Fe-P, Fe-Ni, Fe-Co, Fe-Ni-Mo). These powders are mixed and compacted mechanically with a successive thermal treatment. Depending on the applications, these powder are compacted at different pressures, which will also determine the mechanical strength performance of the magnetic material. In addition to magnetic powder, insulating additives and organic/non-organic layers are used.

Nowadays, the most used composite powders are Soft Magnetic Composites (SMC) materials [6],[22],[23]. Such magnetic materials are prepared with a ferromagnetic base powder, whose particles are covered with an electrically insulating layer to limit the energy dissipation due to eddy current losses. Such layers can be of organic or inorganic origins, and different techniques are adopted to prepare such coatings: mixing, deposition, curing, sol-gel, co-precipitation and others [24–31]. Usually, the organic layers consist of resins, [5],[32] while the inorganic ones are metallic oxides, ferrite, Aluminum, Silicon and others [33],[34]. SMCs present further advantages compared to other magnetic materials: low eddy currents, very high electrical resistivity, low specific losses at medium-high frequencies and more compacted machine geometries; accordingly higher power densities for the same dimension compared to the traditional radial flux machines (RFM) are possible [35]. The low mechanical strength of the material is the weak point. Furthermore, they are materials with not high magnetic permeability.

Depending on the grain size and the particle size distribution, losses are minimized for a wide range of frequencies [36-42]. In general, SMCs materials have a crystalline reticular structure.

The magnetic properties, as well as the BH curves, of some soft magnetic materials, are reported in TABLE VIII and Fig. 14.

TABLE VIII - Magnetic properties of soft magnetic materials [43]

Material Type	Material Composition	Sheet Thickness (mm)	Flux Density at 0.8 kA/m (T)	Flux Density at 2.5 kA/m (T)	Resistivity (μΩcm)	Material Density (g/cm^3)
CoFe	49% cobalt, 49% iron, 2% V	0.2–0.5	2.1	2.23	40	8.12
NiFe	40% nickel, 60% iron	0.1–0.5	1.44	1.48	60	8.2
High-silicon-content SiFe	6.5% silicon, iron balanced	0.1–0.2	1.29	1.4	82	7.49
Thin nonoriented SiFe	3% silicon, 0.4% aluminum, iron balanced	0.1–0.3	1.15	1.63	52	7.65
Nonoriented SiFe	1–3% silicon, iron balanced	0.35–1	—	1.64	20–60	7.6–7.8
Amorphous iron	20% (silicon and boron), 80% iron	0.025	1.55	—	130	7.18
SMC	<1% lubrication, iron balanced	Solid material	0.71	1.22	20,000	7.57

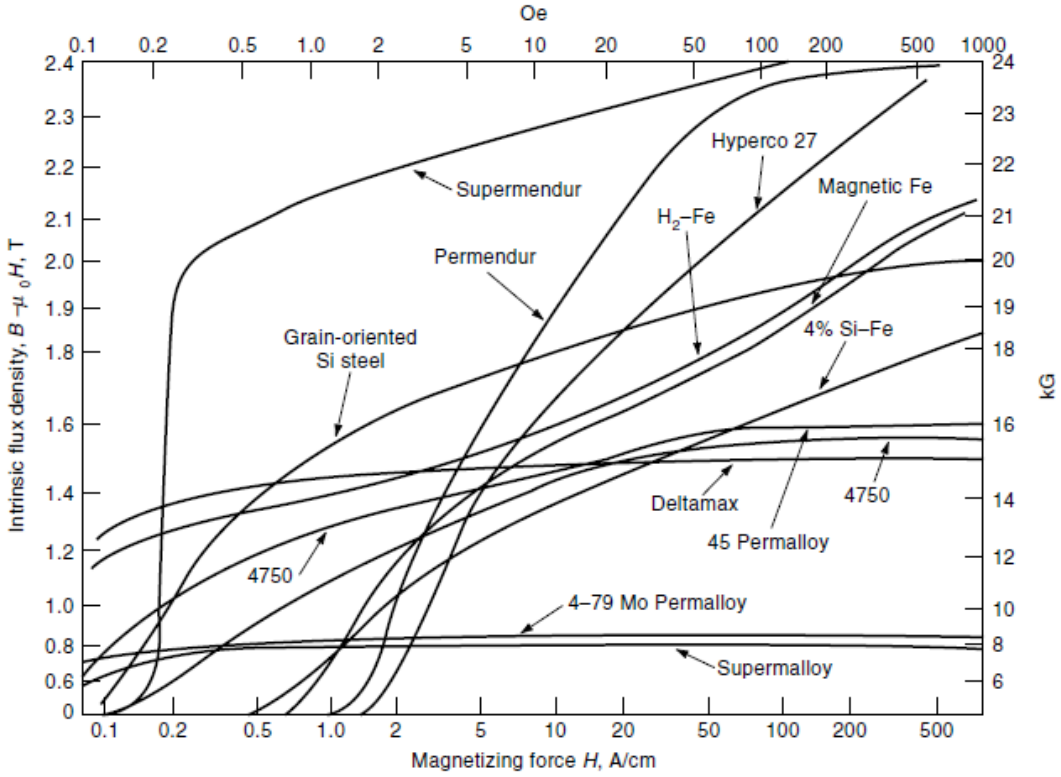

Fig. 14 – BH curves of soft magnetic materials available on the market [44]

II.III Innovative Magnetic Materials: aim of the work

In the research activity, concerning the goal of the doctorate, the novel magnetic materials have been proposed. The study and analysis have been focused on the materials that can improve the performance in electrical machines or provide the new solution in energy conversion and sensor applications. From this point the view, the research activity is divided into material study and characterization, motor design, prototype assembly, and experimental tests.

The proposed materials are:

- BONDED MAGNETS
- SOFT MAGNETIC COMPOSITE
- HYBRID MAGNETIC COMPOSITE

For the aforementioned materials, the investigation has been conducted beginning from products available on the market but mostly with materials developed and produced in the laboratory. The novel and very useful solutions have been realized in relation to motors design and applied in prototypes. Therefore, a brief foreword on the most popular PM electrical machines has been introduced in the following chapter.

III. PERMANENT MAGNET ELECTRIC MACHINES

Permanent magnet electric machines differ from other electric machines due to the presence of hard magnetic materials in the rotor, while the stator is constructively identical or similar to normal electric machines. On the other hand, in DC electric motors the magnets are applied in the stator. There are different types of PM machines, with different operating principles [45-47]; some of them are listed hereafter.

III.I DC Motors

In DC motors the permanent magnets generate the stationary magnetic field. The characteristics torque-speed depend on the type of magnets. For example, the torque density for ferrite magnets is about 0.5 Nm/kg, while if Rare Earths are adopted the torque density will be of about 0.7 Nm/kg. Also, the magnet characteristics affect the stator geometric shape. In Fig. 15 it is possible to note different stator geometric configurations.

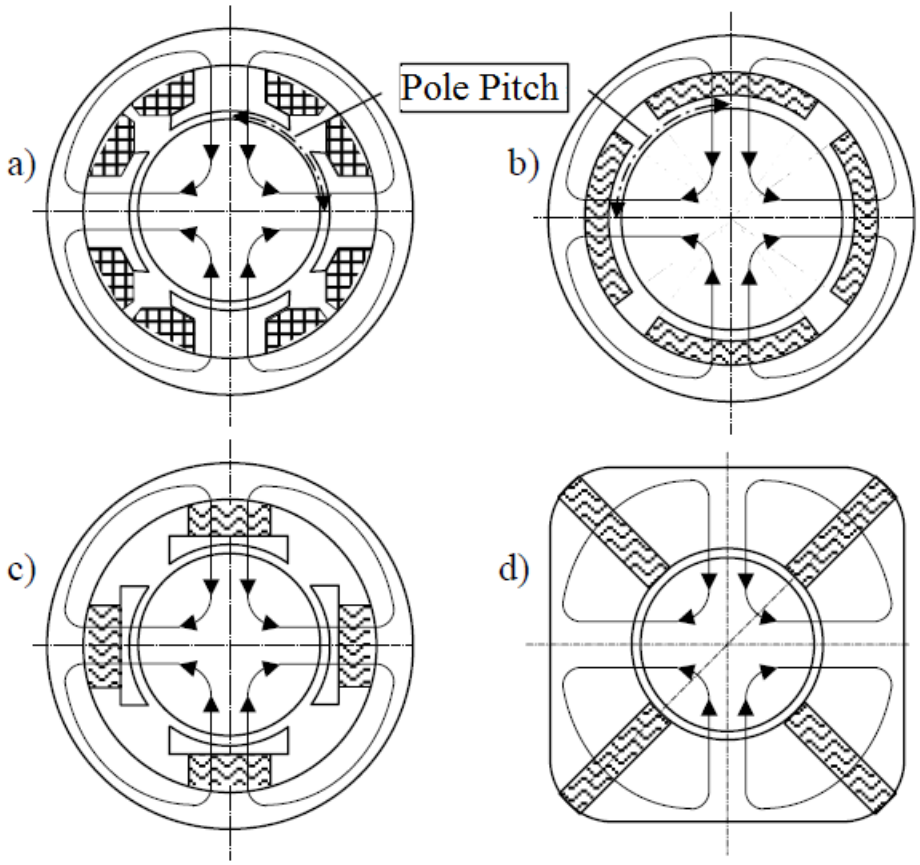

Fig. 15 – Different geometric solutions for stator with two pole pairs: ***a)*** *electromagnets,* ***b)*** *surface permanent magnets,* ***c)*** *interior permanent magnets and* ***d)*** *spoke-type permanent magnet configuration*

III.II Brushless Motors

Brushless motors are synchronous machines equipped with permanent magnets, placed in the rotor. The magnetic flux is generated by permanent magnets, instead of being produced by an excitation circuit in the rotor using its brushes. This certainly allows annulment of Joule rotor losses and also makes the machine more compact and lighter. Unlike in DC machines, the produced field by the magnets is not stationary but is rotating. Moreover, such machines have high efficiency and a wider speed range. While, compared to induction motors, they have better dynamic performances and smaller dimensions for the same power, in addition to a better efficiency. The magnets can be placed superficially or interiorly in the rotor, as shown in Fig. 16.

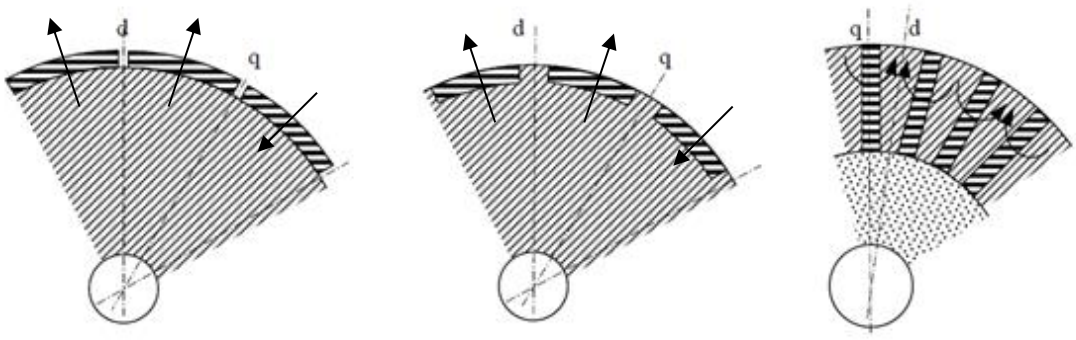

Fig. 16 – The typologies of brushless motors: SPM (surface mounted permanent magnet), IPM (interior permanent magnet) and Spoke type

The control type used and the rotor structure is closely connected. There are two main control techniques for three-phase brushless motors: the trapezoidal and the sinusoidal. The techniques differ according to the waveform of the currents and the counter-electromotive force (back-EMF) of each phase. Brushless trapezoids machines are also called Brushless DC because they are constructively the opposite of DC machines with permanent magnets. The isotropic rotor structure (air gap magnetically invariable) is generally represented from the SPM rotor, i.e. Surface Permanent Magnet (Fig. 17). The anisotropic form is IPM, i.e. Interior Permanent Magnet. Brushless trapezoidal motors are commonly SPM, while sinusoidal brushless motors can be either SPM or IPM. A particular category of brushless motors is Axial Flux Motors (AFM). As the name suggests, they are characterized by an axial and non-radial stator-rotor flux as normally happens in electric motors. The particular constructive form allows realizing multi-stage structures that improve the torque density, efficiency and reduction of machine volume. An example of AFM design, studied in the research activity, is shown in Fig. 18.

The disadvantages in brushless machines are represented by the cogging torque, but different methods are adopted to reduce the amplitude of such torque.

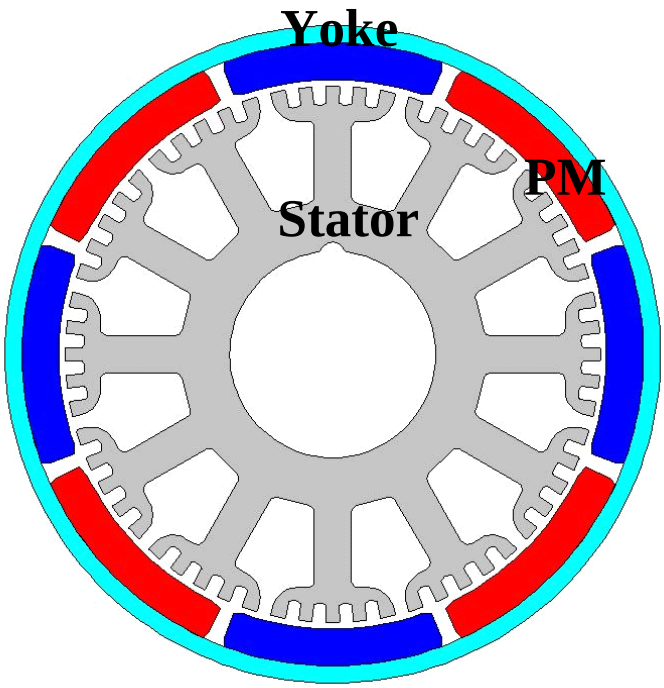

Fig. 17 - Structure of the SPM (surface mounted permanent magnet) used in the research activity

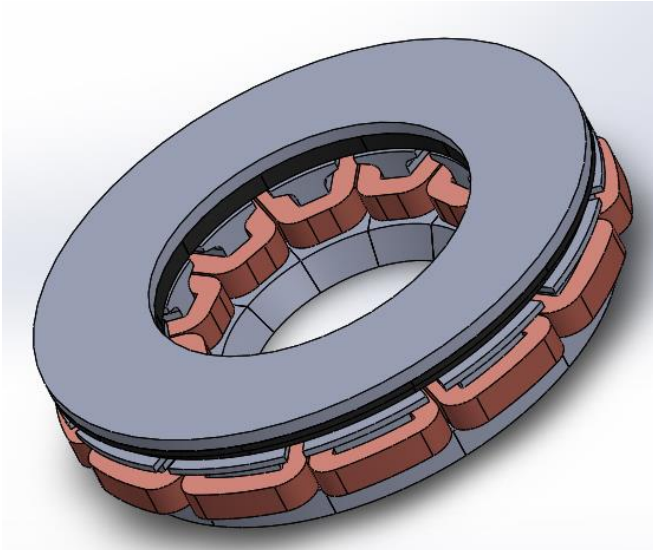

Fig. 18 – Axial flux motor: the design evaluated in the research activity

III.III Assisted Reluctance Motors

In this paragraph, the assisted reluctance machine is described, even though the same typology of the machine will be treated in following chapters. This type of PM machine derives from the synchronous reluctance machine; wherein the permanent magnets have been inserted in flux barriers in order to improve the drawbacks of the original machine. There are two types of reluctance machines: Switched Reluctance, having both rotor and stator with the anisotropic structures, and Synchronous Reluctance, which has flux barriers on the rotor (Fig. 19). The second is like brushless but without permanent

magnets and for that reason, the torque derives from the anisotropy of the rotor. Instead, the stator has a classic construction, like that of an induction motor. The rotor is particularly compact, given the absence of windings and magnets. It is designed in order to form preferential paths for the produced magnetic flux.

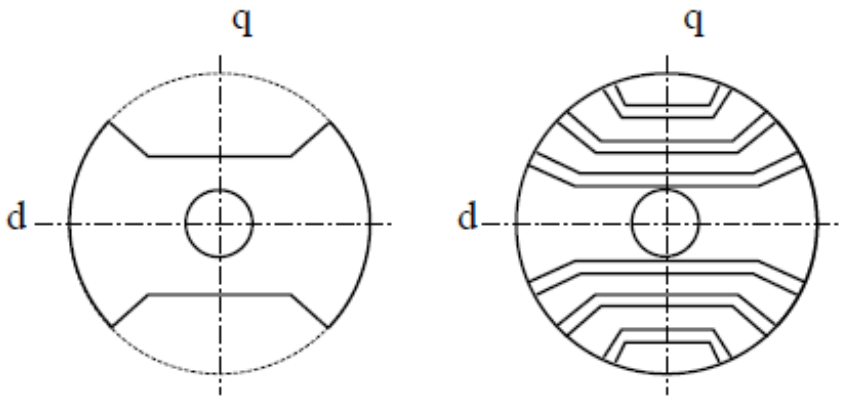

Fig. 19 – Rotor geometry of reluctance machine

In Fig. 19, the axes “d” e “q” show the minimum and maximum reluctance respectively. The assisted reluctance machines is equipped with certain quantity of magnets in the direction of the axis "q", that involves the presence of a flux λ_m. Such flux is a minor part of the total flux. The total flux is the sum of the previous one (produced by magnets in flux barriers) and the one generated by stator windings. The use of permanent magnets in this type of motors makes it suitable for flux-weakening, it also provides another advantage, i.e. it has a higher kVA/kW ratio than the reluctance machine and in some cases even compared to the induction motor. This allows savings in terms of power electronics, because, with the same active power, a smaller inverter will be required than in the case of reluctance machine without the magnets. Furthermore, the use of the magnets improves the torque density. Two different methods of inserting magnets inside the rotor flux barriers are shown in Fig. 20. In the first case, the magnets are simply mechanically inserted (partially filled), in the second case the injection process has been adopted using the ferrite bonded magnets (completely filled).

Different advantages are obtained with PM electrical machines. In particular, in brushless and assisted reluctance machines, the absence of the excitation circuit in the rotor and the use of the magnets guarantees a significant compactness and lightness. Therefore more and more often these machines are chosen in automotive applications. The absence of sliding contacts allows brushless and assisted reluctance motors to receive less maintenance.

While the disadvantages are very complex control, the cost of permanent magnets and of the manufacturing process.

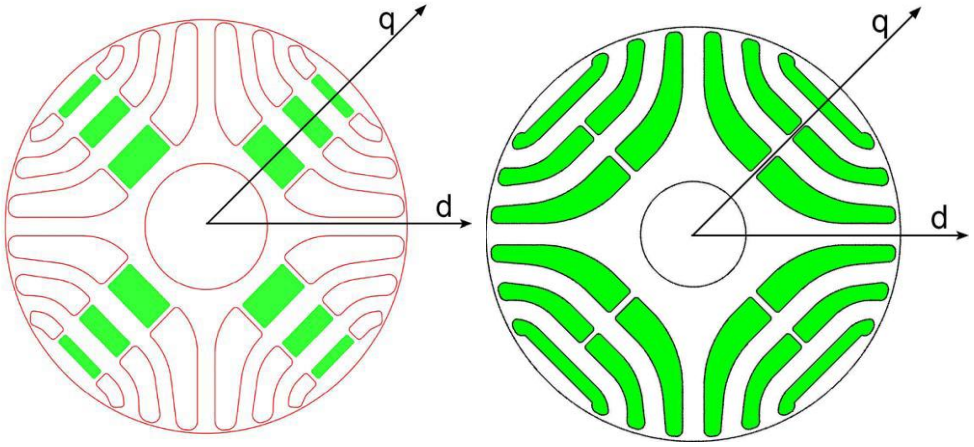

Fig. 20 – Filling of flux barriers with magnets: traditional concept with regular magnets and injection technique with ferrite bonded magnets [48]

III.IV Stator-PM Machines

Stator-PM machines are an attractive structure due to placing both magnets and coils in the stator structure only. Flux Switching PM (FSPM) machines (Fig. 21) and Flux Reversal PM (FRPM) machines (Fig. 22) are two common stator-PM structures [49-52]. Placing the PMs in the stator structure makes these structures an appropriate candidate for transportation applications because they have salient and robust rotor without PMs or windings.

These structures have some advantages like robust structure, high power and torque density, and fault tolerant ability [11],[49-53]. On the other hand, one of the important disadvantages of such structure is that the stator is composed of a large number of components, which makes the construction process so challenging.

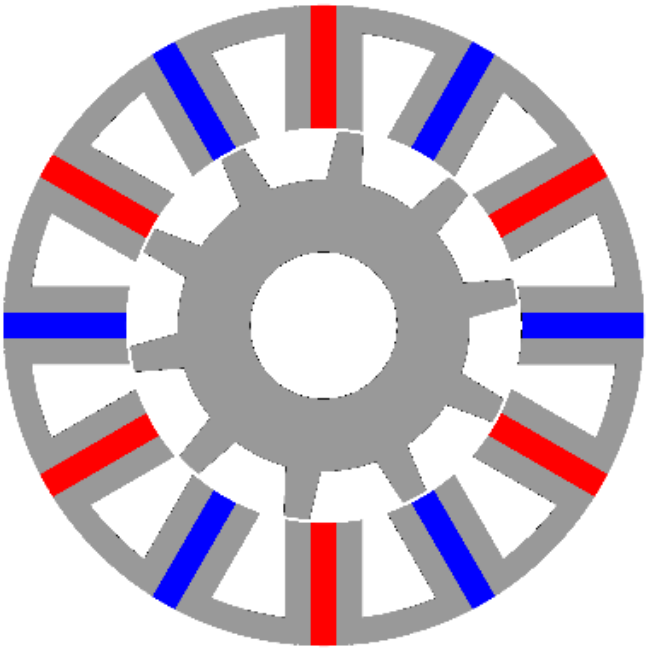

Fig. 21 –Stator structure of flux switching PM machine

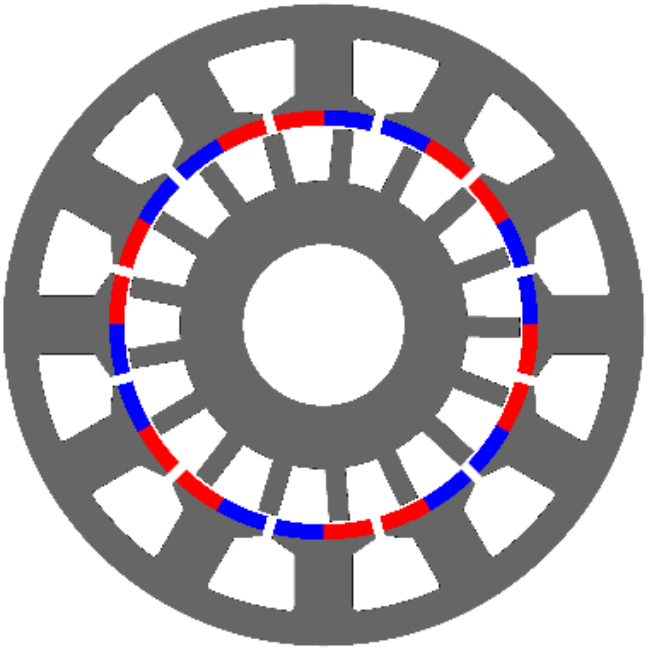

Fig. 22 - Stator structure of flux reversal PM machine

IV. BONDED MAGNETS

Permanent Bonded magnets represent a valid alternative to the traditional sintered magnets [54-57]. Basically, they are made with two components: a hard magnetic powder (such as hard ferrite, NdFeB, SmCo) and a non-magnetic binder mixed for compression or injection molding. The benefits of such materials are represented by the adoption of polymeric binders to prepare the magnetic compound: according to the percentages of the plastic binder, the resulting magnetic characteristic can be "tuned" and adapted to the required characteristics.

The magnets described in the present chapter are the result of an activity that has been carried on in the laboratories for a long time, and which allowed getting experience and knowledge in the materials' selection and the process parameters regulation. However, before starting with the list of the proposed magnets, it is opportune to explain the interpretation of the magnetic curve. The demagnetization curves of the proposed epoxy NdFeB bonded magnets, compared with the tested NdFeB sintered magnets are described in Fig. 23; in particular the curves 1 and 2 represent the magnetic polarization of the NdFeB sintered magnets (1) and epoxy bonded magnets (2), while the curves 3 and 4 represent the magnetic induction obtained by subtracting the term $\mu_0 \times H$ from the previous magnetic polarization curves. The curves (1) and (2) are measured by hysteresisgraph, instead, the (3) and (4) are deduced from the measurements through above-mentioned subtraction. However, the curve (3) and (4) are used in the motor design and simulation tools, while in the curves (1) and (2) the intrinsic coercivity H_{cj} provides information on the maximum overload capability concerning the demagnetization. Further datum can be used to compare the magnets is the maximum magnetic energy product BH_{max} as shown in TABLE IX. The maximum energy product can be good solution for a direct comparison. Nevertheless, the selection of the magnet depends on the application particular and work point, therefore the use exclusive indicator for comparison is not always advisable.

TABLE IX – Magnets comparison: Sintered NdFeB and Epoxy NdFeB Bonded magnet data

Magnet Data					
Sintered NdFeB			**Epoxy NdFeB**		
Remanence B_r	1.163	T	Remanence B_r	0.658	T
Intrinsic Coercivity H_{cJ}	1865	kA/m	Intrinsic Coercivity H_{cJ}	1027	kA/m
Coercivity H_{cB}	856.6	kA/m	Coercivity H_{cB}	450.8	kA/m
BH_{max}	242.5	kJ/m^3	BH_{max}	74.1	kJ/m^3

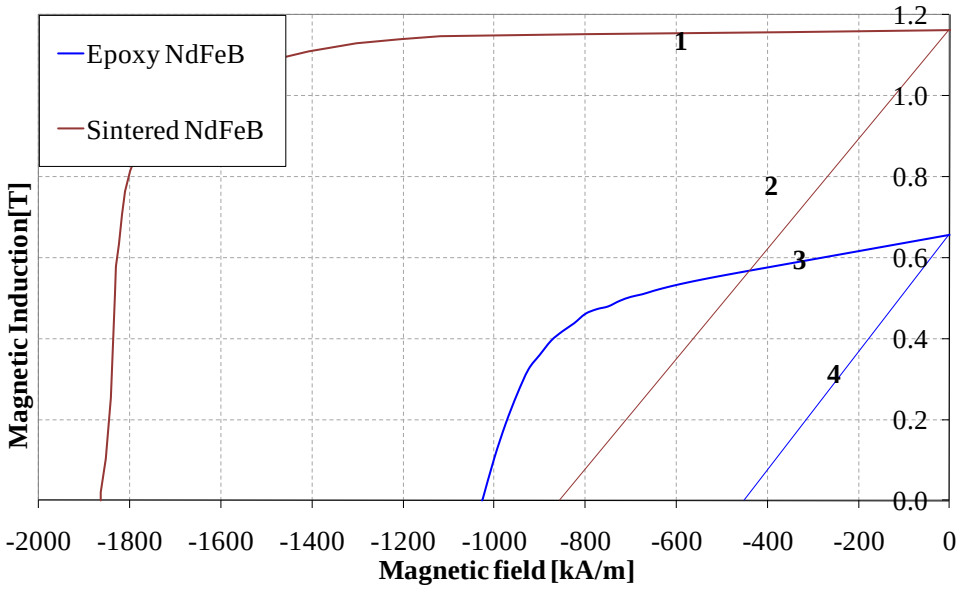

Fig. 23 - Demagnetization curves of the proposed magnets at 20 °C: curve 1-2: magnetic polarization of the NdFeB sintered magnets (1) and epoxy NdFeB bonded magnets (2); curve 3-4: magnetic induction

The magnetic characteristics of the magnets realized have been measured using the hysteresisgraph in Fig. 24. The instrument tools consist of the different measure coils as the function of the magnet dimensions and various polar expansions with the possibility to apply the thermal characterization. All magnets typologies can be measured with this hysteresisgraph.

Different type of bonded magnetic materials has been prepared and characterized; some of them have been used in the prototype production, described in the following chapter.

Fig. 24 - Hystersisgraph: measurement system used for obtaining demagnetization curves

IV.I Materials Selection, Specimens Preparation and Characterization

The first phase consists in the choice of materials, both polymeric and magnetic. At the beginning, a lot of work has been devoted to the selection of the polymeric binders to be utilized; polymeric materials normally used are Polyamide (PA) and resins (epoxy and phenolic). The polymeric technology allows to easily obtain magnets with particular shapes, for example, a curve form, adoptable on external rotating rings. Usually, the thermoset polymer materials, like the resins, are used in the compression moulding, while the thermoplastics are adopted for the injection processes.

The best magnetic properties are obtained with bonded magnets prepared in the laboratories by compression process. The mixture is made using the specific NdFeB powder for bonded magnets, MQP 14-12 for high-temperature applications, together with epoxy or phenolic resin (Fig. 25); the mixing process is prepared by a dedicated machine (turbula in Fig. 26). The specimens have been made in different shapes using a hydraulic press which can operate up to 1GPa (Fig. 27). The final step concerns the thermal treatment, curing at about 150°C for 30 minutes.

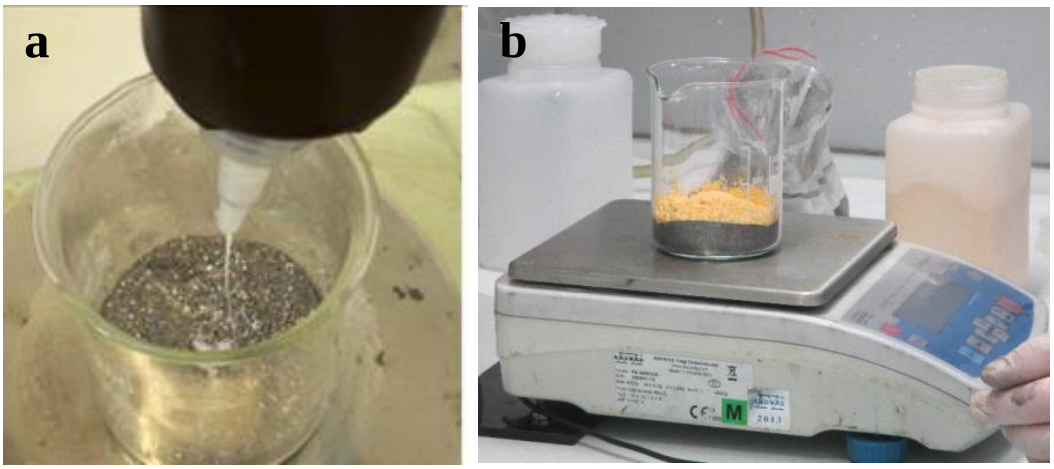

Fig. 25 – The adopted resins: epoxy(a) and phenolic(b)

Fig. 26 – Automatic mixing process with turbula

Fig. 27 - Compression process with the hydraulic press using different pressure levels

The research work has regarded:

- the selection on the binders, in the end, restricted to an epoxy and a phenolic resin as thermosets and PA6 and PA12 as thermoplastics;
- the effect of the compacting pressure, from 220 to 600 MPa;
- the analysis of the percentages to be adopted, explored from 0.5 to 10 wt% in the case of thermosets and from 8 to 40 wt% in the case of thermoplastics.

IV.I.I Compression Molding

Two different binders for compression molding have been adopted; both based on resins: epoxy and phenolic. The epoxy resin is normally used to glue the components in structural parts in different application sectors and presents very high adhesive strength. While the phenolic resin is adopted in brake application and can work at high temperatures. Furthermore this last is more straightforward to mix compared to the epoxy resin and is cheaper.

The effect of compacting pressure has been investigated for both typologies of prepared bonded magnets. Two pressure levels have been selected, both for epoxy (Fig. 28) and

phenolic NdFeB magnets (Fig. 29). The polymer percentage, 1.8% in weight, is the same for both resins. The high-level pressure (600 MPa) is the typical value used in an industrial process for such magnetic powder. Instead, the low one (220 MPa) corresponds to values used in a particular press (hot plates press) adopted in polymer technology. Slightly better results have been obtained with epoxy bonded magnets as reported in TABLE X, and the high difference between the proposed pressure levels involves a slight lowering of magnetic characteristics. Both bonded magnets have magnetic performances much higher than ferrites, mostly as regards the intrinsic coercivity magnetic field.

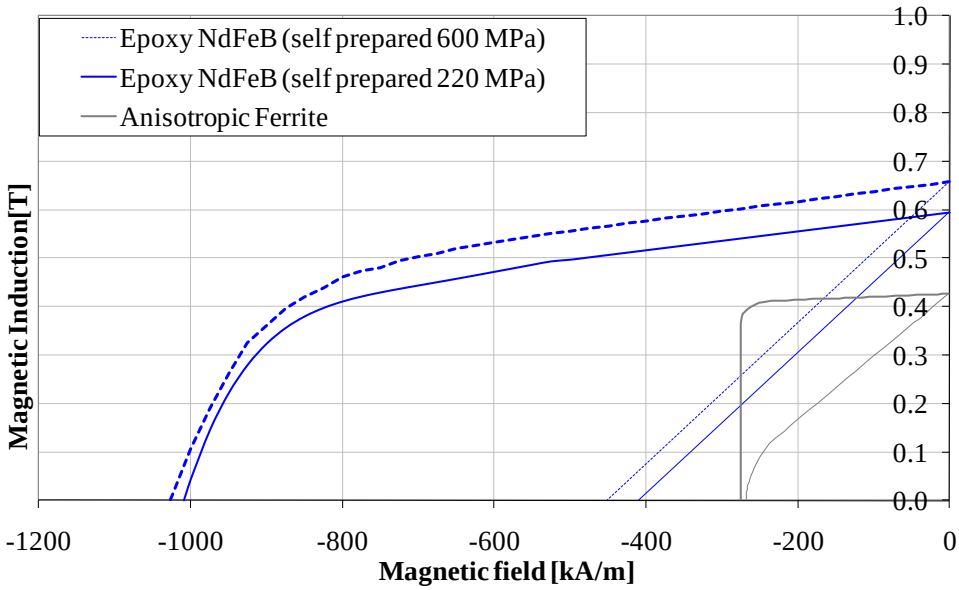

Fig. 28 - Demagnetization curves of epoxy bonded magnets for different pressure levels using the compression molding

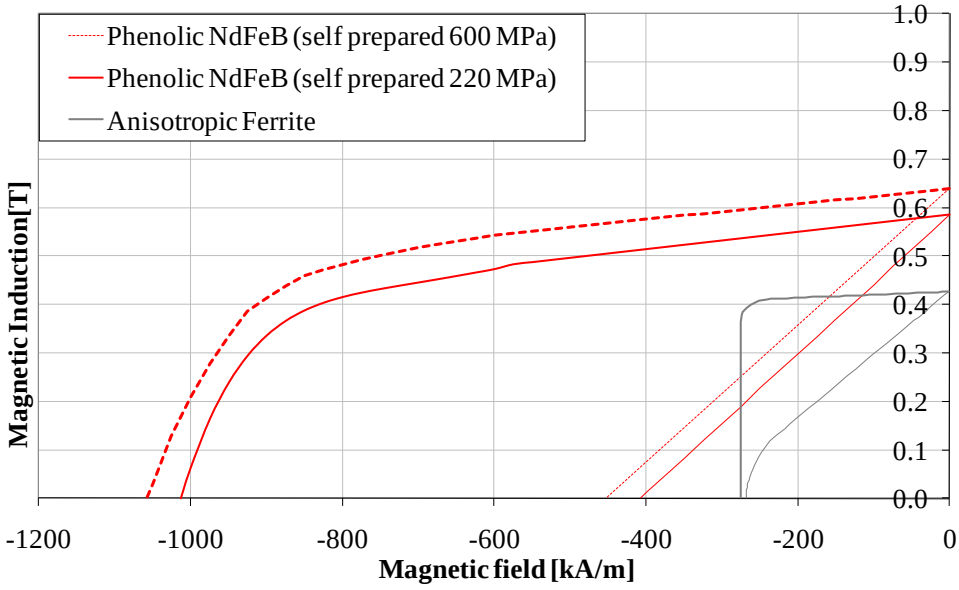

Fig. 29 - Demagnetization curves of phenolic bonded magnets for different pressure levels using the compression molding

TABLE X – Bonded Magnets comparison: Epoxy NdFeB and Phenolic NdFeB magnet data

Magnet Data					
Epoxy NdFeB			**Phenolic NdFeB**		
Remanence Br	0.658	T	Remanence Br	0.639	T
Intrinsic Coercivity HcJ	1027	kA/m	Intrinsic Coercivity HcJ	1057.8	kA/m
Coercivity HcB	450.8	kA/m	Coercivity HcB	451.8	kA/m
BHmax	74.1	kJ/m^3	BHmax	72.1	kJ/m^3

Different binder contents in weight have been used, for the same pressure level (600 MPa). The plastic binder here examined is a phenolic resin, particularly suited for compounds with high resin content, thanks to its minimum volume change after curing. Three binder contents have been chosen: 1.8, 5 and 10 wt%. The results show a high reduction of the remanence value with the amount of binder content, as reported in Fig. 30. It is important to note that the intrinsic coercivity magnetic field remains almost constant. The bonded magnet with a resin content at 1.8 wt% has the maximum magnetic energy BH_{max} of 64.5 kJ/m^3; increasing the resin quantity the BH_{max} values decrees respectively to 54.9 and 22.2 kJ/m^3. It can be noted that the bonded magnet with the lowest magnetic energy has the same high intrinsic coercivity. This means that the magnet can be operated in the applications where high overload capability is required.

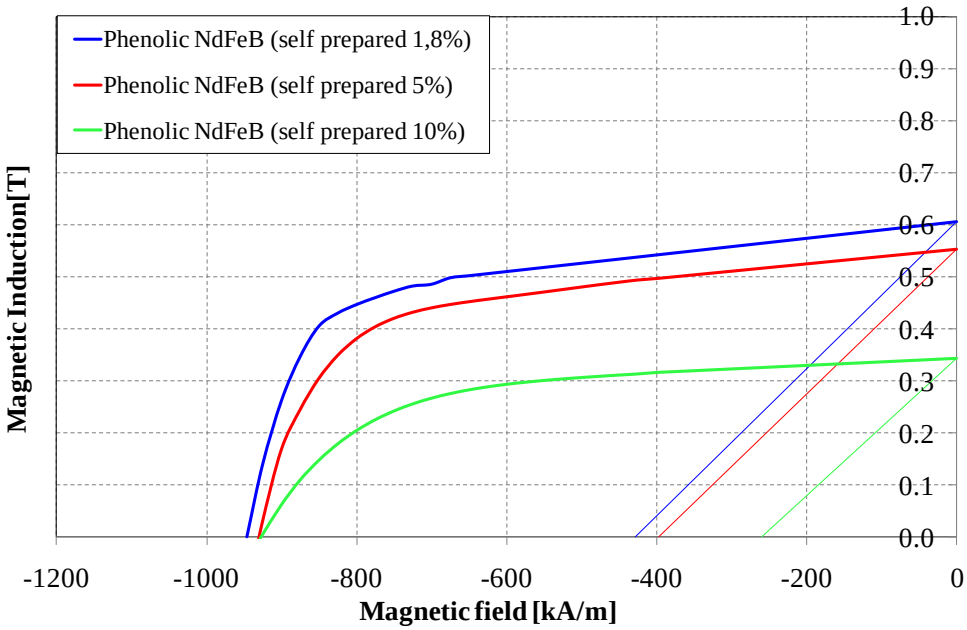

Fig. 30 – Demagnetization curves of phenolic bonded magnets for different binder content and prepared by compression molding

IV.I.II Injection Molding

The injection process allows to realize bonded magnets in very complex shapes and facilitates the mass production. However, reproducing such process in laboratory is very difficult due to the complex settings and expensive tools and components needed; for instance, an extruder is necessary, together with an injector machine with a particualr mould. Therefore, first of all, the magnetic composite has been prepared in a particular plastic mixer at a temperature range of about 260-280°C, always using the same magnetic powder MQP 14-12 and polyamide 6 (PA6) or polyamide 12 (PA12) pellet, as shown in Fig. 31. Such composite has been analyzed and grinded (Fig. 32); once ascertained the good magnetic and mechanical performances the typical extrusion process has been applied (Fig. 33) to obtain the polyamide NdFeB pellet (Fig. 34).

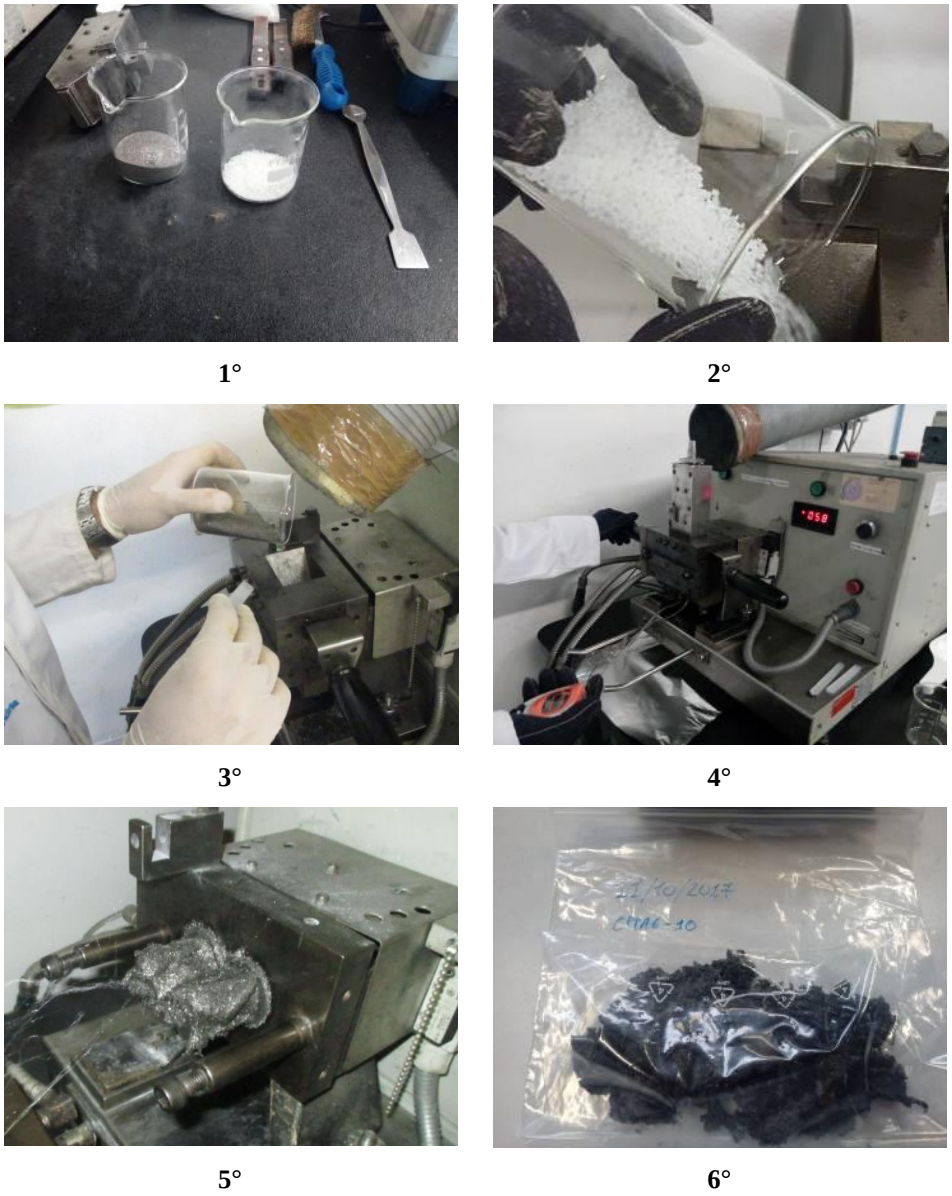

1° **2°**

3° **4°**

5° **6°**

Fig. 31 – Stages of composite production using the dedicated plastic mixer: 1° choice of magnetic and polymeric correct quantities, 2° insert of polymeric binder in pellet form (PA6), 3° insert of magnetic powder, 4° mixed in brabender, 5°extraction of agglomerate material and 6° final compound shape

Fig. 32 – Grinding of produced composite with the aim to make the magnetic powder useful for the molding process

Fig. 33 – Extrusion machine with double screw

Fig. 34 - Pellet production: the case of PA6 NdFeB (self-prepared 20%)

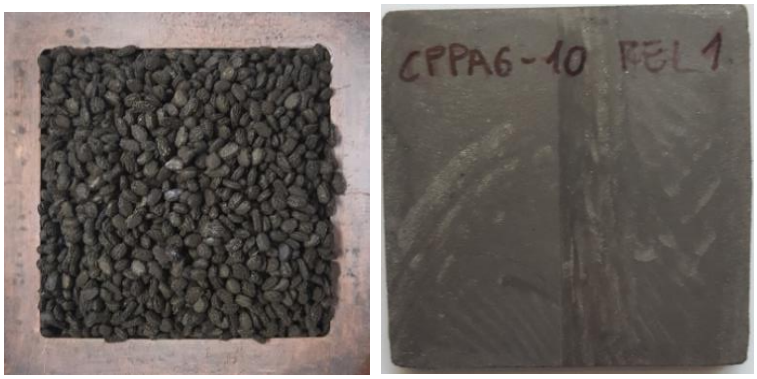

Fig. 35 – Molding of sample: mold with pellet and final plaquette shape of PA6 NdFeB (self-prepared 10%)

Different magnetic shapes have been molded, but above all in plate form, which has been more frequently used (Fig. 35). This typology of sample has been used for several activity: magnetic characterization and machining the pieces for prototype applications.

The effect of the binder content has been studied: some samples have been produced using the above mentioned magnetic powder and the polyamide PA6. The choice of PA6 is due to the lower price compared with other polyamides, especially to the PA12, although the latter has a better degree of mouldability. Various polymer percentages in weight have been tested: 10, 20, 30 and 40%. The best results have been obtained with the lowest percentage of binder, as shown in Fig. 36. The binder content variation also influences, in this case, the remanence value, while the intrinsic coercivity remains almost constant. It is important to note that further reduction of the binder content is very complex, because in the extrusion process the polymer quantity has a lower limit that cannot be exceeded. Furthermore, a high binder content simplifies the production of complex shapes, but the magnetic properties are reduced. The maximum magnetic energy is respectively, 32.9 kJ/m^3 for 10 wt% of PA6, 7.57 kJ/m^3 for 20 wt% of PA6, 3.35 kJ/m^3 for 30 wt% of PA6, and, 1.67 kJ/m^3 for 40 wt% of PA6. The magnetic energy is reduced a lot with the increase of the polymer content.

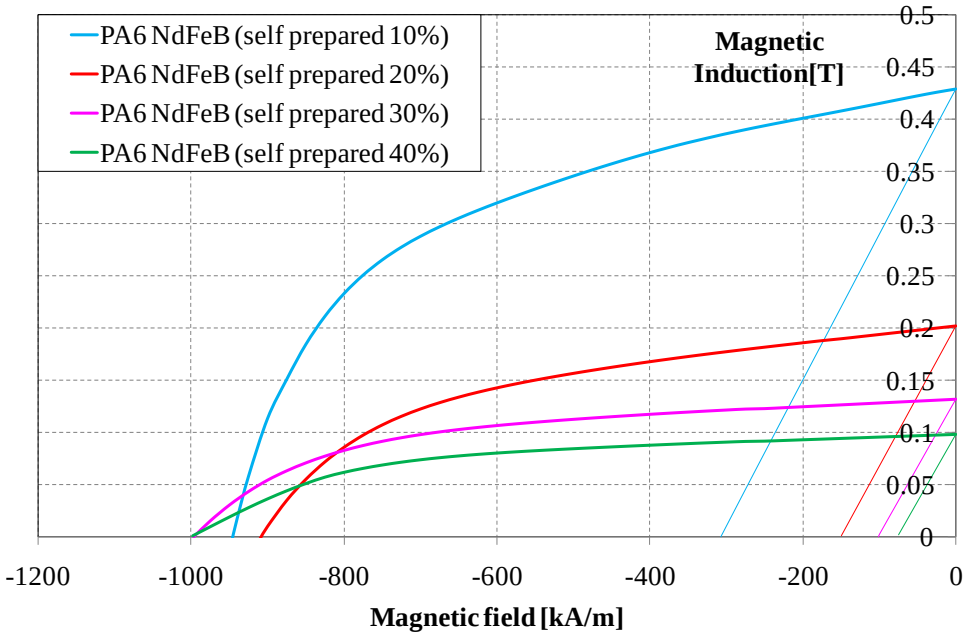

Fig. 36 - Demagnetization curves of polyamide bonded magnets for different polymer content and prepared by injection molding

IV.II Rare-Earth Magnet Recycling

The economic aspect is a primary parameter for the magnet, mainly considering the instability of the raw material price [58], [59]. Rare Earth materials, as Neodymium, are concentrated in a few areas of the planet, and their extraction process is expensive. Therefore the price depends on situations on the markets and geopolitics. For example, the cost of NdFeB powder in 2009 was 30 $/kg; but in 2011 it reached about 300 $/kg, for to end up settling on about 60 $/kg, as is reported in Fig. 37 The same happened to Dysprosium: a material used in minimal quantity in the NdFeB sintered magnets (about 6% in electric generators) and when its price was considerably higher (about 1500 $/kg).

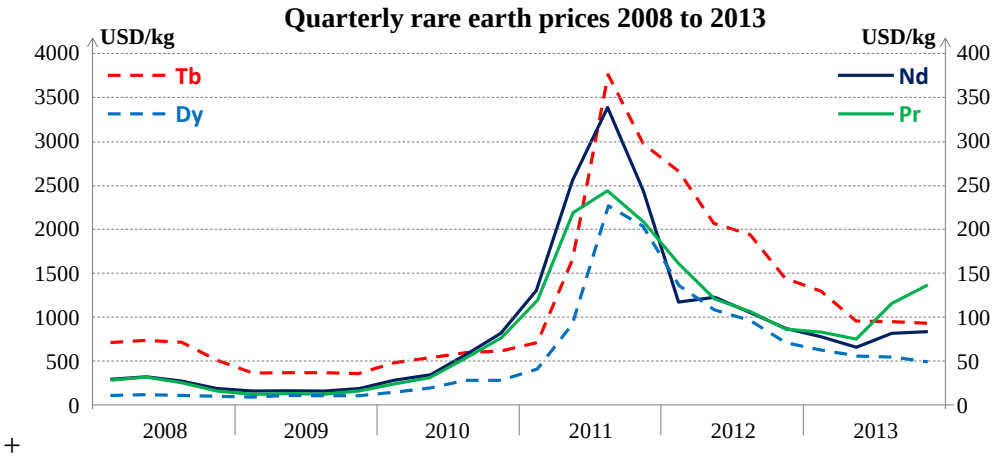

Fig. 37 – Cost rare-earth materials used in NdFeB magnets [60]

An interesting solution could be the recycling of NdFeB magnets. Different techniques are available, but they are in general expensive or very dangerous [61]. Many methods to recover the NdFeB powder from different devices [62] have already been proposed; usually, Hydrogen decrepitation (HD) or hydrometallurgical methods are adopted, and alternatively chemical processes and metallurgy [61],[63-68]. In this work a new method to recycle the NdFeB sintered magnets using a mechanical process has been proposed, without the use of Hydrogen, resulting in a safer, less complicated and cheaper process than chemical methods [69]. To give a better idea about the proposed recycling process, the procedure has been reported in Fig. 38.

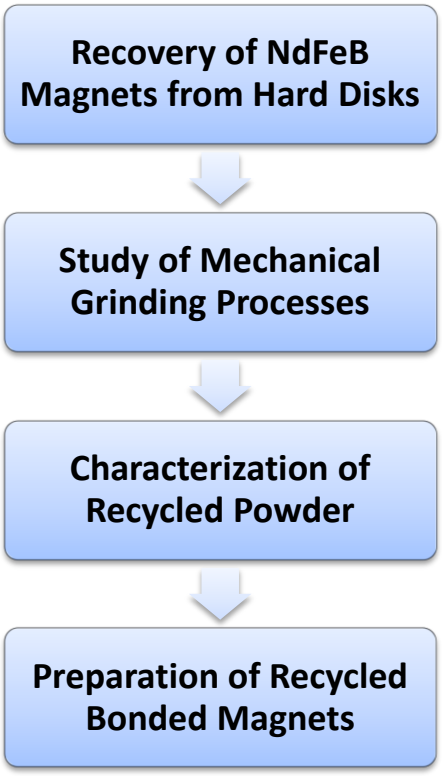

Fig. 38 - The procedure of the proposed recycling process

Several hard disk drivers have been collected, and magnets with different shapes and dimensions have been recovered (Fig. 39). Afterwards, the magnets underwent demagnetization through thermal treatment at 350°C for 1 hour (Fig. 40).

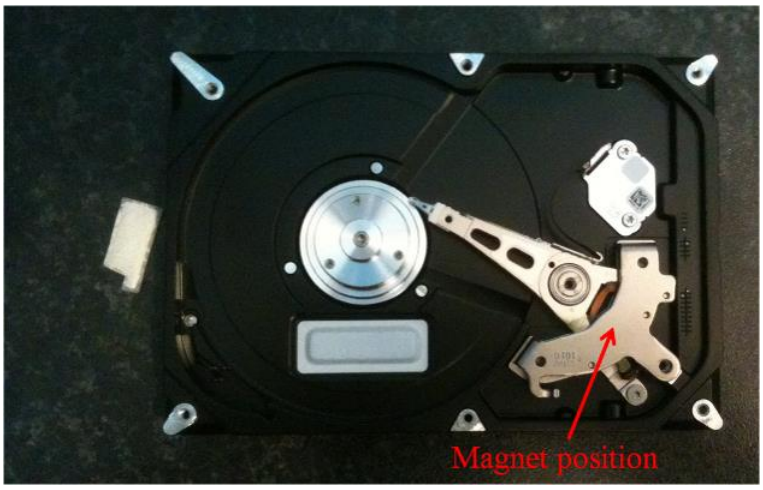

Fig. 39 – Recovery of NdfeB magnets from hard disk drive: the magnet position

Fig. 40 – Various recovered magnets after the demagnetization process

Different mechanical processes have been performed to grind the magnets The method with the impact mill is preferred with respect to others because it is faster to produce the recycled powder (Fig. 41). Two typologies of recycled bonded magnets have been proposed using different washing during the grinding process: in Nitrogen and in Argon. The obtained results show a deep deterioration with respect to the typical bonded magnets prepared with the same binder percentage and pressure level, as reported in Fig. 42. The magnetic material used to prepare the typical bonded magnets is the same commercial powder, MQP 14-12, and the polymer is phenolic resin. Therefore, it is supposed that such results are related to the high concentration of Oxygen in the recycled powder.

Fig. 41 - Mechanical grinding processes used to recycle NdFeB sintered magnets: impact mill

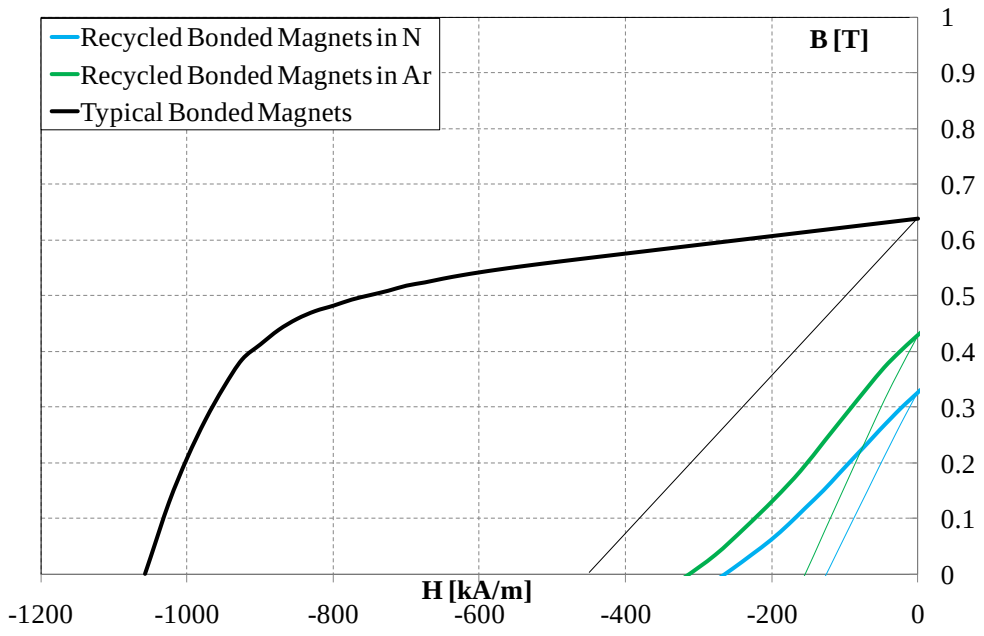

Fig. 42 - Demagnetization curves of recycled bonded magnets compared to typical ones for the same binder percentage (1.8%) and pressure (600 MPa)

The recycled magnets still do not reflect the preferable recycling areas, which are reported in Fig. 43. Imagine to reach the area corresponding to the original magnets is very difficult and it is not necessary. On the other hand, the acceptable recycling area proves to be very satisfactory and useful, and further efforts and studies will be conducted to achieve such zone.

In general, the magnet life is around 10-20 years and depends on the application lifetime where it is used. Any subsequent recycling should be possible.

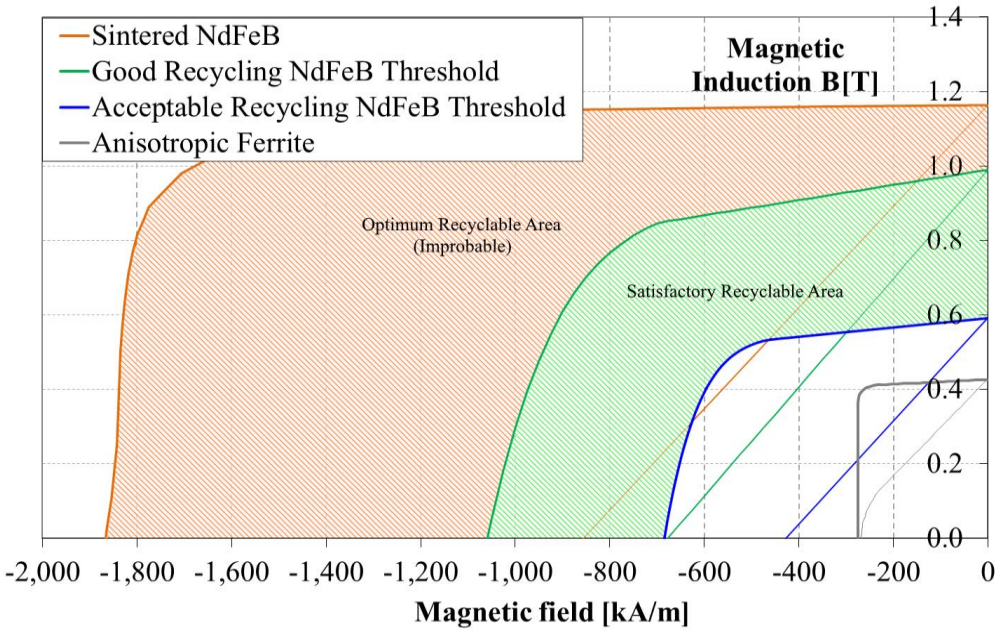

Fig. 43 - Preferable recycling areas of NdFeB magnets

V. BONDED MAGNETS APPLICATION: ASSISTED RELUCTANCE MACHINE

The first case of study of an application with promising use of bonded magnets is the assisted reluctance machine. In general, sintered regular magnets are adopted, mostly ferrite [13],[70] and some case also NdFeB sintered magnets [71], but filling only a part of the volume of the flux barriers [72-74]. Therefore, the flux barriers have very irregular shapes, which the traditional ferrite and sintered NdFeB magnets cannot completely fill [71]. For that reason, the use of bonded magnets can be the solution, which is able to properly fill the flux barriers [75-77]. In this context, different reluctance machine prototypes have been prepared, with and without permanent magnets. The rotor geometry has been studied and designed using a multi-objected differential evolution (DE) algorithm and the finite element analysis (FEA) [78-83].

Before starting with the description of the preparation of the prototypes some hints on the main concepts and behaviors of synchronous reluctance motor (SRM) [84-88] and assisted reluctance machine (PMaSRM) are reported hereafter. Previously some information on the machine typology has been provided (paragraph III.III), but not in detail, without considering the mode of operation.

V.I Concepts and State of the Art of Assisted Reluctance Machine

The SRM is a synchronous motor as the brushless but without magnets on the rotor. It consists of a stator, which is the same as that present in any brushless machine with sinusoidal distribution, and a rotor suitably shaped to have high anisotropy. The anisotropic torque obtained from this machine type has the dependence of inductance L from the distance between stator and rotor references. In particular, this motor has anisotropy only on the rotor which does not contain magnets and can be represented as a single piece of Iron suitably shaped with high anisotropy.

For the development of the motor, assuming magnetic linearity, the expression of the torque is provided:

$$T = \frac{3}{2}p\left(\lambda_d i_q - \lambda_q i_d\right) = \frac{3}{2}p\left(L_d - L_q\right)i_d i_q \quad (1)$$

Therefore, with the same supplied conditions, it can be stated that:

$$T \propto \left(L_d - L_q\right) \qquad (2)$$

Where:

- λ are flux linkages;
- L are inductances;
- p are pole pairs.

This means that to have high torque the difference between the inductances must be maximized [89]. In fact, a high ratio (L_d/L_q) guarantees a high angle between current and flux, but this is not sufficient to have a torque increase, accordingly also the following condition is required:

$$T \uparrow\leftrightarrow (L_d - L_q) \uparrow\leftrightarrow \begin{cases} L_d & high \\ L_q & low \end{cases} \qquad (3)$$

In order to realize a high anisotropy structure (high L_d, low L_q) the rotor is divided into several magnetically isolated segments among them. It is noted that to make a single electrical sheet the various segments must be joined by saturated Iron pieces (flux barrier ends). Therefore, the higher the number of rotor segments (rotor islands), the more the rotor geometry will represent the reluctance machine. Since the flux barriers ends resist to the flexion and less well in traction, ribs are inserted in the radial direction, as reported in Fig. 44. However, the presence of the internal Iron ribs, allows a part of the leakage flux to cross the rotor. This flux corresponds to a reduction in torque and a worsening of the power factor (PF).

Furthermore, the salience ratio (L_d/L_q) is a fundamental parameter for the correct design of a SRM machine. Such ratio, together with the torque value, also affects the power factor and size of the operation region in flux weakening conditions, that is the maximum speed that the machine can reach in constant power operation (Fig. 45).

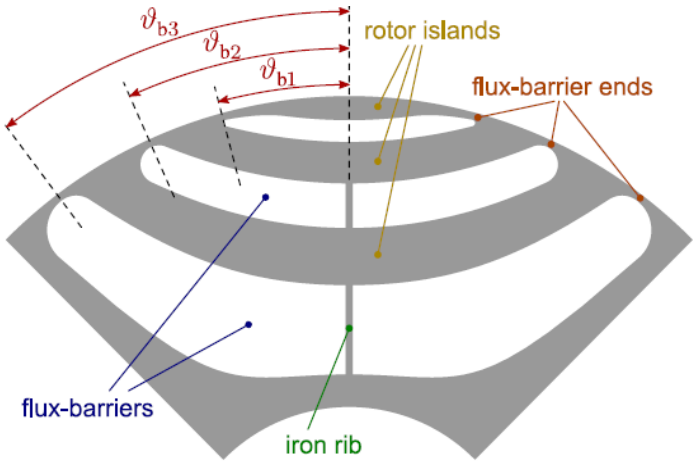

Fig. 44 – Scheme of rotor geometry of a synchronous reluctance machine [89]

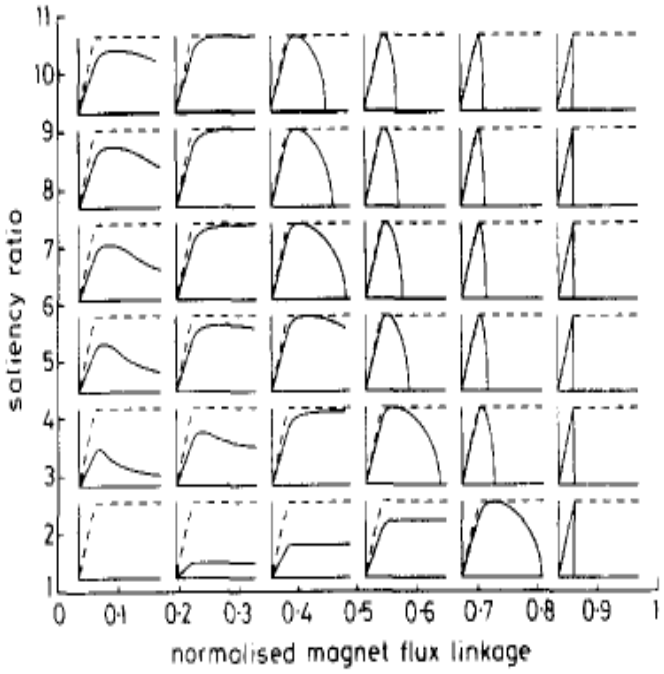

Fig. 45 – Power-speed characteristic in flux weakening conditions as the function of saliency ratio[90], [91]

The reluctance machine can operate in three different zones (Fig. 46):

- zone 1: current limited region, the torque is constant and operate on the maximum torque per ampere (MTPA) locus;
- zone 2: current and voltage limited zone, the torque start decrease (flux weakening condition) but power is constant.
- zone 3: voltage limited region, that is the maximum torque per a limited voltage (MTPV). Torque and power decrease.

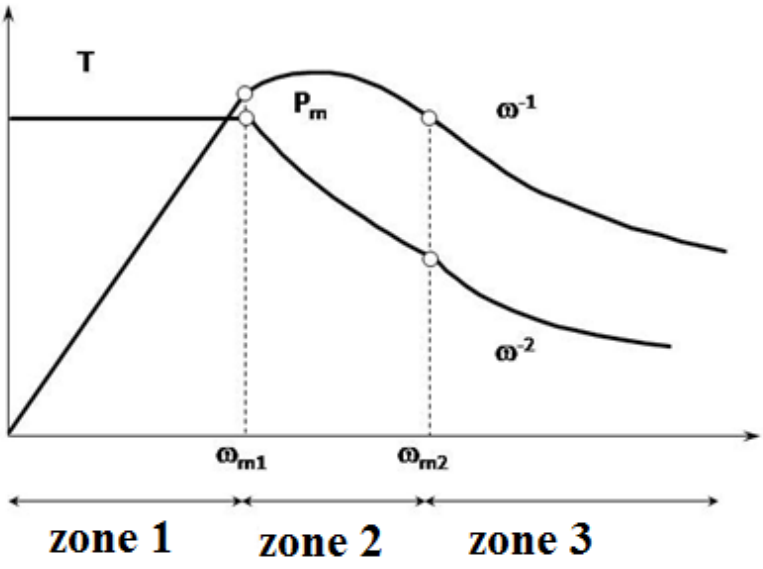

Fig. 46 – Operating regions of a SRM

For spindle-type drives, where a wide speed range is required, the synchronous reluctance machine involves an over-dimensioning of the inverter. In order to solve this problem, the assisted reluctance machine has been adopted, which has the same geometry as the SRM but with the addition of magnets inside the flux barriers. The vector diagram with the magnets flux λ_m is shown in Fig. 47. In general, the salience ratio for SRM is about 4, this means very low power factor and short flux weakening region. On the other hand, the use of permanent magnets in flux barriers improves/stretches the range of flux weakening. That means that the torque value in PMaSRM decreases slowly with respect to the SRM. Obviously the power factor increase with the use of permanent magnets in the flux barriers (Fig. 48).

The disadvantages of PMaSRM are the cost of permanent magnets, especially if NdFeB sintered magnets are adopted, and the control by inverters. The inverter involves more time to invert the torque because it is not able to change the sign of i_q, as it could be done with the SRM, as to avoid worsening the effect of the magnets must always be opposite to λ_m. Alternatively, the i_d is reversed, but the times are longer [92].

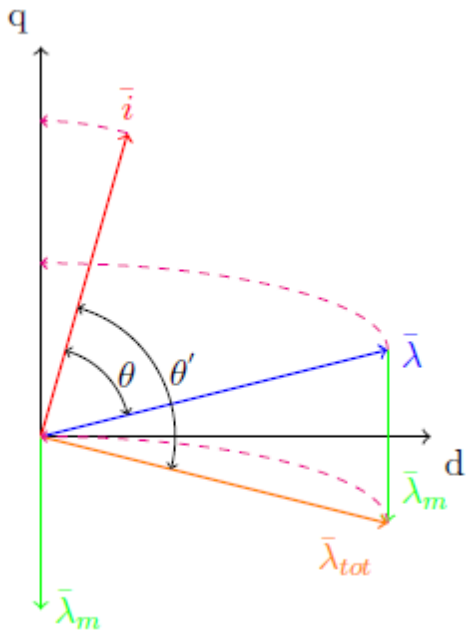

Fig. 47 – Effect of magnets on the trajectories of current and flux in axes d and q

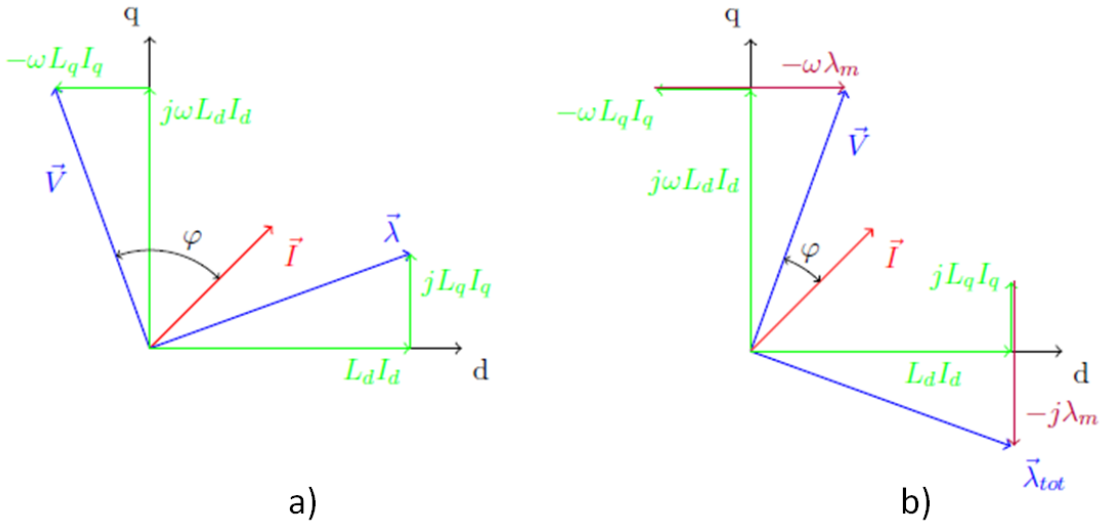

Fig. 48 – Vector diagram of SRM a) and PMaSRM b)machines: the power factor improvements in the case of the use of permanent magnets

A typical drawback of reluctance machines and PMaSRM is the strong torque oscillation, produced above all by the rotor anisotropy that interacts with the harmonics of the magnetomotive force of the stator. The technique is used to reduce torque ripple is the skewing, but unfortunately, in motors with the permanent magnets in the rotor it is possible to implement only a stepping or step-skewing, that is a "discrete" inclination of the rotor, which reduces the torque oscillation by about 10%. But it is possible to further reduce the torque ripple by using flux barriers with particular shapes. In practice, the laminations alternate with two different profiles of flux barriers to compensate the torque harmonics. Or use only one type of electrical sheet that already contains two different types of flux barriers [93].

Another particular subdivision concerns rotors lamination typology, that can be conventional or axial. Axial lamination, also called "ALA" (Axially-Laminated Anisotropic), consists of the use of differently shaped laminations, installed axially to the rotor shaft, as shown in Fig. 49. This structure presents a considerable anisotropy if it is well dimensioned since it is possible to realize a high number of flux barriers, but it is not very used due to the impossibility of skewing and above all by the fact that, given its constructive complexity, it is impractical for mass production. The high iron losses characterize this type of lamination.

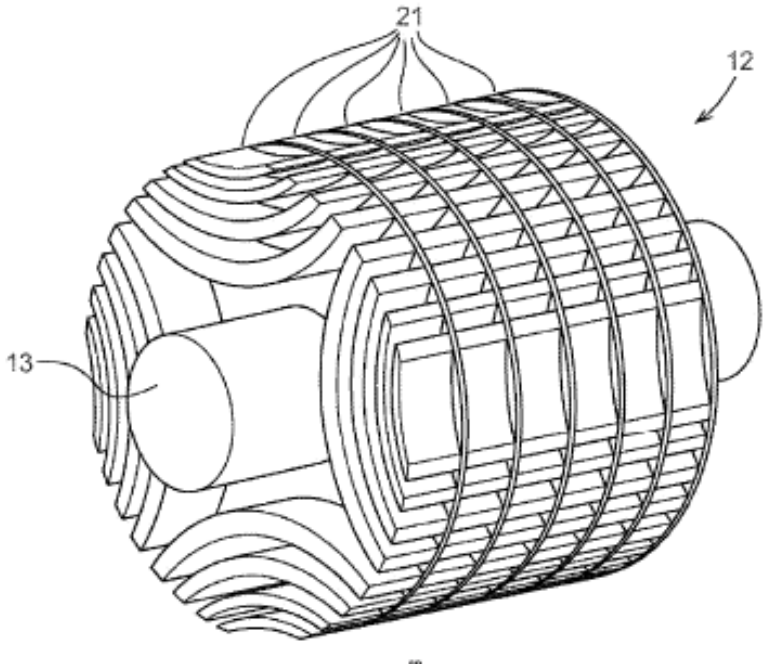

Fig. 49 – Axial lamination structure of reluctance machines

V.II Selection of Motor Design

The rotor geometry has been optimized by means of a multi-objected differential evolution (DE) algorithm. The optimization has been carried out without PMs (REL rotor) setting the maximum average torque and the minimum torque ripple as objectives. The flux barriers angles and thicknesses and the iron channel widths have been set as geometrical parameters [79],[94],[95]. The number of flux barriers per pole has been kept fixed to two to limit the minimum flux barrier area and to easy the filling process.

The proposed rotor geometry, after careful analysis by an optimization algorithm, is reported in Fig. 50. The next investigation considers the use of the magnets, therefore different magnets have been examined by simulation tools to find the optimal solution or cases to prepare the prototypes. The rotor design with bonded magnets concept is shown in Fig. 51 and this geometry will be adopted for finite element analysis (FEA).

Fig. 50 – Rotor geometry after optimization algorithm

General data

$p = 2$	pole pairs
$Lstk = 40\ mm$	stack length
$kpack = 0.96$	packaging factor
$I_{rated} = 3\ A$	rated current
$I_{rated} = 5.5\ Nm$	rated torque

Windings data

$nc = 100$	number of series conductors per slot
$npp = 1$	number of parallel paths
$kfill = 0.45$	slot fill factor

Stator data

$Qs = 36$	number of slots (total in the stator)
$De = 150\ mm$	outer diameter
$Ds = 96\ mm$	inner diameter
$wt = 4.45\ mm$	width of the stator tooth

$wso = 2.5\,mm$	slot opening
$hs = 13.85\,mm$	slot height
$hso = 0.7\,mm$	slot opening height
$hwed = 1\,mm$	wedge height
$ws = 4.3\,mm$	slot width (outwards)
$wse = 6.5\,mm$	slot width (inwards)
$angleSlot1 = 5$	(deg) angle of the first slot ("Islot1")

Rotor data

$rotor\ alignment = 0$	rotor initial position
$Dre = 95.2\,mm$	outer diameter
$Dri = 40\,mm$	inner diameter
$tm = 0\,mm$	magnet thickness
$hri = 6.92\,mm$	inner rib height
$dbi = 0.6\,mm$	distance PM - airgap
$hre = 4\,mm$	outer rib height
$dbe = 0.5\,mm$	distance PM - out

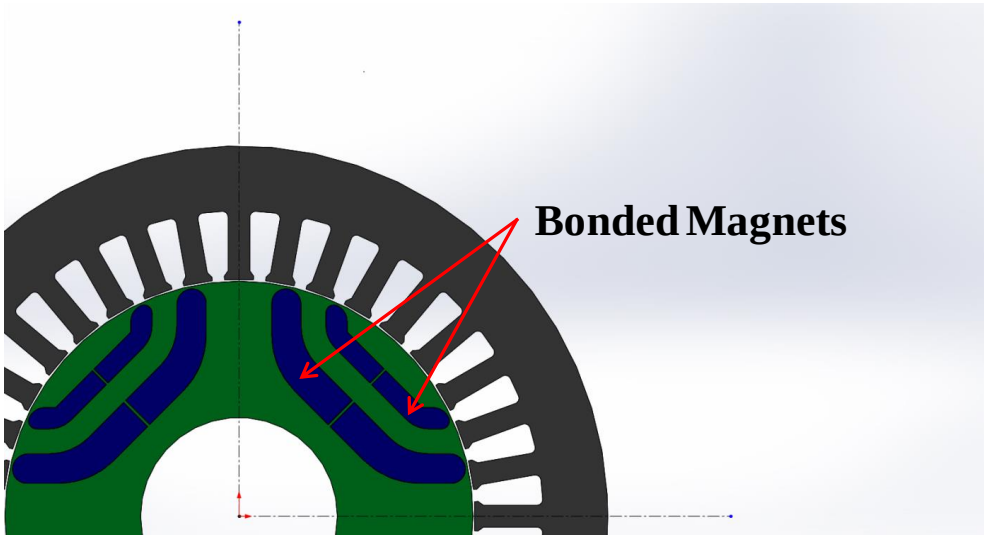

Fig. 51 - The proposed prototype geometry and filling of the flux barriers with the bonded magnets

V.III Finite Element Analysis

The finite element analysis has been adopted to estimate the behaviour of the proposed prototypes before their preparation, in order to choose the most appropriate bonded magnets. Therefore different quantities have been considered for the comparison: maximum torque per ampere, torque ripple, fluxes, torque maps etc. Besides these results, the simulation has been used to evaluate the skewing effect. The skewed model is shown in Fig. 52 and has been made with 8 steps of slot pitch (10°), as described in Fig. 53 and Fig. 54. For this purpose, it is necessary to divide the rotor into packs of electrical sheets with a thickness of 5 mm for a total of 8 groups for a motor stack length of 40 mm. Each group of laminations must be rotated with respect to the previous one by an angle of:

$$\tau_{c,skew} = \frac{10^{\circ}}{8} = 1.250^{\circ} \qquad (4)$$

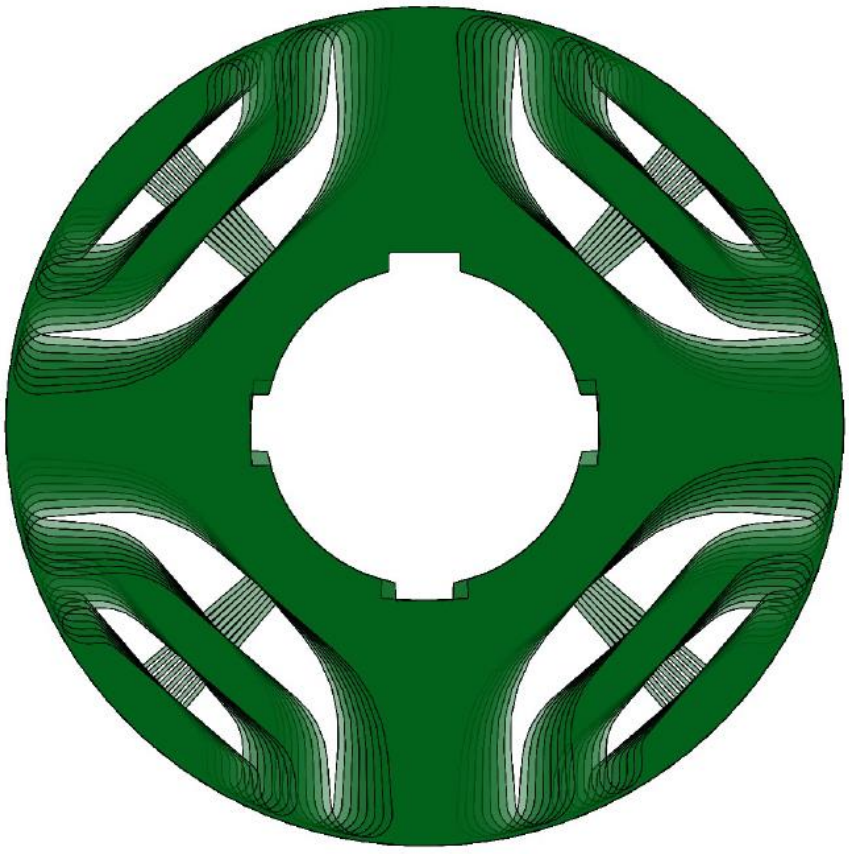

Fig. 52 – The skewing model with 8 steps for slot pitch

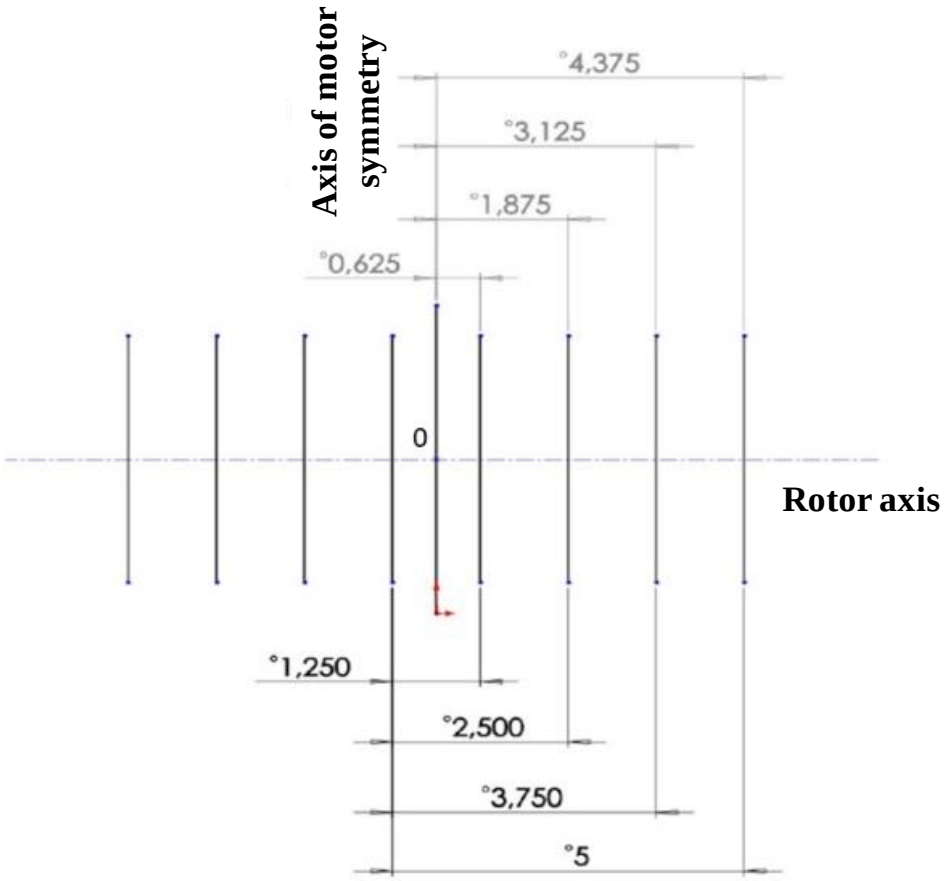

Fig. 53 - Key skewing sequence

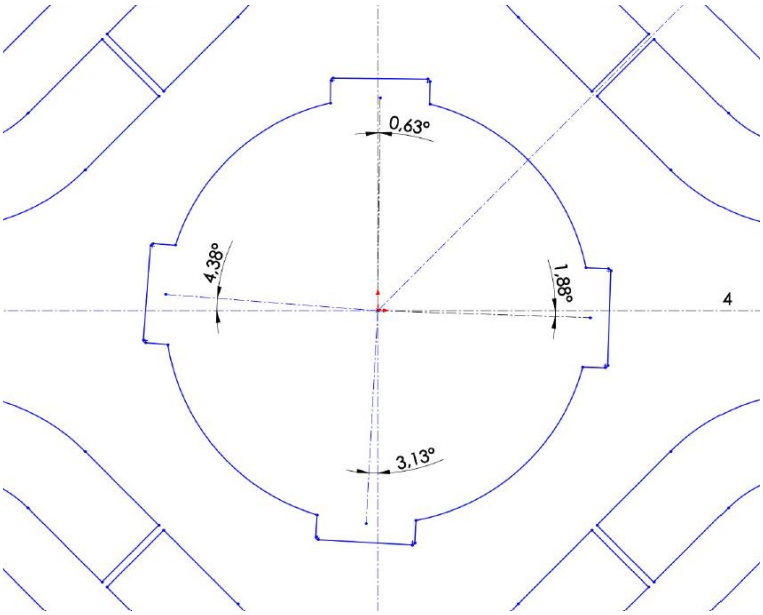

Fig. 54 – Key housing for skewing

The simulation results for the SRM motor have been illustrated in Fig. 55 for rated current. The skewing effect reduces the torque ripple of 73%. On the other hand, the average torque value goes down slightly from 5.5 Nm to about 5.25 Nm. Therefore,

hereafter the prototypes will be prepared only with skewing rotors, with or without magnets.

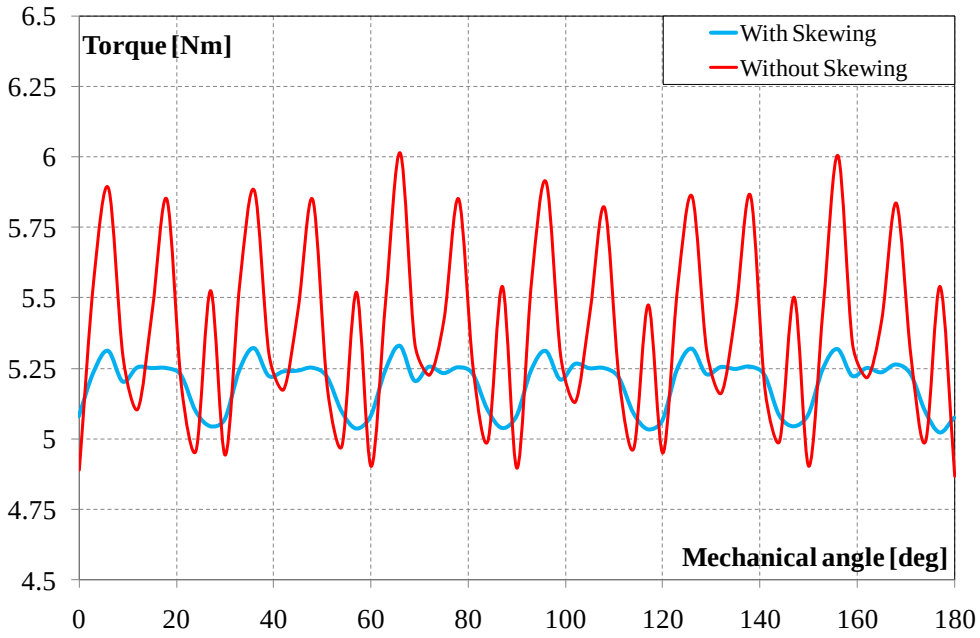

Fig. 55 – The simulation comparison for torque ripple between the use of skewing or no use of skewing

V.III.I Magnets Evaluation

Various permanent magnets have been considered in this phase of the study. The investigation has been primarily focused on the bonded magnets, available on the market in pellet form and mainly self-prepared in the laboratory. Also, the particular flexible magnets, promising under the point of view of the insertion, have been tested for the application in an assisted reluctance machine. All these magnets allow a total filling of the flux barriers, which have a complex shape geometry.

Furthermore, the sintered regular magnets, usually adopted in assisted reluctance machine and considered as the traditional concept, have been analyzed for a wider comparison. In this case, the adopted motor design is shown in Fig. 56, where the volume of regular magnets has been maximized. In the following, the magnetic characteristic of each magnet has been listed.

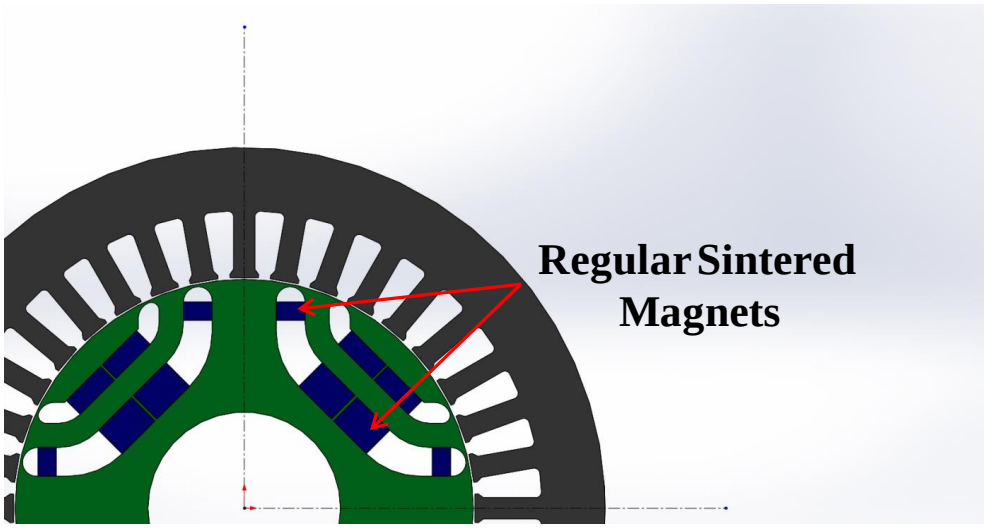

Fig. 56 - The proposed prototype geometry with the filling of the flux barriers with the sintered magnets

- *Injection molding magnets self-prepared* in the lab using the magnetic powder MQP 14-12 and PA6 as the polymeric binder. The demagnetization curves with the different percentage in the weight of binder content are shown in Fig. 57.

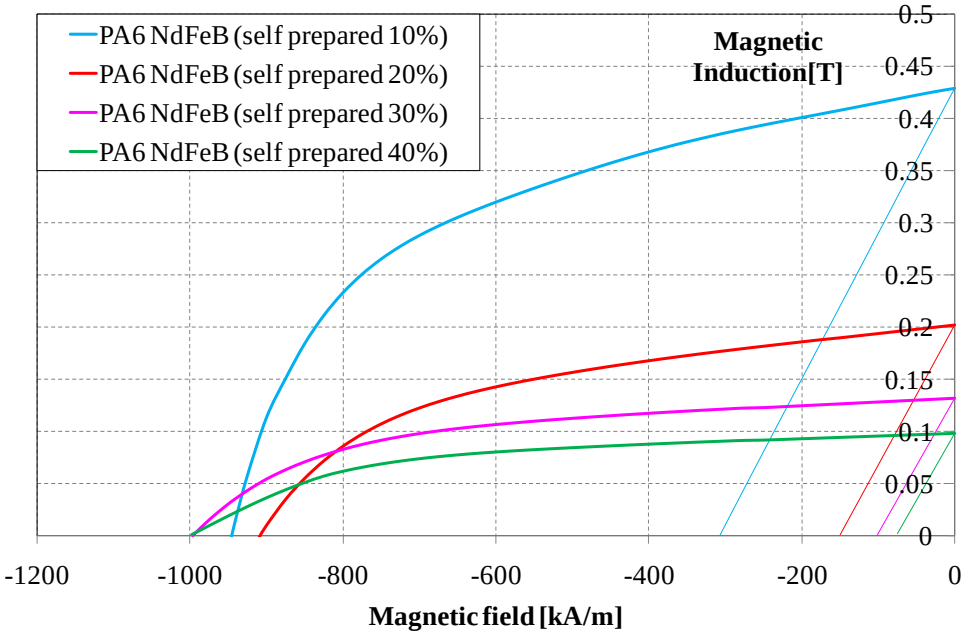

Fig. 57 – Demagnetization curves of injection molding self-prepared NdFeB bonded magnets for different polymer content

- *Compression molding magnets self-prepared* in the lab using the magnetic powder MQP 14-12 and phenolic resin. The demagnetization curves with the different percentage in weight of resin are shown in Fig. 58. The differences in the intrinsic coercivity are not typical to expect, and unfortunately, are due to different lots of magnetic powders (this should not happen); the resin aging affects more mechanical performance and corrosion resistance and very slightly

on the magnetic properties. The magnets with the resin content less than 5 wt% have the similar maximum magnetic energy BH_{max} in that order: 63.7 kJ/m^3 for 3.3 wt% of phenolic resin, 62.1 kJ/m^3 for 4 wt% of phenolic resin, and 54.9 kJ/m^3 for 5 wt% of phenolic resin. So basically, it is necessary to take into account the intrinsic coercivity value.

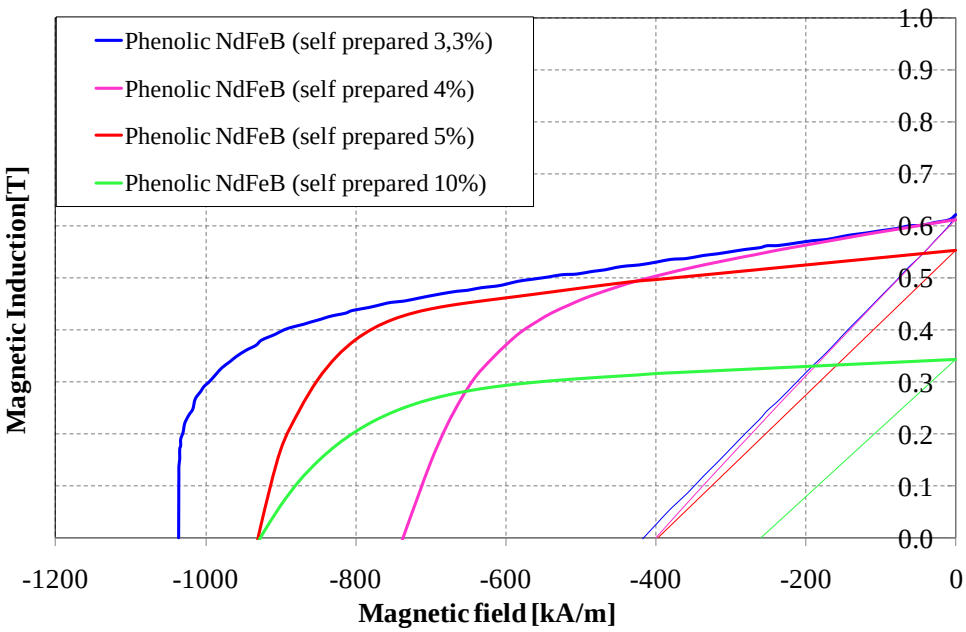

Fig. 58 - Demagnetization curves of compression molding self-prepared NdFeB bonded magnets for different resin content

- The particular *flexible magnets Plastoren 8* are proposed for current research activity (Fig. 59). It is a commercial product and is supposed to facilitate coupling with flux barriers. In this way, it is possible to magnetize the magnet in a single direction and then flex it to vary the direction of the magnetic field following the shape of the barriers (Fig. 60). The magnetic characteristic is reported in Fig. 61 and the main magnetic data are described in TABLE XI.

Fig. 59 –Flexible magnets: Plastoren 8

Fig. 60 – Magnetized sample of flexible magnet adopted in flux barriers

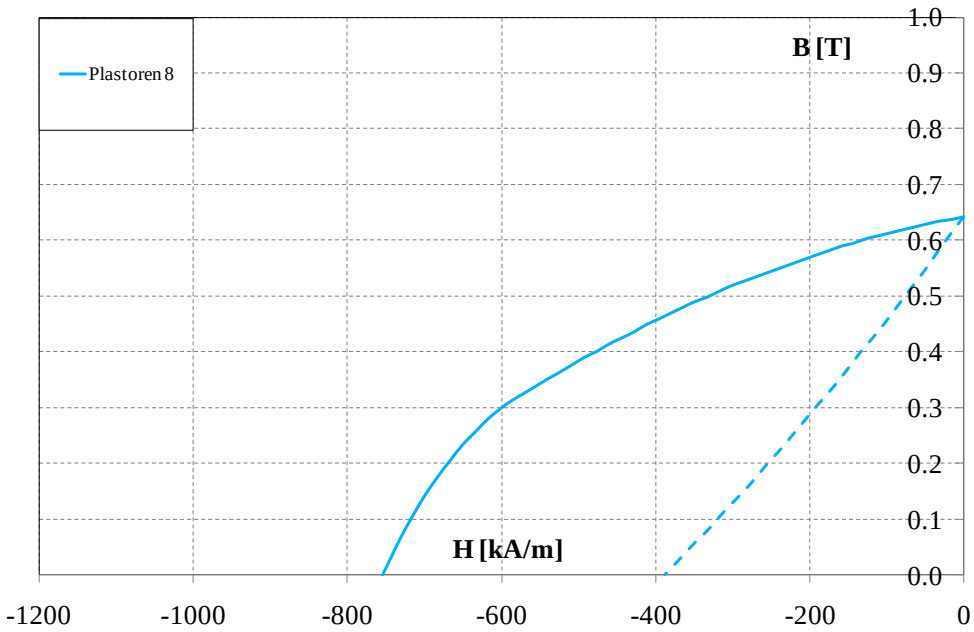

Fig. 61 - Demagnetization curves of flexible NdFeB bonded magnets

TABLE XI – Magnetic properties of flexible NdFeB bonded magnets (Plastoren 8)

Magnet Data		
Remanence Br	0.643	T
Intrinsic Coercivity HcJ	755.2	kA/m
Coercivity HcB	388.4	kA/m
BHmax	57.9	kJ/m^3

- *The NdFeB pellets* are available on the market and used to mold by means to the injection process (Fig. 62). All final pieces are molded in laboratories starting from commercial compound (MQIP-M260) and the results of characterization are shown in Fig. 63, and the magnetic properties are reported in TABLE XII. The polymer content is 10 wt%.

Fig. 62 – Commercial NdFeB pellets used in injection process

TABLE XII - Magnetic properties of NdFeB bonded magnets (MQIP-M260 pellets)

Magnet Data		
Remanence Br	0.409	T
Intrinsic Coercivity H_{cJ}	928	kA/m
Coercivity H_{cB}	286.6	kA/m
BH_{max}	28.9	kJ/m^3

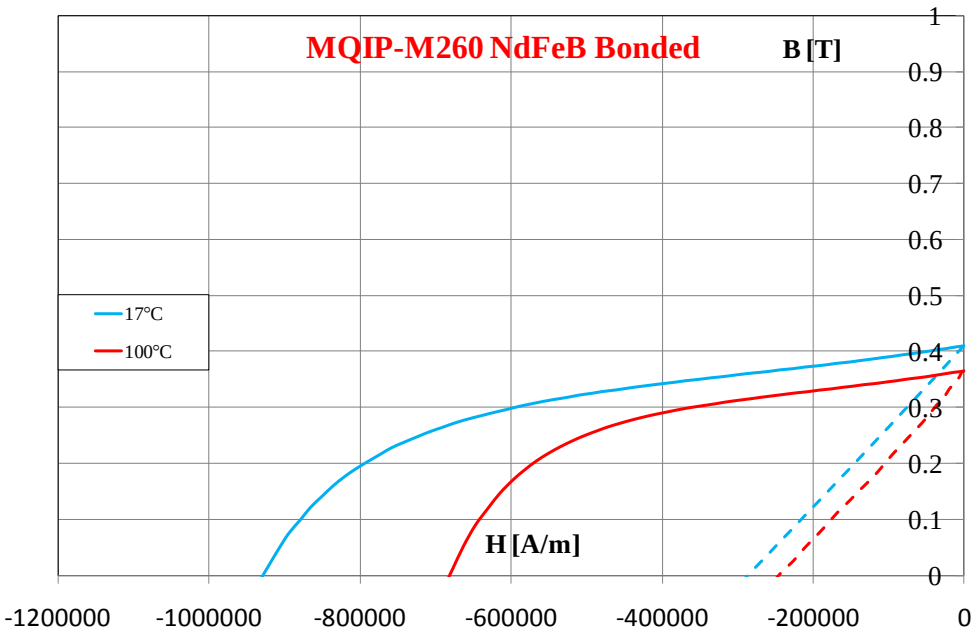

Fig. 63 - Demagnetization curves of NdFeB bonded magnets prepared by injection process using commercial compound

- *The ferrite pellets* reported in Fig. 64, have been adopted as above-mentioned NdFeB pellets, supplied by the market and molded in the laboratory. Such magnets have the lowest magnetic characteristic as shown in Fig. 65, on the other hand, they have a possible economic saving. In this case, the polymer content is about 9 wt%. Furthermore, the magnetic properties are reported in TABLE XIII, it is noted that the maximum magnetic energy is very low.

Fig. 64 - Commercial ferrite pellets used in injection process

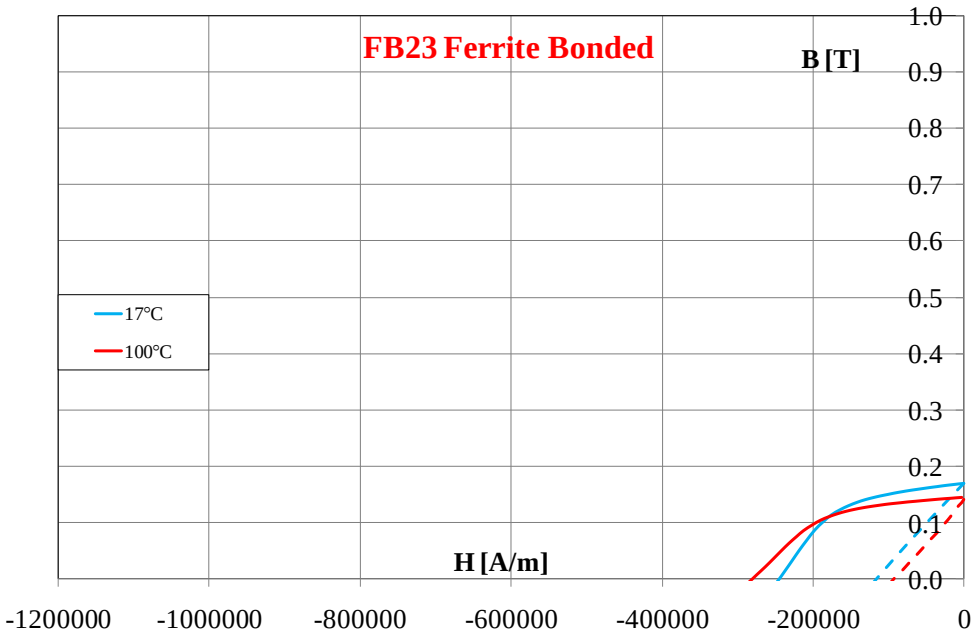

Fig. 65 – Demagnetization curves of ferrite bonded magnets prepared by injection process using commercial compound

TABLE XIII - Magnetic properties of Ferrite bonded magnets (FB23 pellets)

Magnet Data		
Remanence Br	0.170	T
Intrinsic Coercivity HcJ	246	kA/m
Coercivity HcB	116	kA/m
BHmax	5.02	kJ/m^3

- *The anisotropic ferrite* is adopted as regular magnet. This is the traditional concept already used in PMaSRM. This shape allows to reduce the quantity of material (Fig. 66), and therefore the costs. The magnetization process for regular parallelepiped shape is very simple with respect to the newly proposed concept using the bonded magnets. The magnetic characteristic is reported in Fig. 67, and the main magnetic data are shown in TABLE XIV.

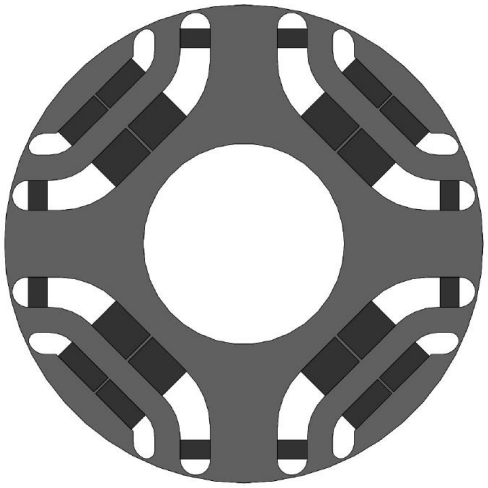

Fig. 66 –The proposed regular shape using traditional concept

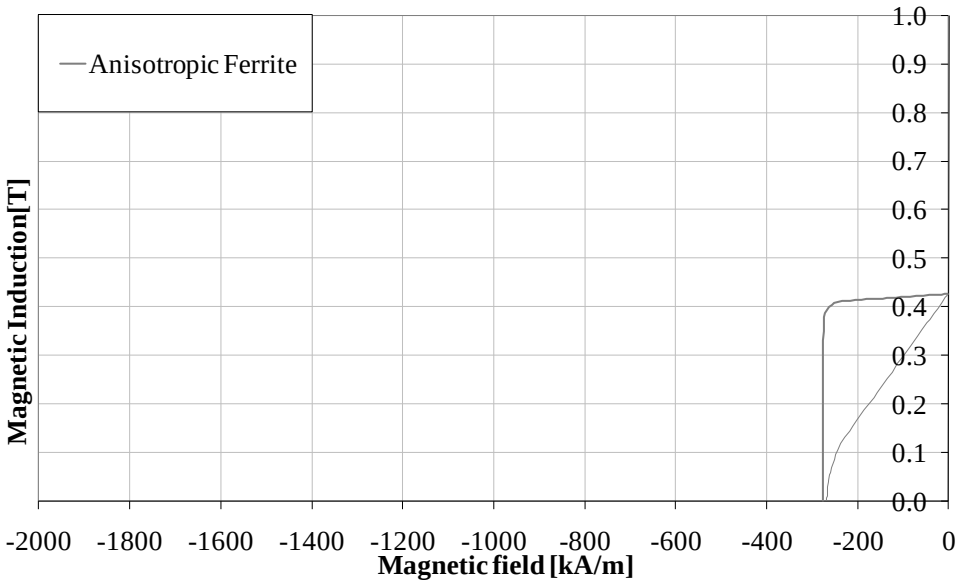

Fig. 67 - Demagnetization curves of anisotropic ferrite: regular commercial magnets

TABLE XIV - Magnetic properties of Anisotropic Ferrite regular magnets

Magnet Data		
Remanence Br	0.426	T
Intrinsic Coercivity HcJ	275	kA/m
Coercivity HcB	268	kA/m
BHmax	35.2	kJ/m^3

- *The NdFeB sintered magnets* are used as the regular magnets, identically to anisotropic ferrite. Such magnets have very high magnetic properties and sometimes are involved in PMaSRM. The demagnetization curves are reported in Fig. 68, and magnetic properties are described in TABLE XV

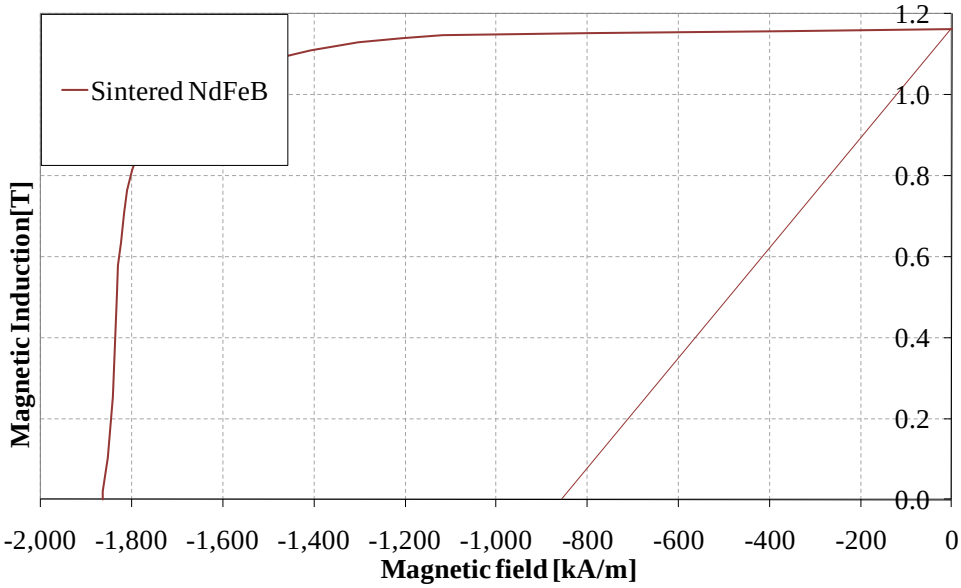

Fig. 68 - Demagnetization curves of NdFeB sintered magnets: regular commercial magnets

TABLE XV - Magnetic properties of NdFeB sintered magnets

Magnet Data		
Remanence Br	1.163	T
Intrinsic Coercivity HcJ	1865	kA/m
Coercivity HcB	856.6	kA/m
BHmax	242.5	kJ/m^3

In order to have a broader view of the performances of the considered magnets, two comparisons have been elaborated. The first concerns the maximum magnetic energy BH_{max} as reported in Fig. 69. It is possible to note the bonded magnets prepared by the compression molding process have better values, about double compared to anisotropic ferrite. The best bonded magnets prepared by the injection molding process have similar value to anisotropic ferrite. The second comparison is about intrinsic coercivity values (Fig. 70): the NdFeB magnets show very high resistance to demagnetization independently of NdFeB bonded magnets typology or process. Moreover, it is also evident that bonded magnets with low BH_{max} have high H_{cj} values, and then can be used in the proposed electrical machine.

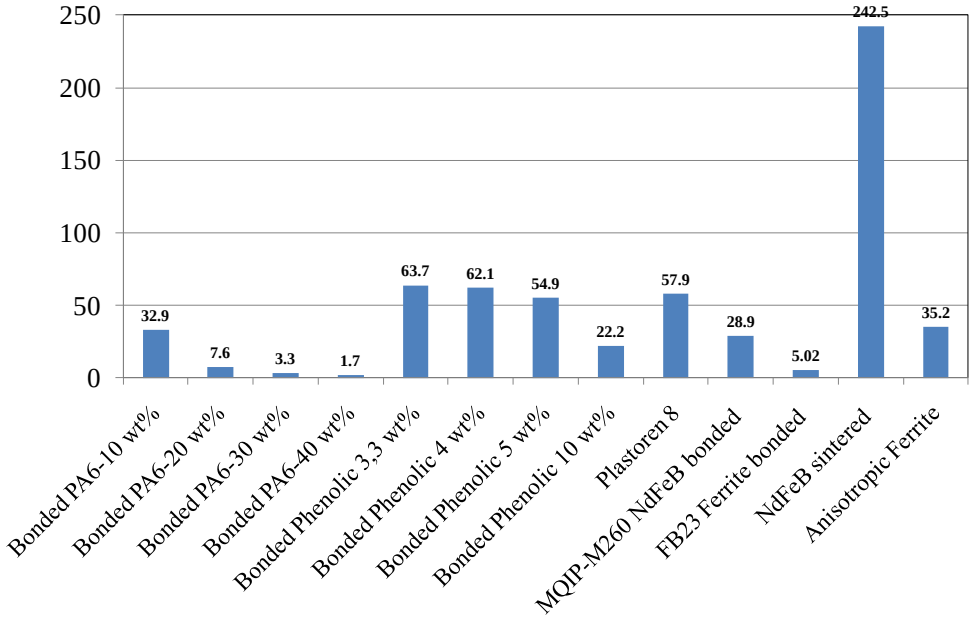

Fig. 69 – Maximum Magnetic Energy (BH_{max}) for considered magnets

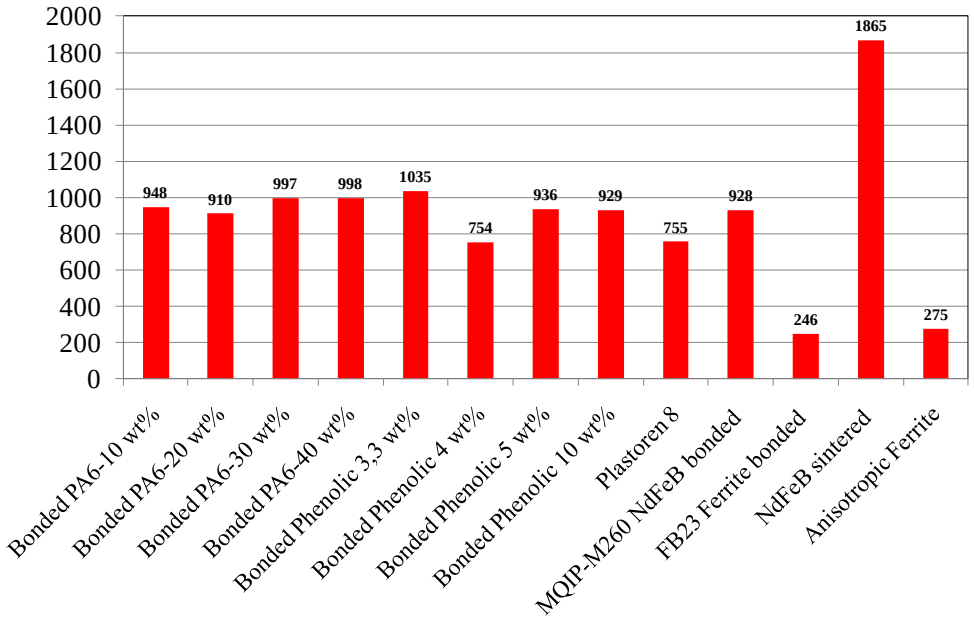

Fig. 70 - Intrinsic Coercivity (H_{cj}) for considered magnets

Simulation results are reported for more significant parameters: torque value and power factor. The torque ripple is not so important to select the suitable magnets. In Fig. 71 are reported the torque values as a function of the current; the maximum selected current is 10 A, limit given by the control system. It is noted that the phenolic NdFeB magnets with lower binder content reach about 50% higher torque value with respect to SRM. Also, interesting results have been noted for PA6 NdFeB magnets with 10% of polymeric binder. The regular magnets, NdFeB sintered and anisotropic ferrite, have lower performance compared with self-prepared compression bonded magnets. All magnets improve torque density. In Fig. 72 the power factor (PF) is shown as function

of the current considering the MTPA locus, the results over 0.85 have been obtained for the compression and some injection bonded magnets (PA6 in 10 wt%). The increases of the PF are remarkable compared to no PM machine.

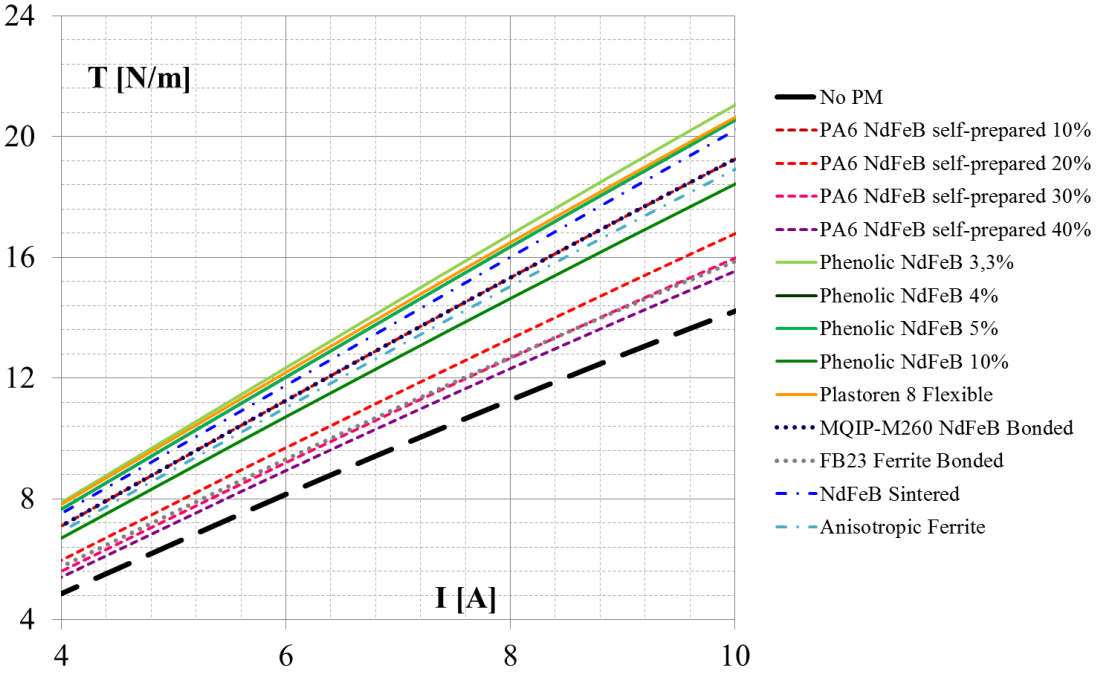

Fig. 71 – Torque simulation estimates as the function of current

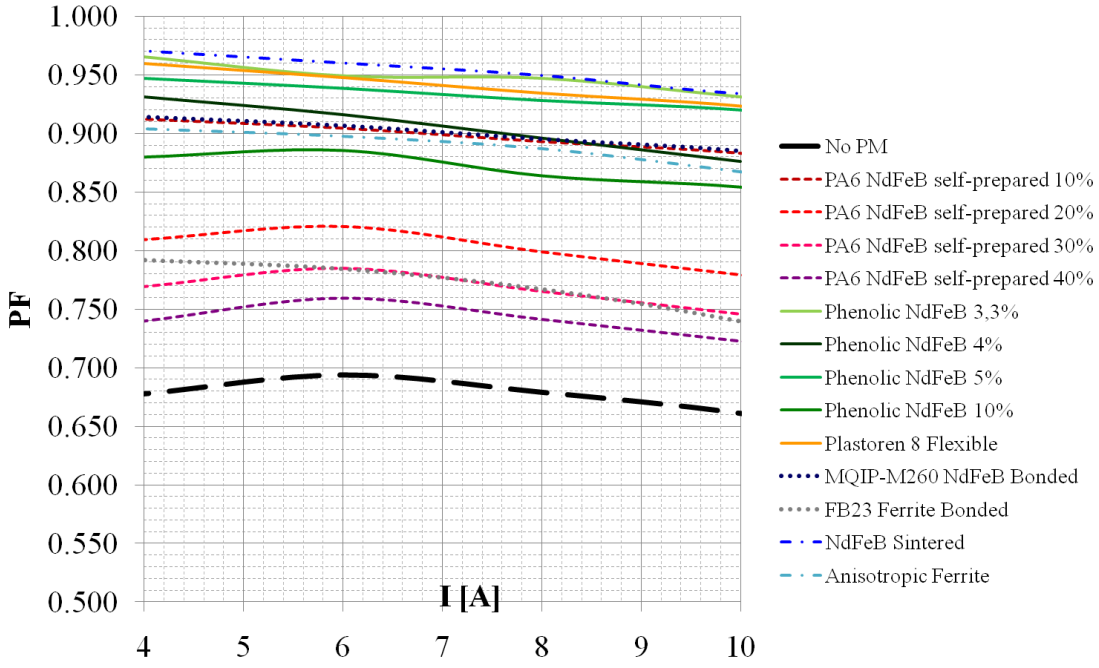

Fig. 72 – Power factor simulation estimates as the function of current

TABLE XVI – Comparison of torque and PF estimations with respect to No PM machine at maximum supplied current

Proposed Magnets			MTPA @ I=10 A		
Source	**Process**	**Name**	**T (Nm)**	**DT %**	**PF**
Lab	*N.A.*	**No PM**	14.22	0%	0.66
Lab	*Injection*	**Bonded PA6-10 wt%**	19.25	35%	0.88
Lab	*Injection*	**Bonded PA6-20 wt%**	16.79	18%	0.78
Lab	*Injection*	**Bonded PA6-30 wt%**	15.98	12%	0.75
Lab	*Injection*	**Bonded PA6-40 wt%**	15.54	9%	0.72
Lab	*Compression*	**Bonded Phenolic 3,3 wt%**	21.05	48%	0.93
Lab	*Compression*	**Bonded Phenolic 4 wt%**	20.54	44%	0.92
Lab	*Compression*	**Bonded Phenolic 5 wt%**	20.88	47%	0.93
Lab	*Compression*	**Bonded Phenolic 10 wt%**	18.43	30%	0.85
Commercial	*Flexible*	**Plastoren 8**	20.64	45%	0.92
Commercial	*Injection*	**MQIP-M260 NdFeB bonded**	19.26	35%	0.89
Commercial	*Injection*	**FB23 Ferrite bonded**	15.87	12%	0.74
Commercial	*Regular*	**NdFeB sintered**	20.21	42%	0.93
Commercial	*Regular*	**Anisotropic Ferrite**	18.92	33%	0.87

In TABLE XVI the estimates of torque and PF for maximum current value, 10 A, are reported. Moreover, the percentage increment for torque value with respect to SRM has been obtained. After careful analysis, the five typologies of bonded magnets have been chosen to produce the prototypes. They are highlighted in TABLE XVI: in green color, four distinct magnets based on different processes, which allow high increment of torque density and in yellow color, cheaper solution ones. The list of the proposed magnets is reported hereafter:

- Laboratory prepared bonded magnets using the compression moulding with phenolic resin (4% in the weight) and NdFeB powder. This solution has the best magnetic properties;
- Laboratory prepared bonded magnets using the injection process of polyamide 6-PA6 (polymer content is 10% in the weight) and NdFeB powder;
- Commercial NdFeB compound for bonded magnets (PA content is 10% wt.) moulded in the laboratory through the injection process;
- Commercial NdFeB flexible magnets, useful for faster and simpler filling of the flux barriers;

- Commercial ferrite compound for bonded magnets (PA content is 9% wt.) moulded in the laboratory through the injection process. This solution has the lower magnetic properties but also can have the lower cost.

V.III.II Flux Density

By means of simulation, it is possible to observe the magnetic flux density distribution. For each proposed case the respective figure has been shown. In Fig. 73 the flux density has been represented; it is possible to note the flux barriers are discharged regions. The most stressed case is with compression self-prepared bonded magnets (Fig. 74). The two magnet types, produced by injection, have similar magnetic behavior (Fig. 75 and Fig. 76). The last case corresponds to magnets prepared by ferrites pellet; for an increase of the current the flux density is practically zero in the flux barriers (Fig. 77).

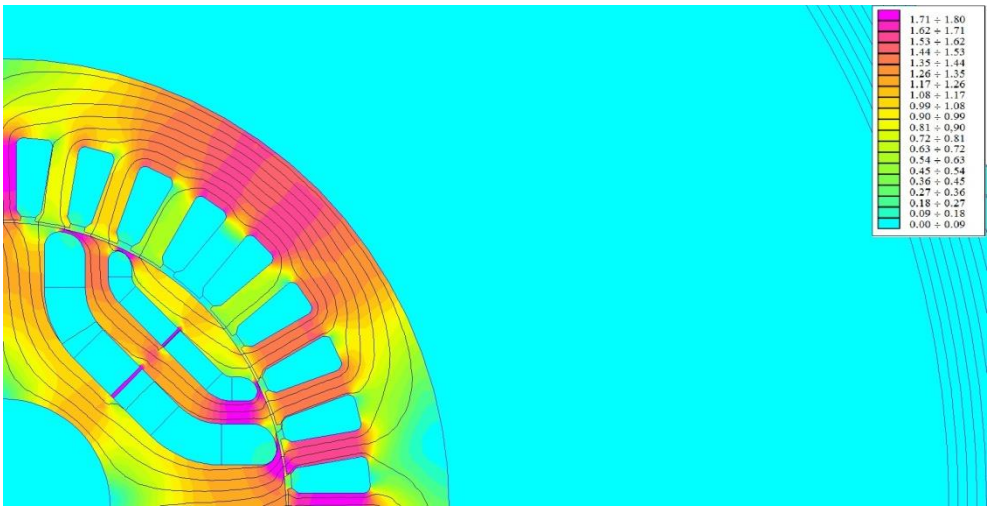

Fig. 73 – NoPM flux density for the rated conditions in MTPA loci

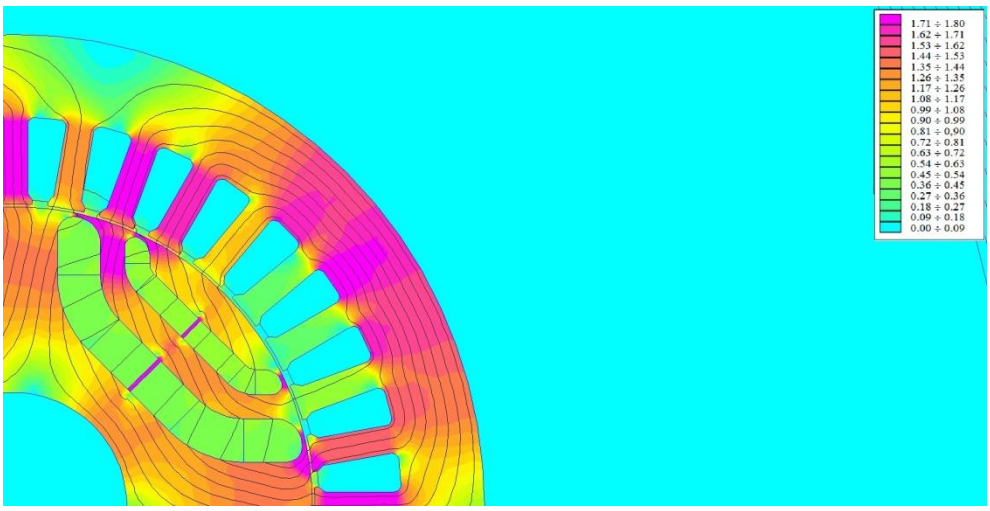

Fig. 74 - Compression self-prepared NdFeB bonded magnets flux density for the rated conditions in MTPA loci

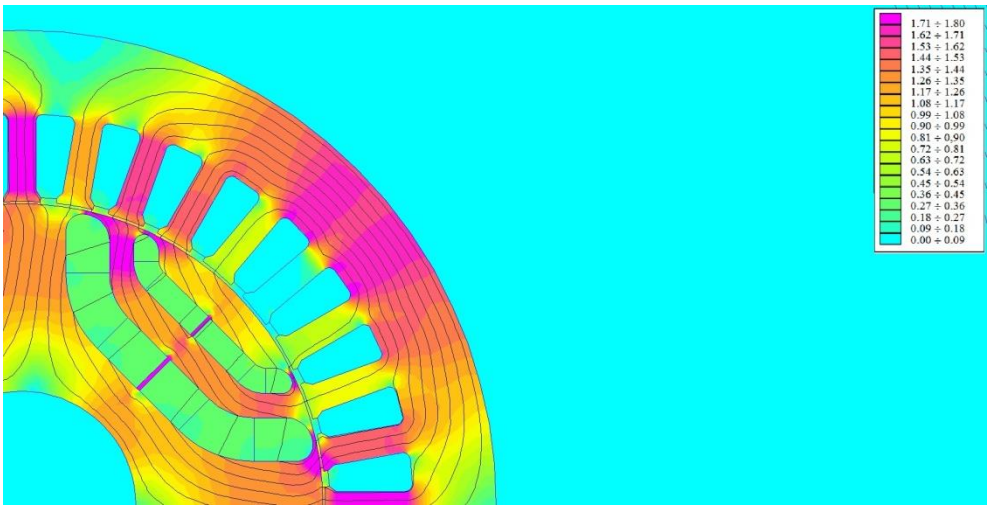

Fig. 75 – Injection self-prepared NdFeB bonded magnets flux density for the rated conditions in MTPA loci

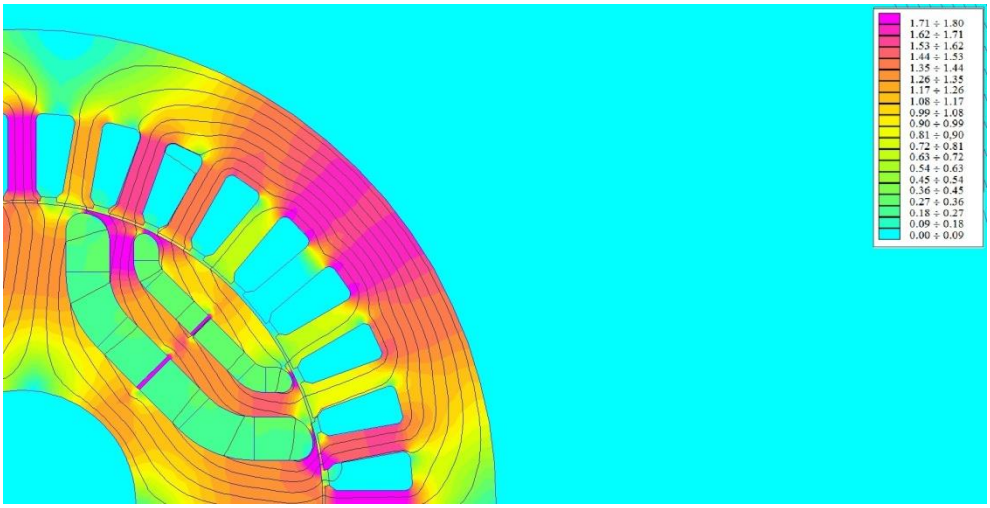

Fig. 76 - Flux density of injection prepared bonded magnets in the laboratory by means of commercial NdFeB pellets in the rated conditions for MTPA loci

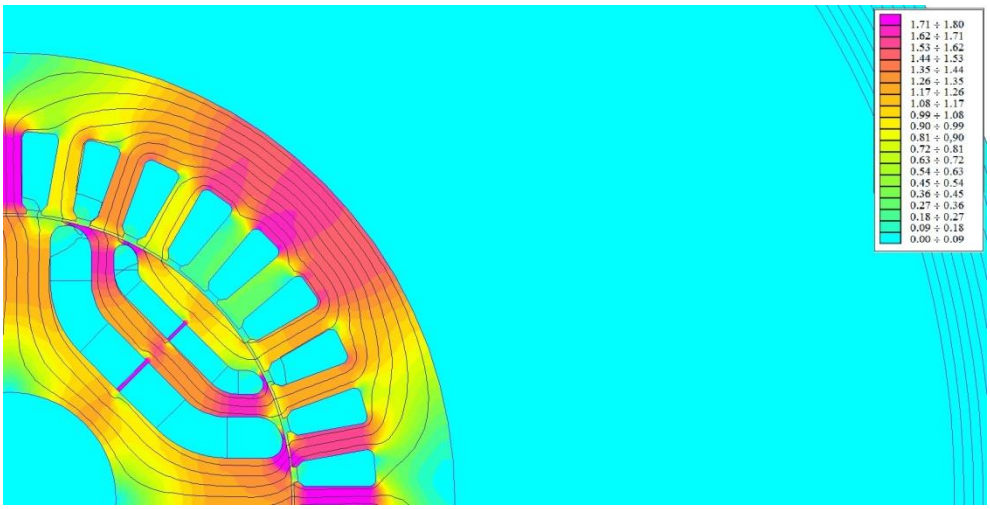

Fig. 77 - Flux density of injection prepared bonded magnets in the laboratory by means of commercial ferrite pellets in the rated conditions for MTPA loci

The magnetic direction of permanent magnets is shown in Fig. 78. The orientation is opposite with respect to IPM machines.

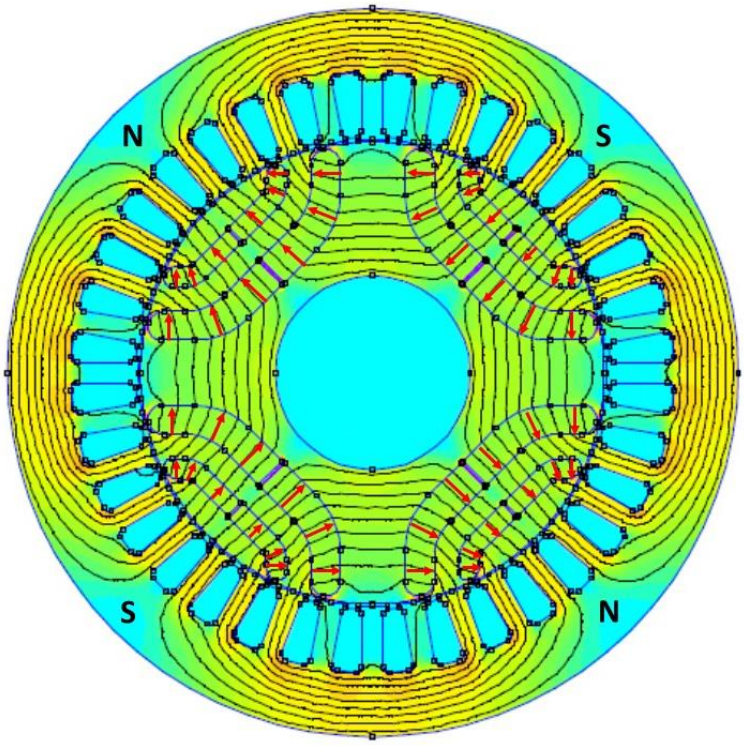

Fig. 78 – Magnetic direction of PM

V.IV Magnets Production

The selection of bonded magnets has been conducted in order to obtain the best performances considering the actual production techniques and costs. Therefore, five different bonded magnets were prepared based on moulding technologies.

V.IV.I Compression Bonded Magnets Preparation

In the case of compression technique, the phenolic resin has been used as the polymeric binder and mixed with NdFeB powder. For such process the binder content range in weight is affected by compacted pressure levels, as shown in Fig. 79, and type of resin, but, in general, such values are from to 0.8% to 5% in weight. Higher polymer content means lower magnetic properties but better mechanical strength. In this research activity the chosen weight percentage (wt%) is 4 %, therefore the first step consisted in the mixture preparation using the mentioned phenolic resin and MQP 14-12 NdFeB powder, a magnetic powder adopted for applications at high temperature (until to 180°C) [96].

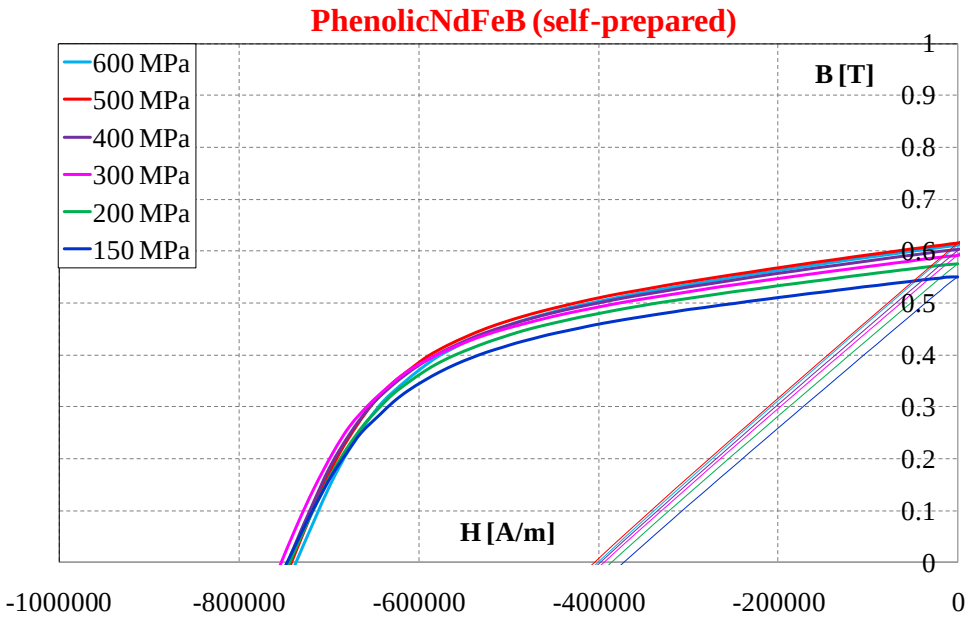

Fig. 79 – Different compacting pressure adopted for Phenolic NdFeB 4wt%

The following process is the compression moulding at 600 MPa followed by thermal treatment at 150°C for 45 minutes. The mixed powder has been compacted in the discoid form by means of a hydraulic press and machined afterwards (Fig. 80). The demanded geometry was designed on a SolidWorks platform from which it was possible to obtain the format compatible with the dedicated cutter software (Fig. 81). Such software allows to obtain the sequence of points to be interpolated of a specific geometry. The final obtained shapes are shown in Fig. 82.

Fig. 80 - Working process of the compacted disk

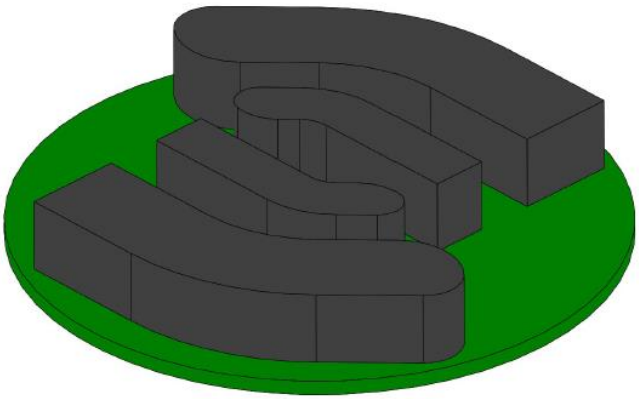

Fig. 81 – Drawings of the final magnets produced by one pressed disk

Fig. 82 – The final shape of compression self-prepared magnets

V.IV.II Injection Bonded Magnets Preparation

For injection moulding, the bonded magnets are prepared using the commercial pellets MQIP-M260 and FB23, shown in Fig. 83, or compound self-prepared in the laboratory. The preparation of compound has been explained in IV.I.II, using the NdFeB powder MQP 14-12 with polyamide 12 (PA12) in 10 wt% in pellet form. The process moulding consists in the fusion of the pellet at a range between 240°C and 280°C (Fig. 84), the following cooling at 80°C (Fig. 85), which allows solidifying in the molded shape (Fig. 86) [96]. Before the molding process, the pellets or compound must be dried (Fig. 87).

Fig. 83 – Filling of the mold with the pellets

Fig. 84 – Platen press: the fusion process at 275°C

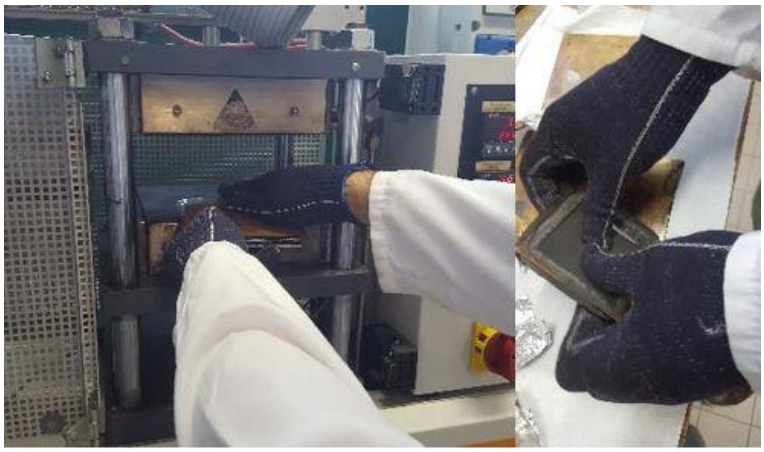

Fig. 85 – Platen press: cooling phase/solidification at 80°C

Fig. 86 – The molded form of MQIP M260 NdFeB Bonded magnets

Fig. 87 – The dryer system used for about 4 hours at temperature of 80°C

The particular drawings have been involved to allow the machining of the magnets in the final flux barriers forms (Fig. 88). For this reason, there are 2 mm high mechanical bridges, which have the function of maintaining the robustness structure during the milling process. The molded sample, once milled, was removed from the holder and the individual magnets were recovered by manually breaking mechanical bridges (Fig. 89).

A transparent varnish, acrylic-based, is used to create a protective layer on magnets (Fig. 90), which helps to avoid oxidation in case of contact with water or in case of use in damp and corrosive environments.

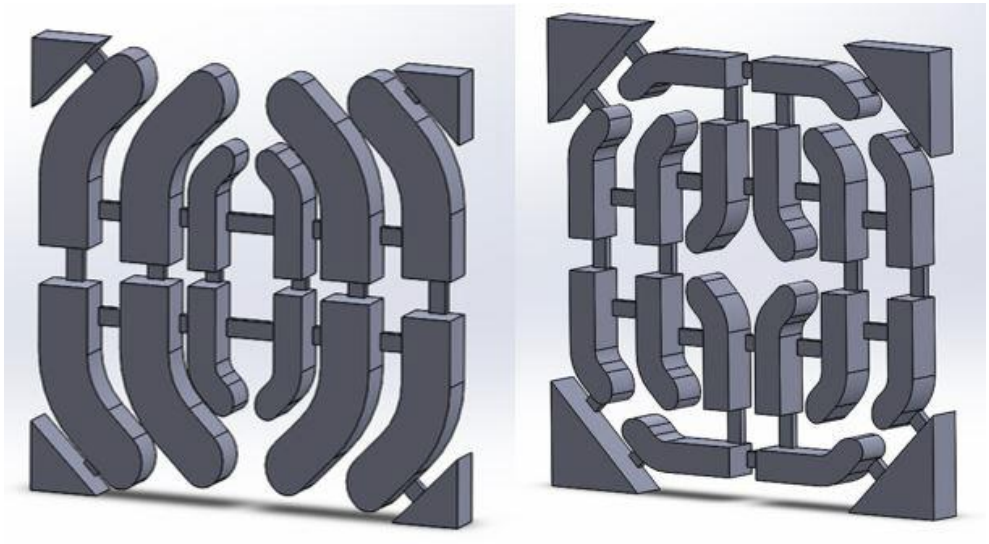

Fig. 88 – Drawings used to obtain the final flux barrier shape

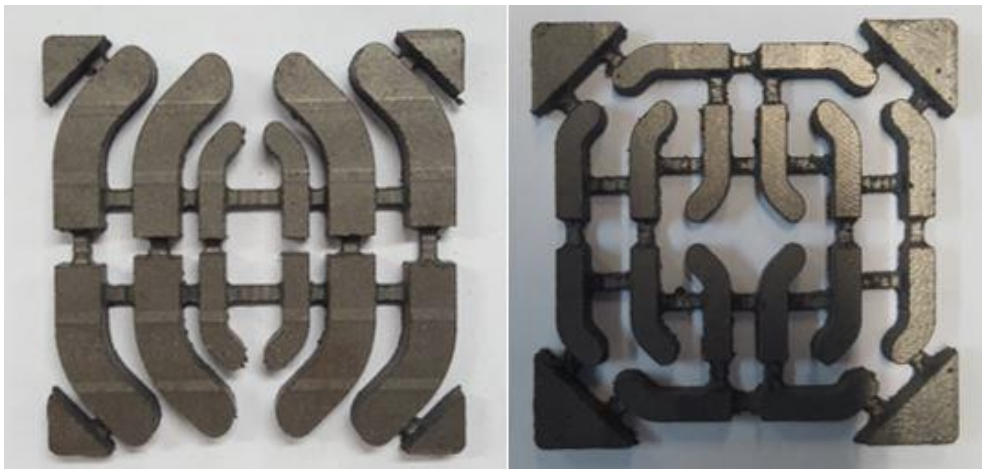

Fig. 89 – The final phase bonded magnets by means of injection moulding

Fig. 90 – Magnets surface protection applying a protective spray

The same process has been repeated for all injection adopted bonded magnets. The temperature and times are different during the process, accordingly, the used technique is defined in dependence of the typology of the proposed magnets. The molded sample

for FB23 ferrite bonded and self-prepared PA6 bonded magnets are respectively shown in Fig. 91 and Fig. 92.

Fig. 91 - The molded sample of FB23 Ferrite Bonded magnets

Fig. 92 - The molded sample of self-prepared PA6 NdFeB Bonded magnets

V.IV.III Flexible Magnets Preparation

An investigation on the use of flexible bonded magnets in the flux barriers geometry has been carried out: this type of bonded magnets cannot use in the proposed rotor geometry for poor mechanics. While attempting to insert the flexible magnets into flux barriers; the samples has been broken and cracked, as shown in Fig. 93 and Fig. 94.

Fig. 93 – Failed insert of flexible magnets

Fig. 94 – Broken flexible magnets

V.IV.IV Magnetization Process

The obtained bonded magnets have been magnetized by means of a particular holder (Fig. 95 and Fig. 96) to be inserted in the coil of a magnetizer, getting the demagnetization curves. It should be noted that during both molding processes no one magnetization procedure or alignment has been applied. The holder has been designed to obtain the magnetization direction close to the desired one, used in the simulation. With a particular type of paper, it is possible to view the flux density distribution and evaluate the magnetic direction. The small difference is represented to the extremity of

the magnets (Fig. 97); to obtain the magnetization direction adopted in the simulation it would have been necessary to magnetize in situ using the assembled prototype with very high current (over 50 A). The designed stator cannot operate at such current value and for this reason, the differences in the magnetization direction have been considered acceptable.

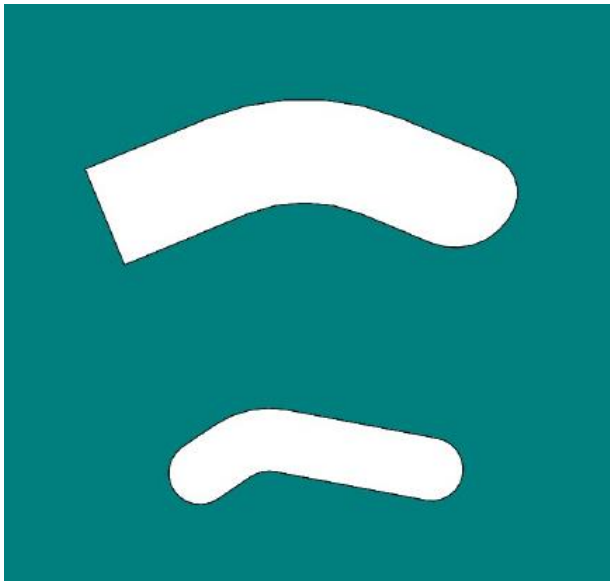

Fig. 95 - Drawing of particular holder

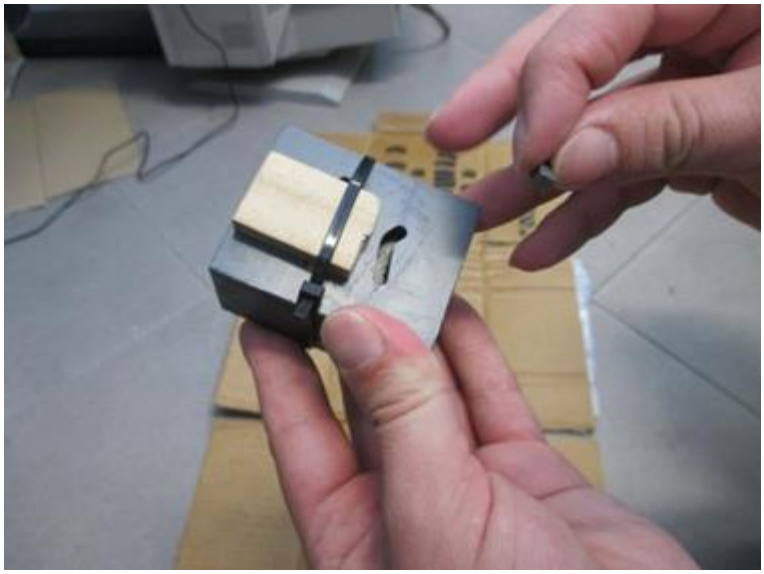

Fig. 96 - The insertion of the magnet inside of the holder

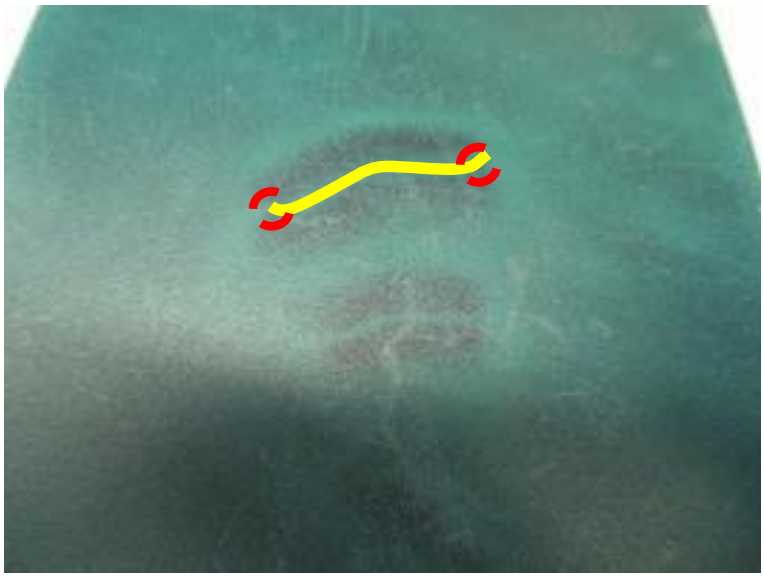

Fig. 97 - Magnetic flux density of prepared magnets: the differences between the magnetization process and simulation one

V.V Prototypes Assembly

In Fig. 98 there are all the components used to compose the rotor: on the right are noted some electrical sheets (Fig. 99), in the middle there are two plates that serve to keep the pack of laminations compact, on the top the shaft and the center there is a nut that has the function of locking one of the plates.

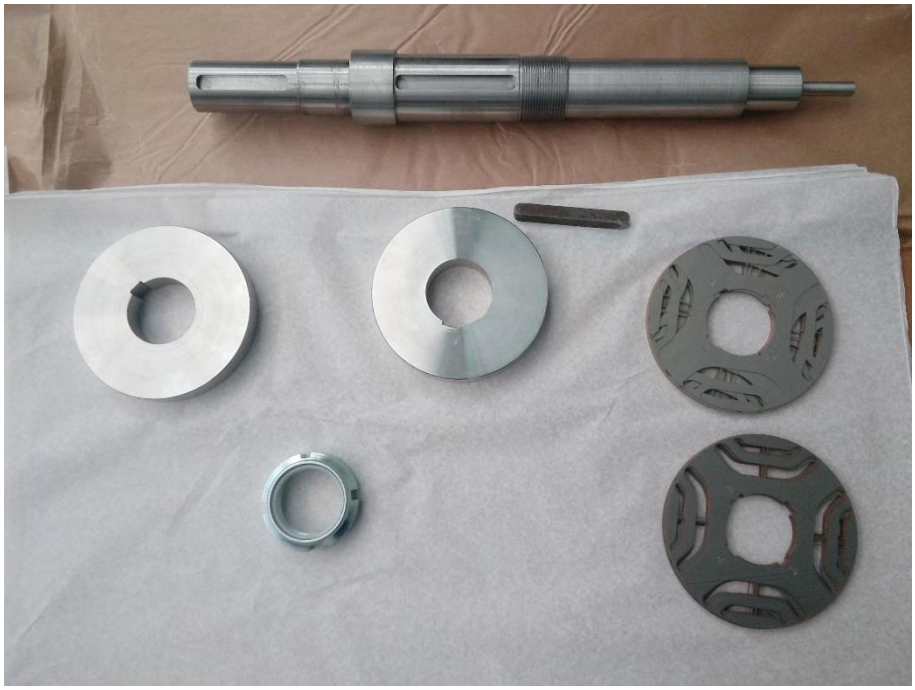

Fig. 98 – The main components of the rotor

Fig. 99 – Electrical sheets/laminated steel with the flux barriers

In Fig. 100 it is possible to observe the stacking of the electrical sheets that have been specifically designed to have a 10° stepping (skewing). There are 80 sheets for each prototype, divided into 8 groups of 10. The insertion of the magnets in the flux barriers (Fig. 101) is not at all trivial since the magnets must have the right tolerance to be able to enter in the barriers without too much friction, but at the same time, they must remain inside them. This is not obvious, as the mutual repulsive force of the magnets tends to separate them and then to lift the rotor pack. Obviously this effect is much greater as more magnets are taken into consideration, so the assembly of the last layers was more difficult than the first ones.

Fig. 100 - Electrical sheet stacking

Fig. 101 - The insertion of the magnets in the flux barriers

During the preparation of the rotors, it is possible to verify the correct assembly through the skewing pattern observation. The particular magnetic green paper can be used to evaluate the flux density distribution on the rotor surface (Fig. 102) and is therefore well-suited for displaying the skewing effect, as is shown in Fig. 103. The right inclination and its periodicity confirm the success of mounting of rotor.

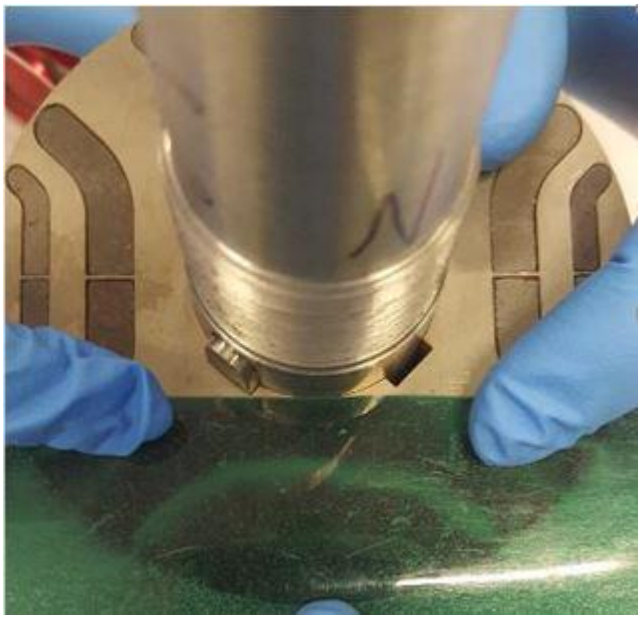

Fig. 102 – The magnet flux distribution

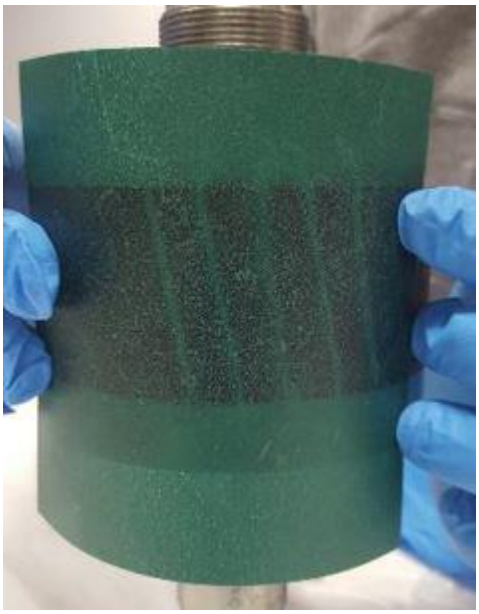

Fig. 103 - Skewing effect visualization to confirm the correct assembly of the rotor

Once the rotor is assembled (Fig. 104) it proceeds with mechanical coupling with the stator, as shown in Fig. 105. The series conductors number for slot is 100 and diameter of each conductor is 0.56 mm. The rated current is 3A, and rated torque is 5.5 Nm. The final prepared prototypes are shown in Fig. 106.

Fig. 104 – Assembled rotor

Fig. 105 – Rotor-stator assembly

Fig. 106 – Some prepared prototypes of PMaSRM

V.VI Results Analysis

Five reluctance machines prototypes have been assembled: a SRM without magnets and four PMaSRM with bonded magnets. The experimental results have been deduced by means of two dedicated test bench (Fig. 107), slowly and speedy test bench, and compared to the simulation ones. The maximum torque per Ampere (MTPA) locus has been analyzed for each machine in order to estimate the performances and compare them to the experimental data. Furthermore, the torque ripples have been evaluated at rated current for the proposed prototypes, as also torque maps as the function of I_d and I_q current. For each prototype it is important to recognize the order of the phases for a correct connection of supply, control and measurement devices (Fig. 108). The SRM has been considered as reference machine to make opportune assessments and comparison.

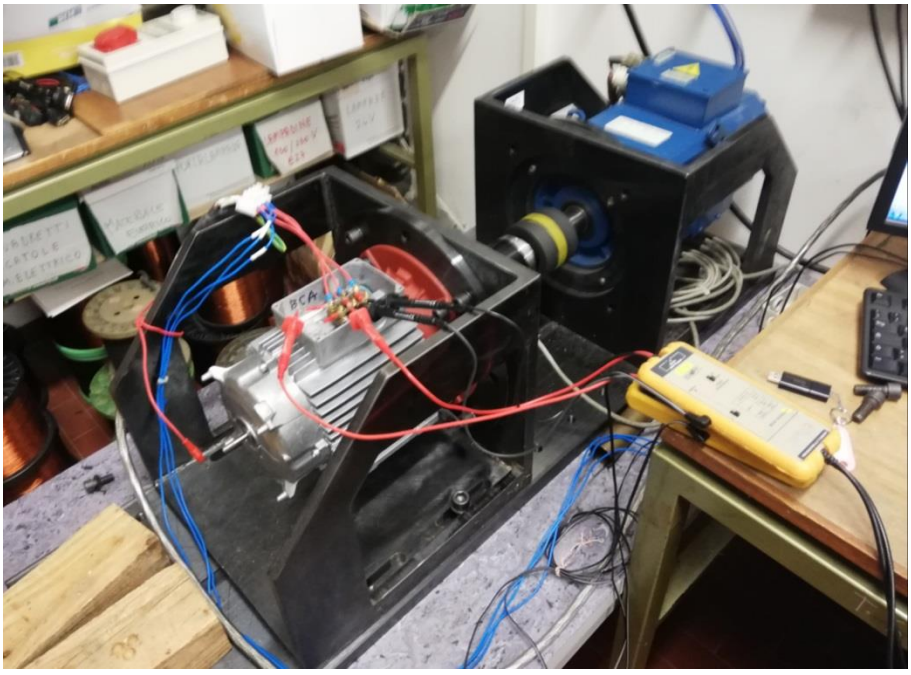

Fig. 107 – Dedicated test bench for dragged measurements

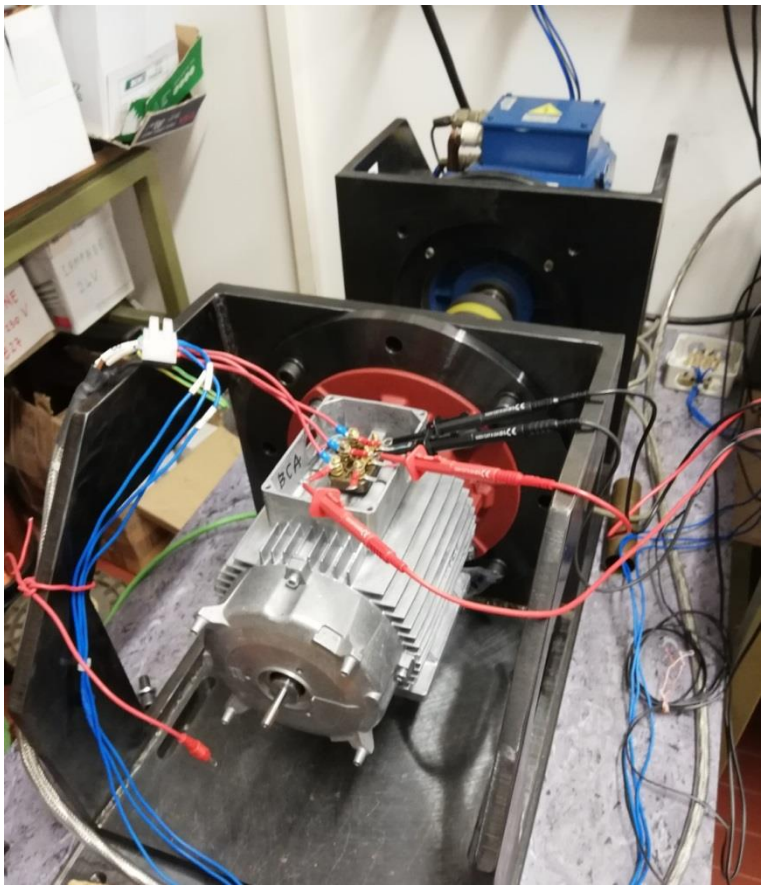

Fig. 108 – Connection setup

V.VI.I Torque Versus Current Vector Angle

The comparison, for both simulation and experimental results, has been carried out on the basis of the average torque versus the current angle. For a comprehensive analysis, different current values were chosen, mostly in the case of the FEM simulation. The torque trends have been obtained in the range from 0.5 A to 6 A with the steps of 0.5 A, being 6 A the double of the machine's rated current. The torque versus current angle for the reference SRM are shown in Fig. 109. The simulation data are indicated by means of lines; the measurement values are represented by the points instead. The MTPA trajectory is reported in red line, instead the measured one is in blue line.

The measurement results are slightly lower than the simulated ones, this is probably due to the temperature condition inside the motors. In particular, this consideration applies to PMaSRM prototypes where the magnetic characteristics at 100°C have been used in the simulation tools. Therefore the inner temperature is probably slightly higher during the measurements than in the simulations.

The difference between simulation and measurement results for SRM machine, at the rated condition (3 A), is about 3%. Also, the MTPA trajectories are very near each other.

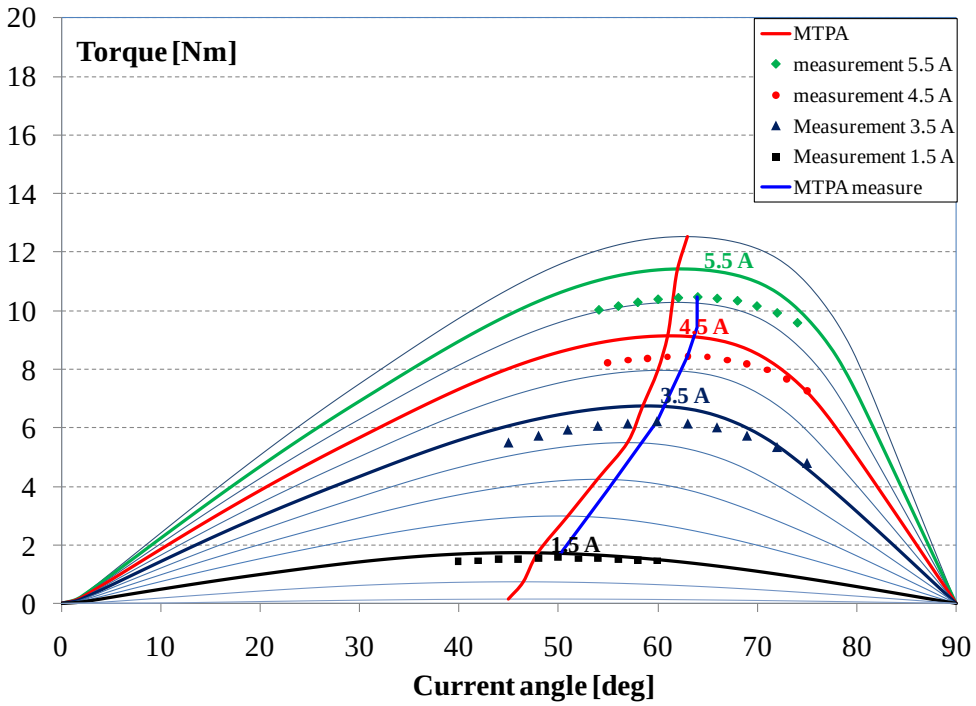

Fig. 109 – Average torque versus current angle of the reference SRM (No PM): comparison between simulation and measurement results

The torque trends of the PMaSRM with compression self-prepared bonded magnets are reported in Fig. 110. The matching between measurement and simulation results is about 4% for rated current. Also, the prototype with the bonded magnets has better torque performances compared to the reference reluctance machine without magnets. From this point of view, the average torque increases well as 55%.

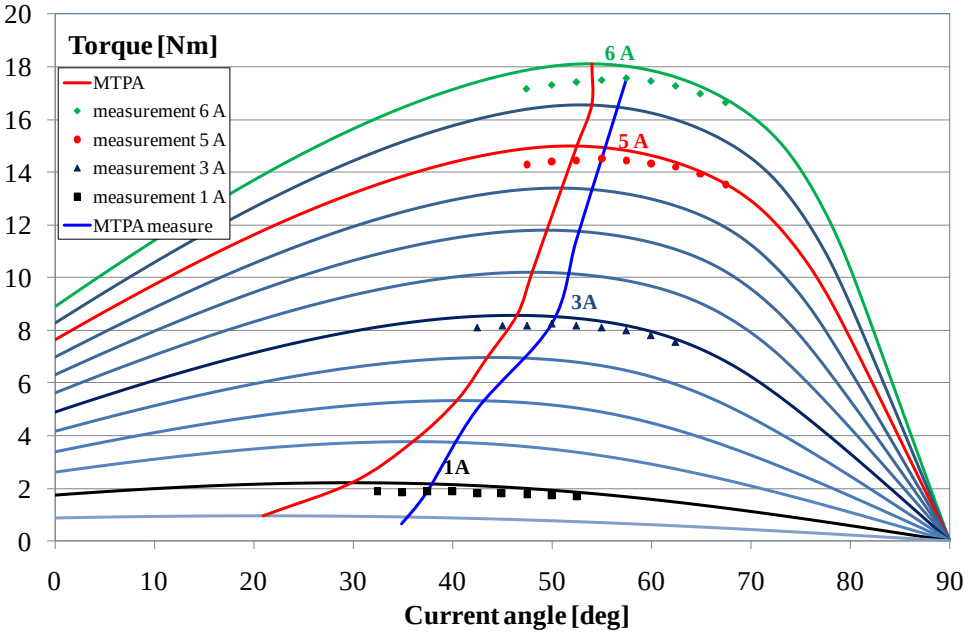

Fig. 110 – Average torque versus current angle of the PMaSRM with compression self-prepared bonded magnets (Phenolic Bonded 4wt%): comparison between simulation and measurement results

For PMaSRM with injection self-prepared bonded magnets the torque versus current angle waveforms are reported in Fig. 111. For such a prototype, the errors between measurements and simulations are of 5%. The torque increment with respect to SRM is of 41%. In this case, as in the previous one, the MTPA trajectories are a bit distant with respect to SRM machine.

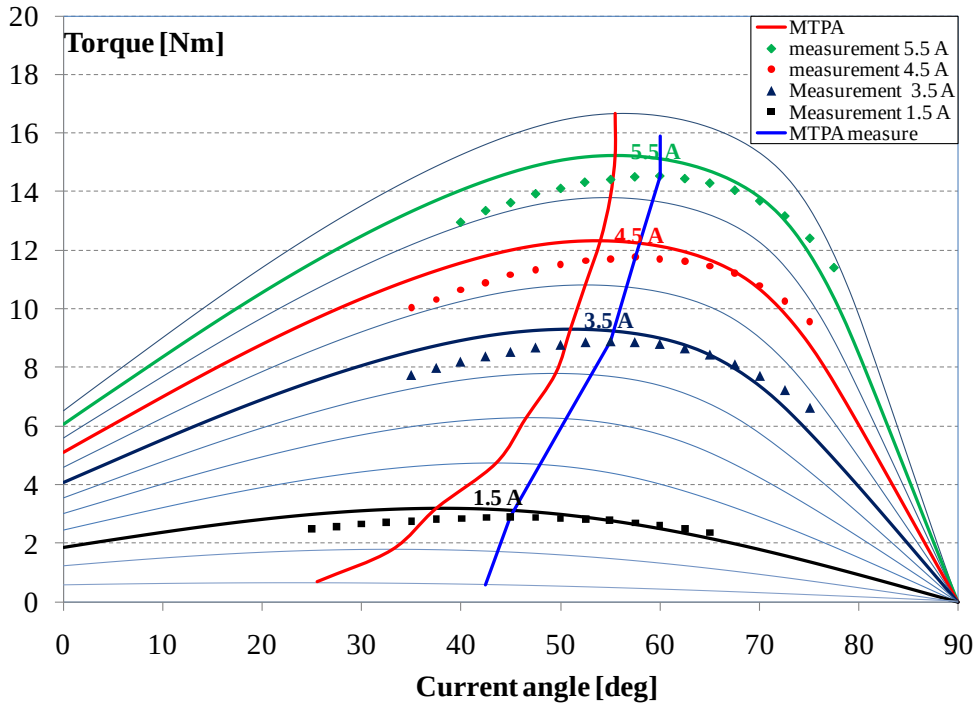

Fig. 111 - Average torque versus current angle of the PMaSRM with injection self-prepared bonded magnets (PA6 Bonded 10wt%): comparison between simulation and measurement results

In the case of MQIP-M260 bonded magnets (commercial pellets) the torque trends are shown in Fig. 112. The same matching between measurements and simulations as in the previous case, have been obtained (around 5%). On the other hand, the torque improvement is of 39% for the rated condition. For this reason, it can be concluded that the self-prepared magnets allow to obtain better performances than commercial ones.

The PMaSRM with FB23 bonded magnets (Ferrite pellets) has torques versus current angle shown in Fig. 113. The best matching between measurements and simulations results have been obtained, about 1%. The MTPA trajectories are very close to each other. However, the average torque increases only of about 16% for the rated current. And, although the improvement is less significant with respect to other considered bonded magnets, it represents the cheaper solution with good torque density compared to SRM.

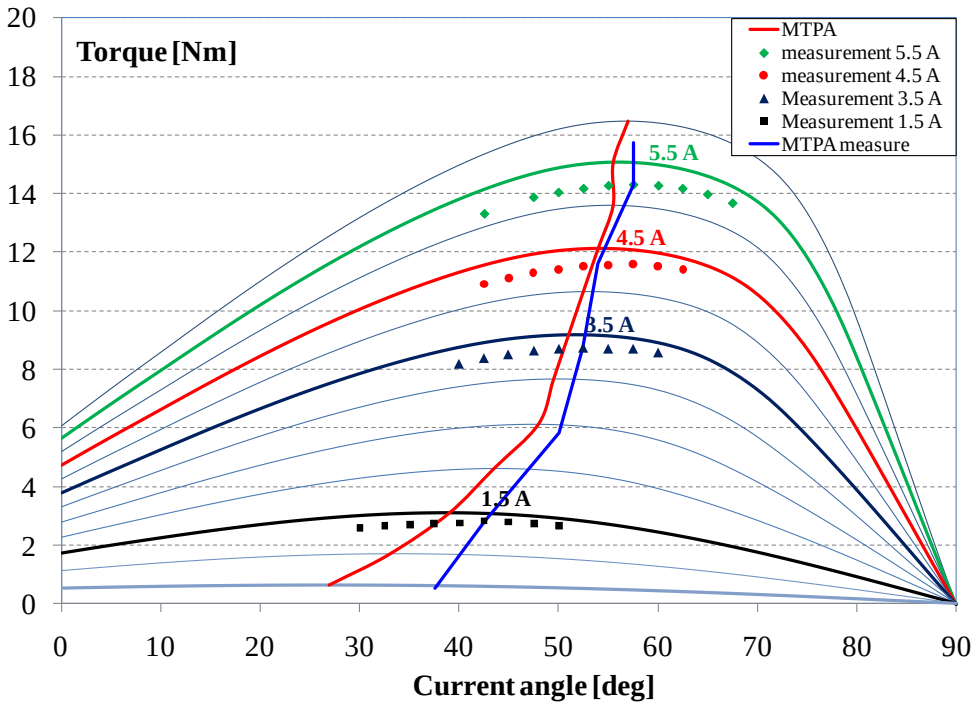

Fig. 112 – Average torque versus current angle of the PMaSRM with MQIP-M260 bonded magnets (NdFeB pellets): comparison between simulation and measurement results

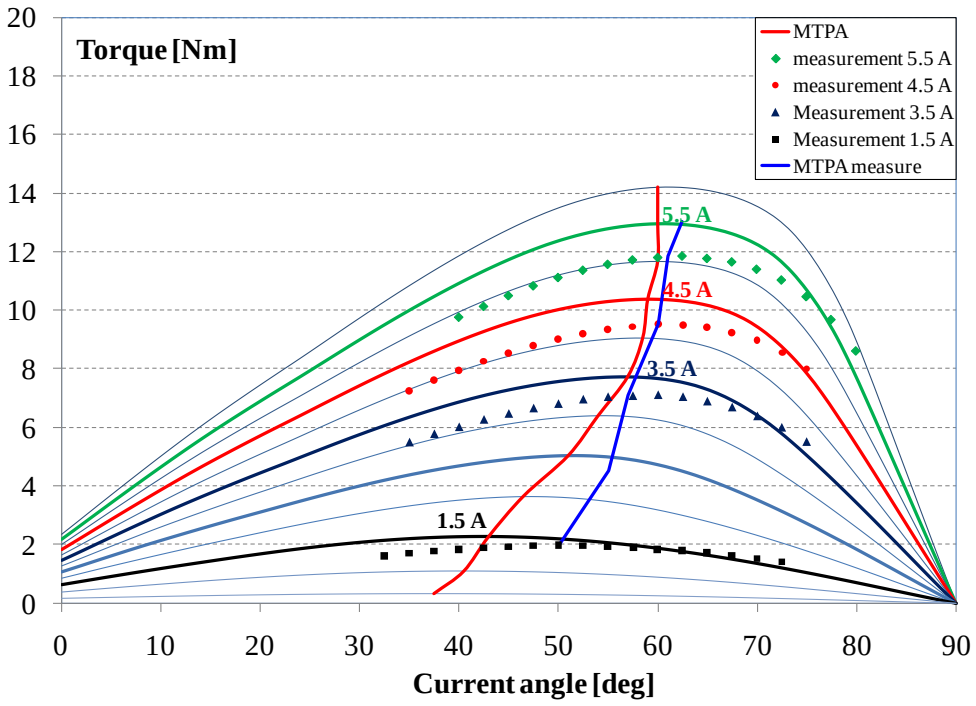

Fig. 113 – Average torque versus current angle of the PMaSRM with FB23 bonded magnets (Ferrite pellets): comparison between simulation and measurement results

V.VI.II Torque Ripple

The torque ripple has been evaluated for all the proposed prototypes, also considering the comparison between measurements and simulation data. The torque ripple results, for both measurement and FE analysis, are reported respectively in Fig. 114 for SRM, in Fig. 115 for the PMaSRM with compression moulded bonded magnets (self-prepared) and in Fig. 116 for the PMaSRM with injection moulded bonded magnets (also self-prepared).

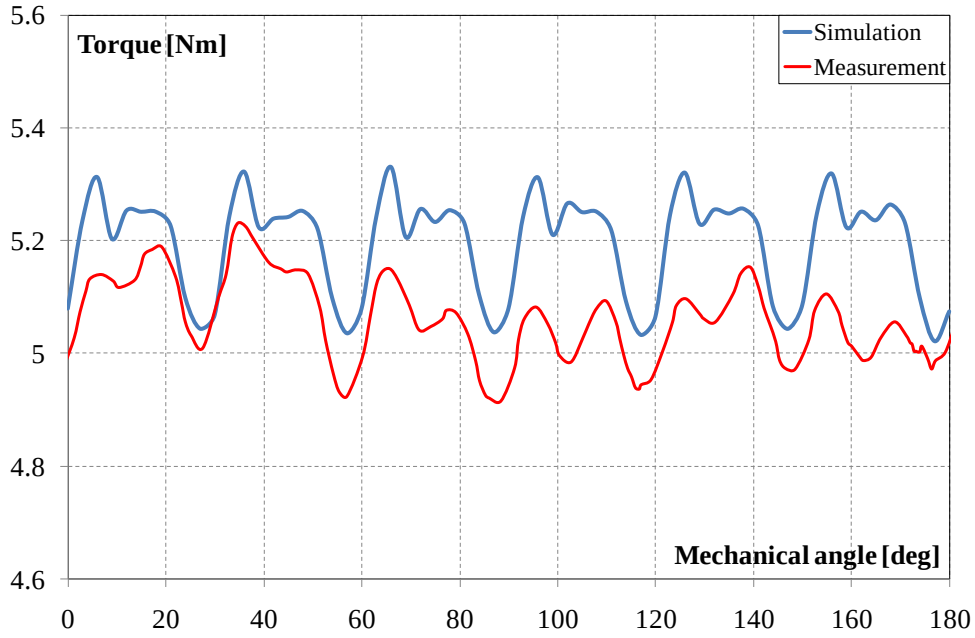

Fig. 114 – Torque ripple of SRM (No PM): comparison between simulation and measurement results

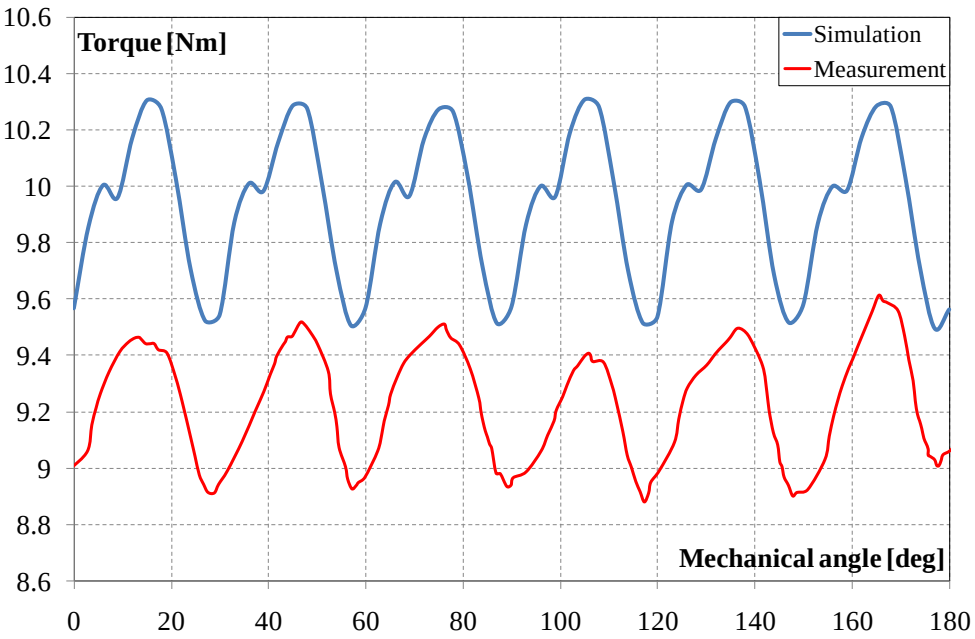

Fig. 115 – Torque ripple of PMaSRM with self-prepared compression bonded magnets (Phenolic Bonded 4wt%): comparison between simulation and measurement results

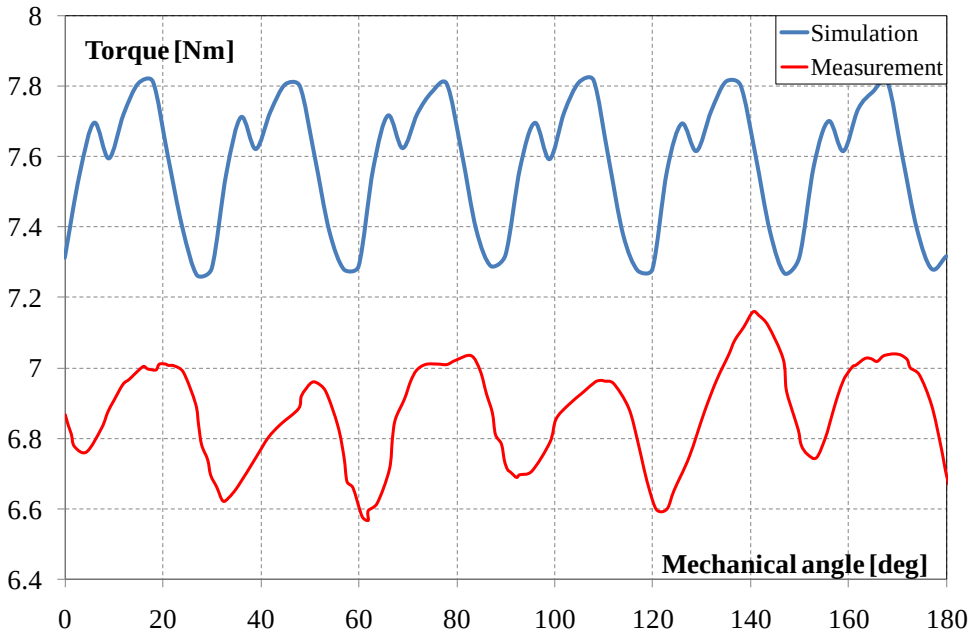

Fig. 116 - Torque ripple of PMaSRM with self-prepared injection bonded magnets (PA6 Bonded 10wt%): comparison between simulation and measurement results

In the case of the reference SRM, the matching between measurement and simulation data for average torque value, is about 3%. For what concerns the ripple values, the difference is of 6%. For the PMaSRM with bonded magnets made through compression moulding, the average torque difference is 7% while the ripple difference is 1%. Instead for PMaSRM with bonded magnets prepared by injection moulding the average torque has a matching of 9%, while the ripple is of 8%.

For all cases, the measurement waveforms are similar to the simulated ones. The difference in average torque for both PMaSRM is always taken into account to the temperature condition. Furthermore, it is important to note that was not the equal magnetization pattern adopted in the simulation and realized in the laboratory. There are small differences in magnetic field lines in the extremities of the prepared magnets, little folds just described in V.IV.IV. This also involves the further difference between simulation and measurement data.

In the case of prototypes with MQIP-M260 bonded magnets (NdFeB pellets) and FB23 bonded magnets (Ferrite pellets) the average torque differences, between simulation and measurement, are respectively 7% and 1%, as shown in Fig. 117 and Fig. 118. As in the previous subparagraph, the best matching between simulation and measurement results has been obtained for Ferrite bonded magnets. On the other hand, the ripple shows a matching of 9% for the prototype with MQIP-M260 bonded magnets, instead for FB23 bonded magnets (Ferrite pellets) machine has a matching of 23%.

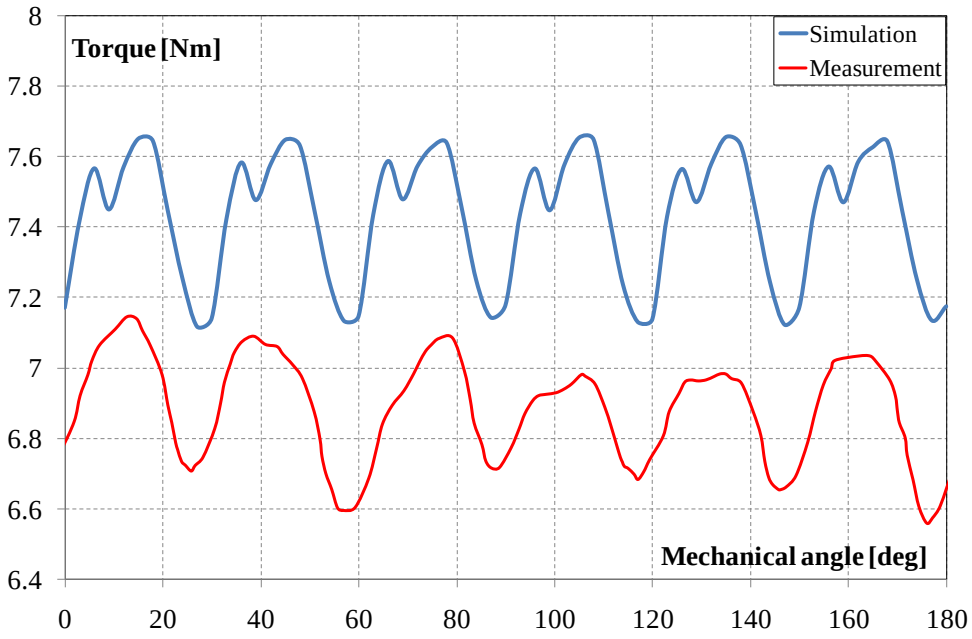

Fig. 117 – Torque ripple of PMaSRM with injection MQIP-M260 bonded magnets (NdFeB pellets): comparison between simulation and measurement results

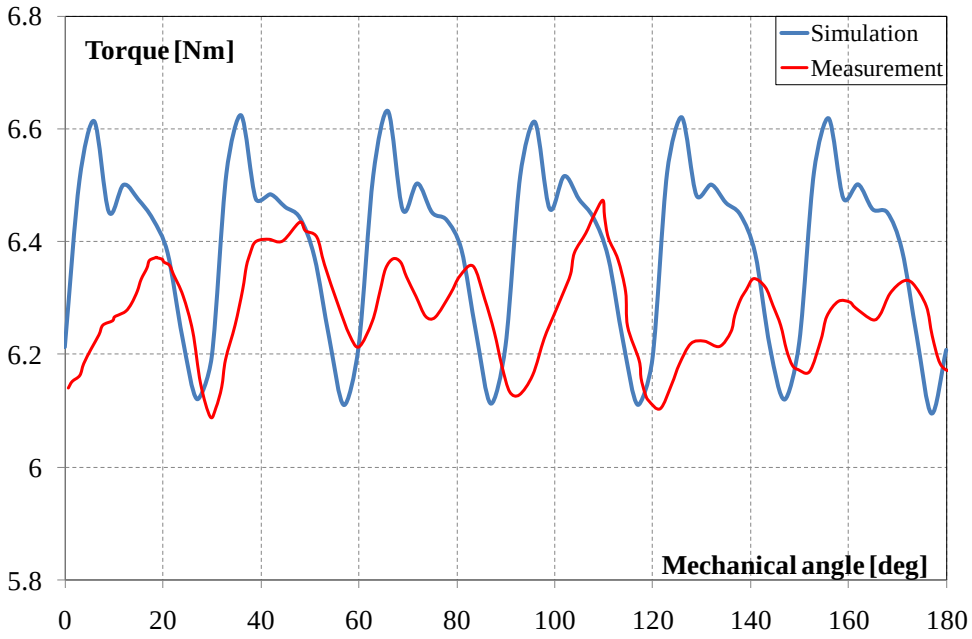

Fig. 118 - Torque ripple of PMaSRM with injection FB23 bonded magnets (Ferrite pellets): comparison between simulation and measurement results

The use of bonded magnets increases the ripple respectively of 145% for the PMaSRM with compression moulded bonded magnets, of 83% for PMaSRM with injection moulded bonded magnets (self-prepared), of 80% for with injection moulded MQIP-M260 bonded magnets (commercial NdFeB pellets), and 26% for injection moulded FB23 bonded magnets (commercial Ferrite pellets).

V.VI.III Torque Maps

The torque maps for all prototypes are shown respectively in Fig. 119 for SRM, in Fig. 120 for PMaSRM with self-prepared compression bonded magnets, in Fig. 121 for PMaSRM with self-prepared injection bonded magnets, in Fig. 122 for PMaSRM with injection MQIP –M260 bonded magnets, and in Fig. 123 for PMaSRM with injection FB23 bonded magnets.

For SRM and PMaSRM with ferrite bonded magnets, a very good matching between simulation and measurement results has been obtained. On the other hand, for other PM prototypes, the differences are higher and not linear and constant. Probably, such disparities are due to not perfectly magnetization pattern to the normal direction of the surface. As already mentioned (V.IV.IV), there are magnetic field folds on the extremities of the magnets, which do not exist in the simulation model.

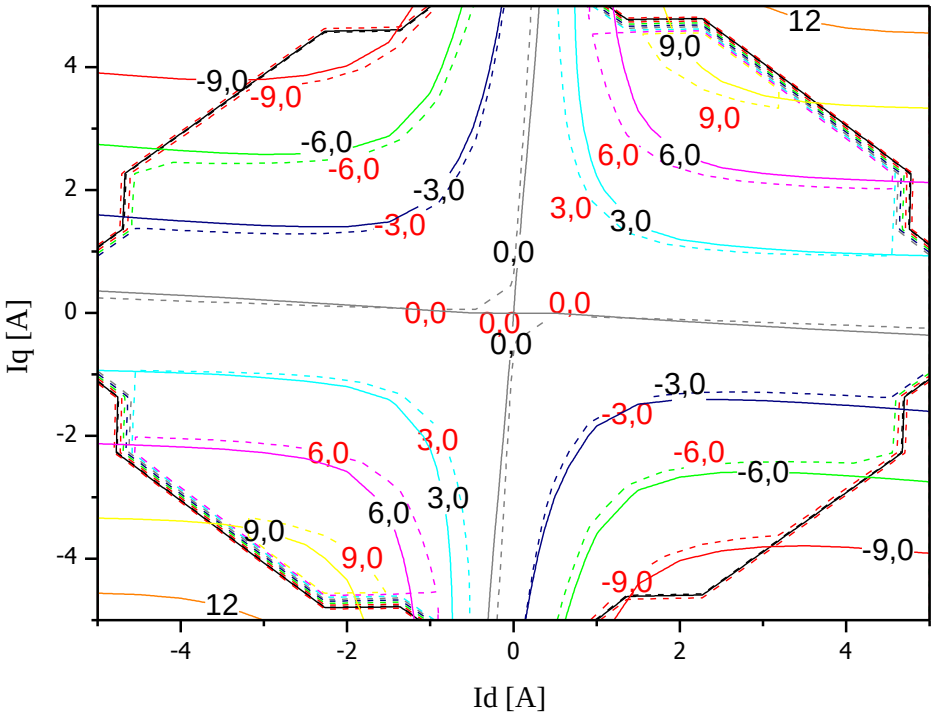

Fig. 119 – Torque maps of SRM (No PM): comparison between simulation and measurement results

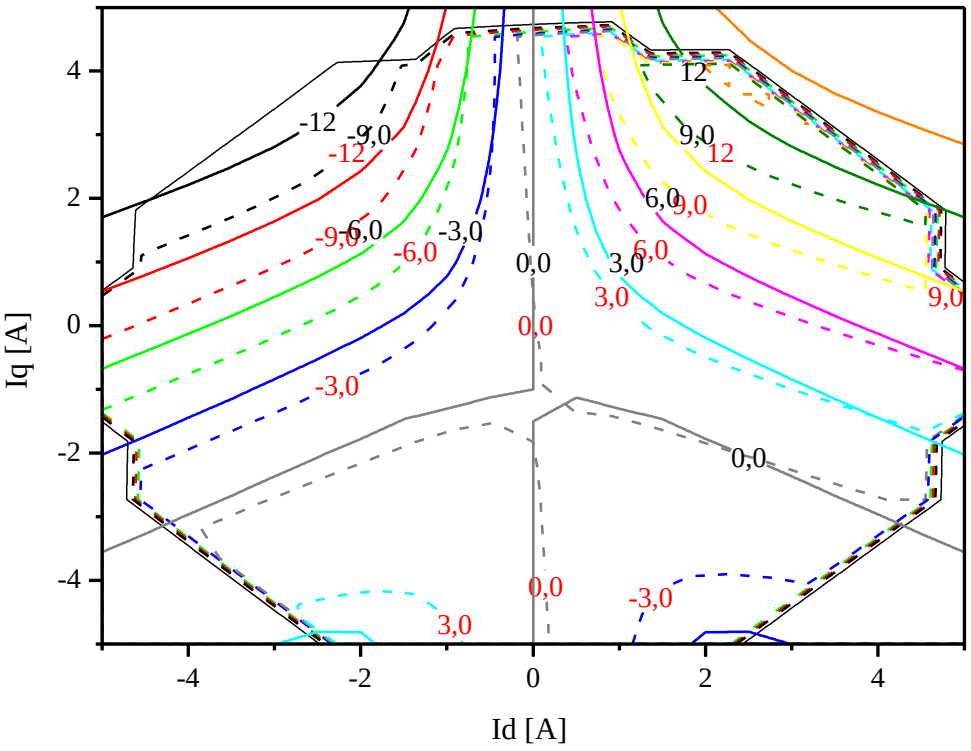

Fig. 120 - Torque maps of PMaSRM with self-prepared compression bonded magnets (Phenolic Bonded 4wt%): comparison between simulation and measurement results

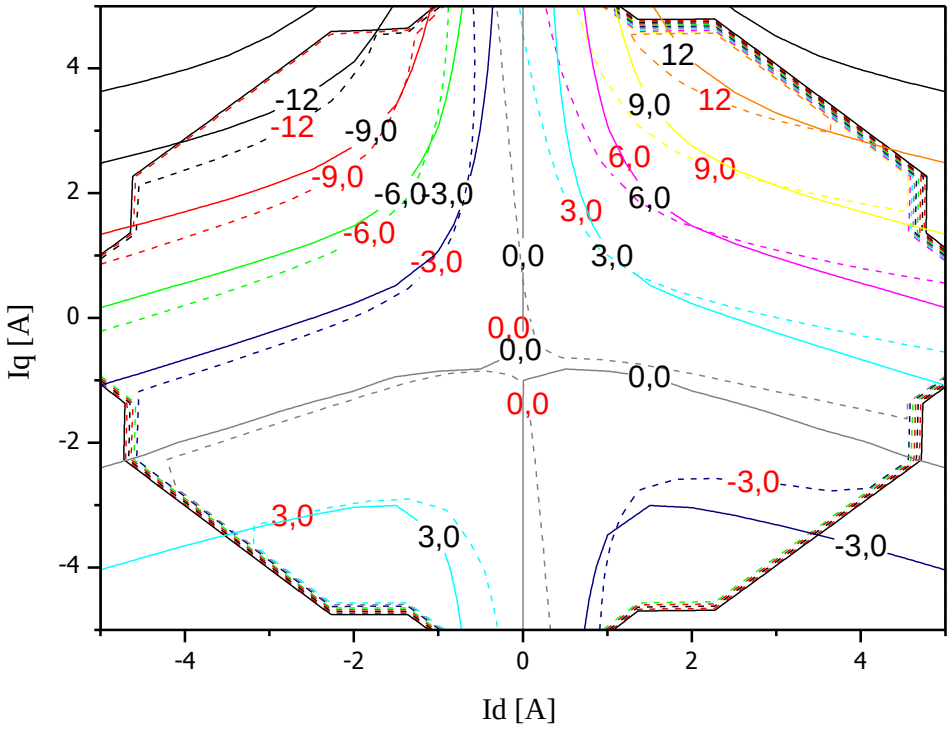

Fig. 121 - Torque maps of PMaSRM with self-prepared injection bonded magnets (PA6 Bonded 10wt%): comparison between simulation and measurement results

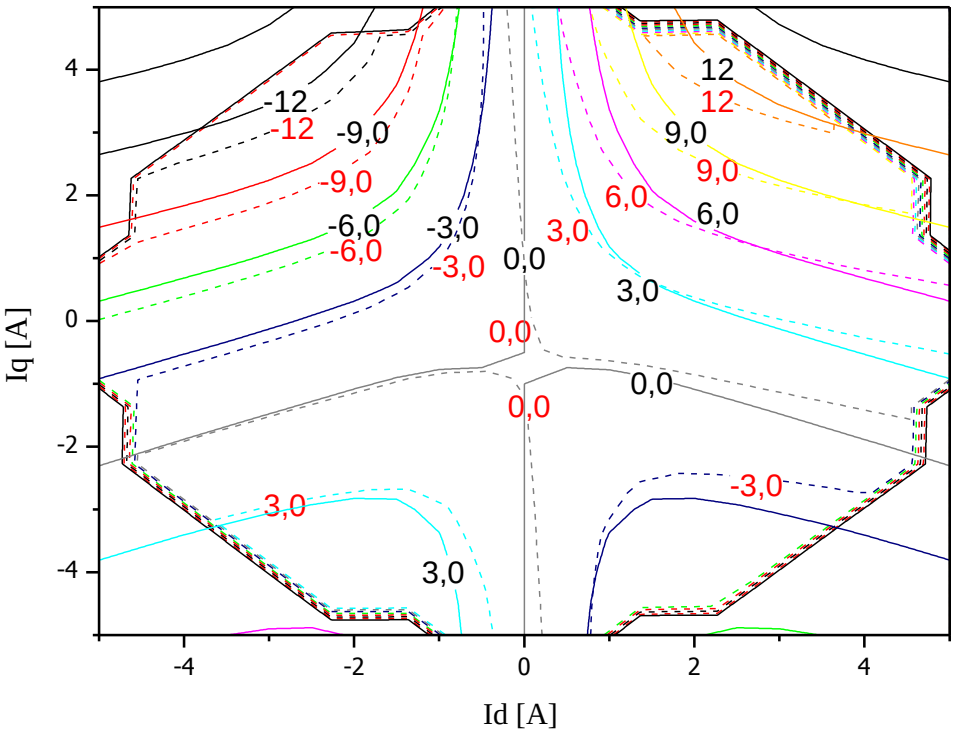

Fig. 122 - Torque maps of PMaSRM with injection MQIP –M260 bonded magnets (NdFeB pellets): comparison between simulation and measurement results

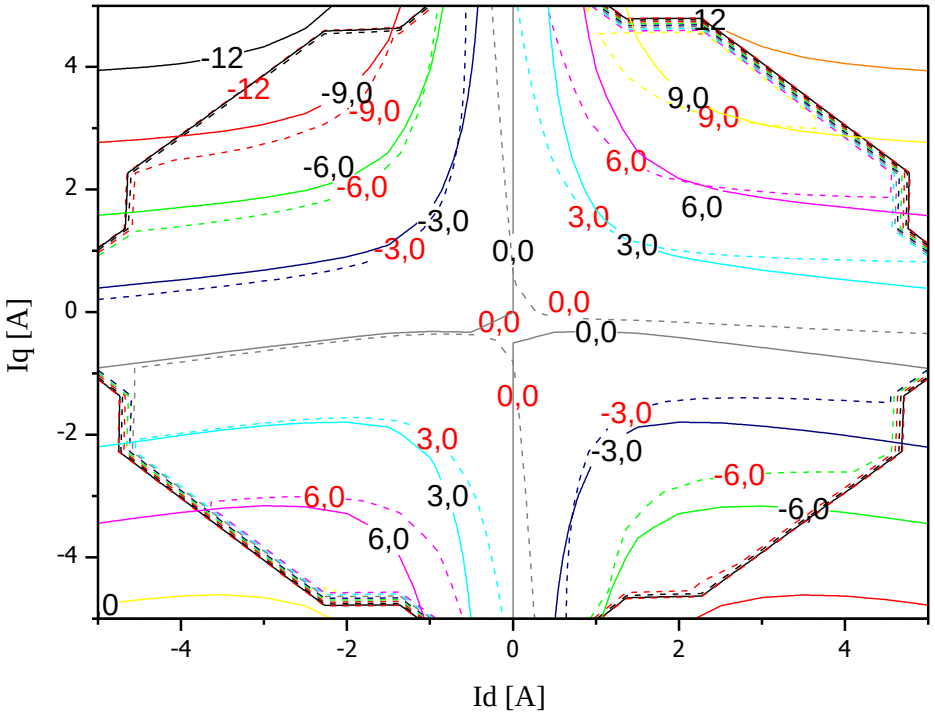

Fig. 123 - Torque maps of PMaSRM with injection FB23 bonded magnets (Ferrite pellets): comparison between simulation and measurement results

V.VI.IV Power Factor

Further interesting results concern the power factor. For all prototypes, the power factor has been deduced for the rated current. The assisted reluctance machines have higher power factor with respect to the reference SRM, as it is reported in TABLE XVII, mainly for the PMaSRM equipped with compression moulded bonded magnets.

TABLE XVII – The power factor of the prepared prototypes

Motor Types	**MTPA for I=3 A**
	PF
SRM	0.70
PMaSRM compression self-pre. NdFeB	0.96
PMaSRM injection self-pre. NdFeB	0.93
PMaSRM injection NdFeB	0.90
PMaSRM injection Ferrite	0.80

V.VI.V Magnets Demagnetization Risk

The opportunity to operate in the overload condition in assisted reluctance machine can be limited by the use of permanent magnets. The increase of current could lead to partial or complete demagnetization of the magnets. Therefore, the investigation concerns such risk has been evaluated by means of simulation tools for all prepared prototypes with the permanent magnets. Different values of supply current have been considered: 0, 3, 10, 15, 20, until 50 A. It is important to remember that the maximum supply current during the tests in the laboratory is 10 A, due to the control system. In this context, the first phase of analyses has been done by means of FEA, and only then some experimental tests will be performed.

For PMaSRM with NdFeB bonded magnets made through compression moulding the flux density at 10 A supply condition is shown in Fig. 124. It is possible to note that different parts of the magnetic circuit seem no completely saturated. As a result, the load lines for three different currents (0, 3 and 10 A) are drawn and intercepted with the magnetic characteristic of the considered magnet as illustrated in Fig. 125. For 10 A no one demagnetization effect has been reached, the bonded magnets prepared by

compression moulding have good overload capability. The slight demagnetization begins for a current of about 15 A.

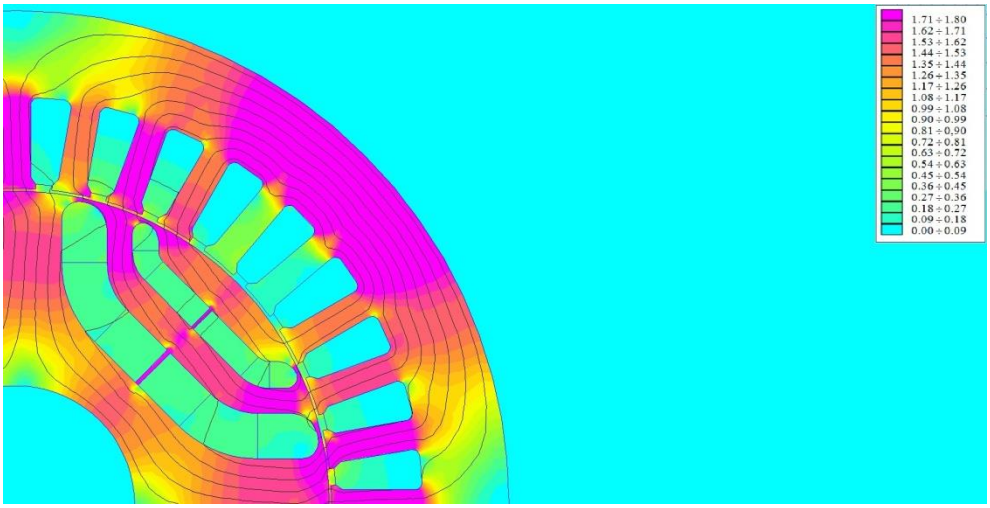

Fig. 124 - Compression self-prepared NdFeB bonded magnets flux density for the supply current of 10 A in MTPA loci condition

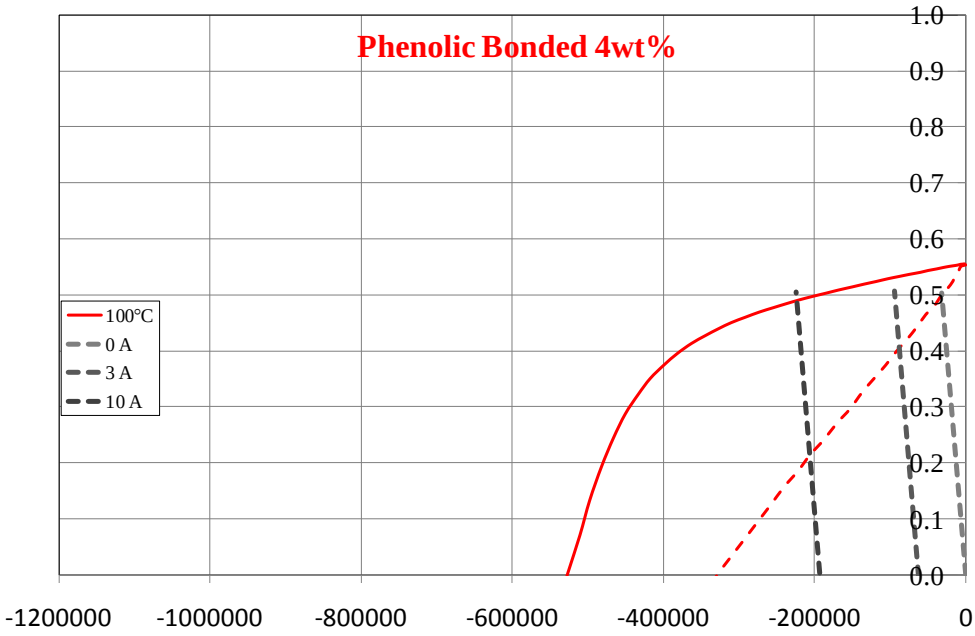

Fig. 125 – Interception between the demagnetization curve and load lines (0, 3 and 10 A) for Phenolic NdFeB Bonded 4wt% magnets

The flux density of the PMaSRM prototype with the bonded magnets self-prepared by the injection moulding process, and at the condition of 10 A is shown in Fig. 126. Also in this case, the saturation of the magnetic circuit is not complete, however, it is more saturated than bonded magnets made with the compression moulding. In Fig. 127 is shown the interception of the load lines (0, 3 and 10 A) with magnetic characteristic of PA6 Bonded 10wt% magnets. Also, the magnets prepared by injection moulding have good overload capability. The demagnetization begins around 20 A.

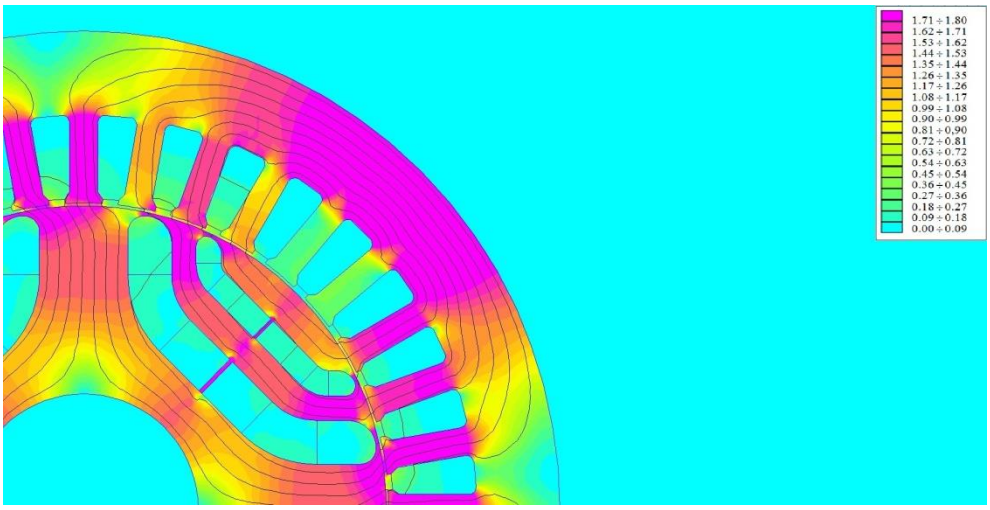

Fig. 126 - Injection self-prepared NdFeB bonded magnets flux density for the supply current of 10 A in MTPA loci condition

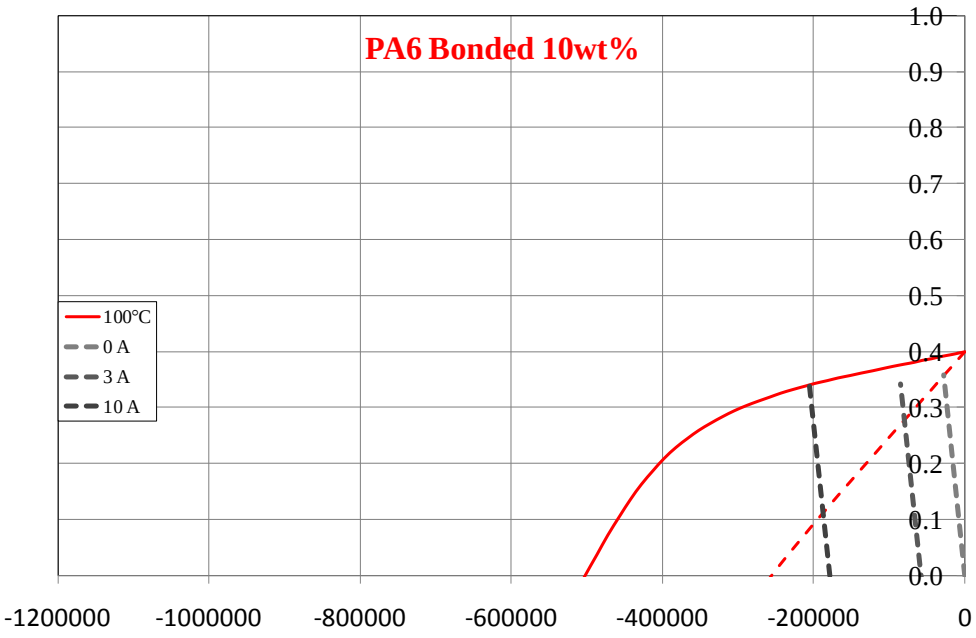

Fig. 127 - Interception between the demagnetization curve and load lines (0, 3 and 10 A) for PA6 NdFeB Bonded 10wt% magnets

In Fig. 128 is shown the flux density at the supply condition of 10 A for PMaSRM with injection MQIP –M260 bonded magnets. The saturation is very close to the previous case. In Fig. 129 the load lines (0, 3 and 10 A) intercept the demagnetization curve of MQIP-M260 bonded magnets. Very high overload capability has been observed, but lower points of the work have been obtained with respect to the previous cases. The effect of demagnetization can be detected around 40 A.

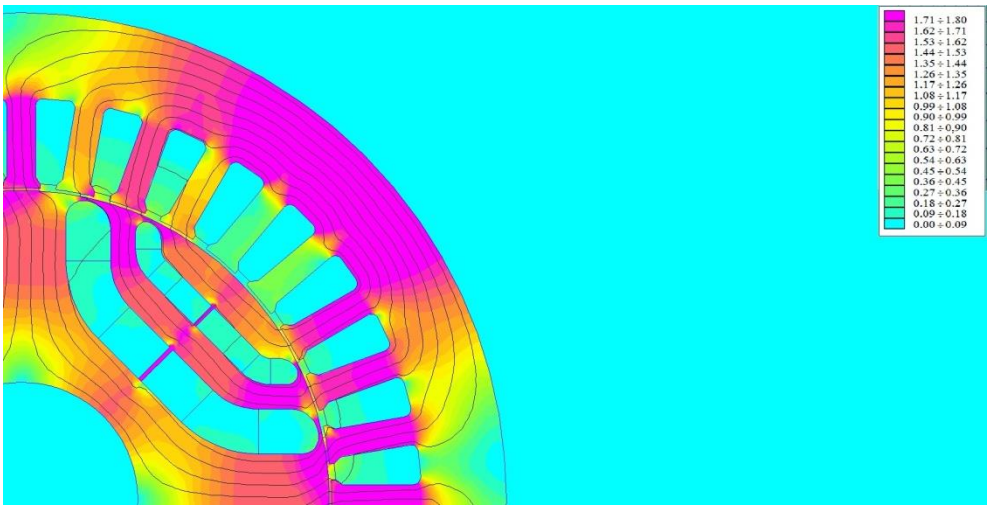

Fig. 128 - Flux density of injection prepared bonded magnets in the laboratory by means of commercial NdFeB pellets at the supply current of 10 A in MTPA loci condition

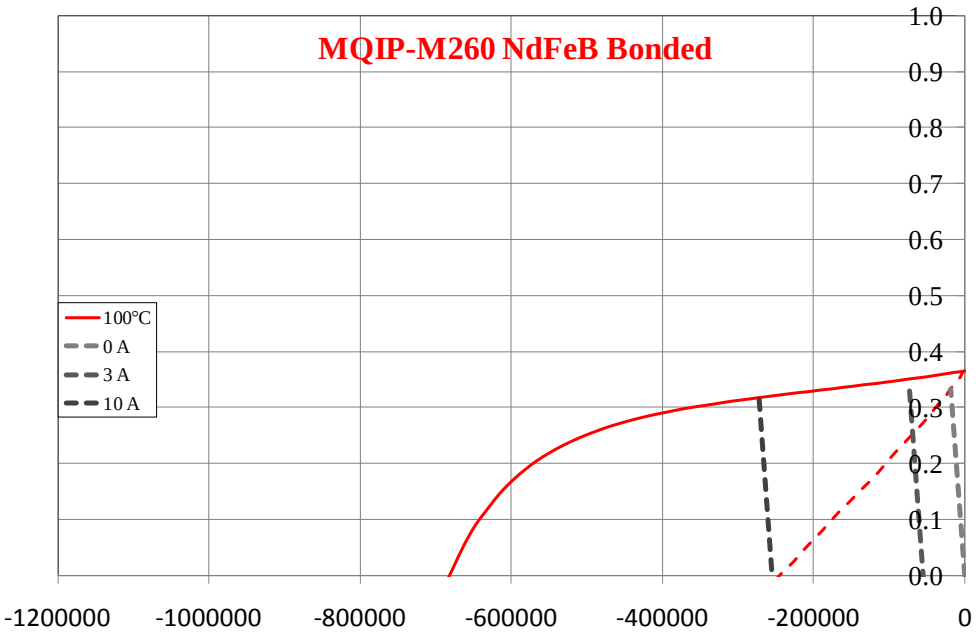

Fig. 129 - Interception between the demagnetization curve and load lines (0, 3 and 10 A) for MQIP-M260 NdFeB Bonded magnets (commercial pellets)

The same consideration have been done for the prototype with the Ferrite bonded magnet. In Fig. 130 the flux density for the supply current of 10 A has been shown. In these condition, the magnets operate in the third quadrant. In Fig. 131 the load lines (0, 3 and 10 A) with the interception of Ferrite bonded magnets demagnetization curve are reported. The overload capability is the lowest one, on the other hand, the demagnetization effect begins about 10 A proving an acceptable result. The complete demagnetization has been estimated for 25 A.

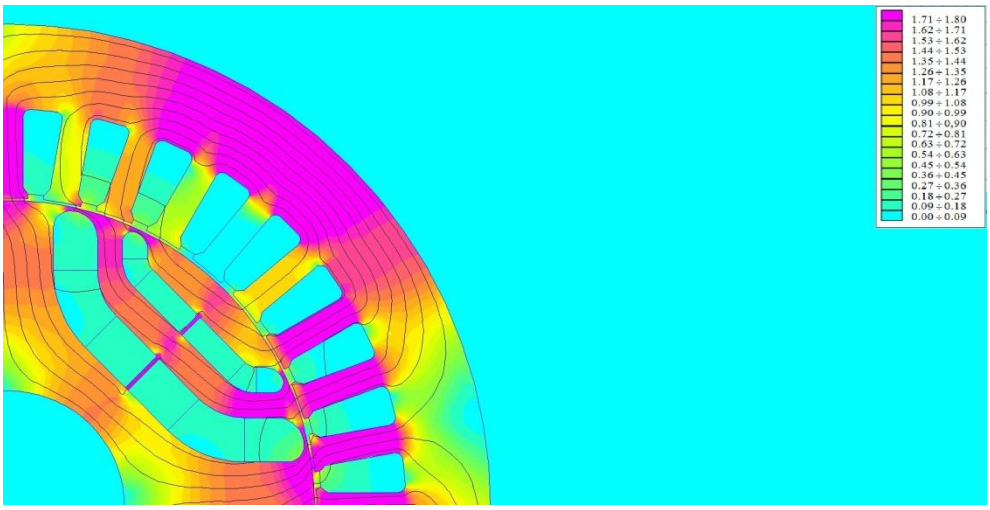

Fig. 130 - Flux density of injection prepared bonded magnets in the laboratory by means of commercial Ferrite pellets at the supply current of 10 A in MTPA loci condition

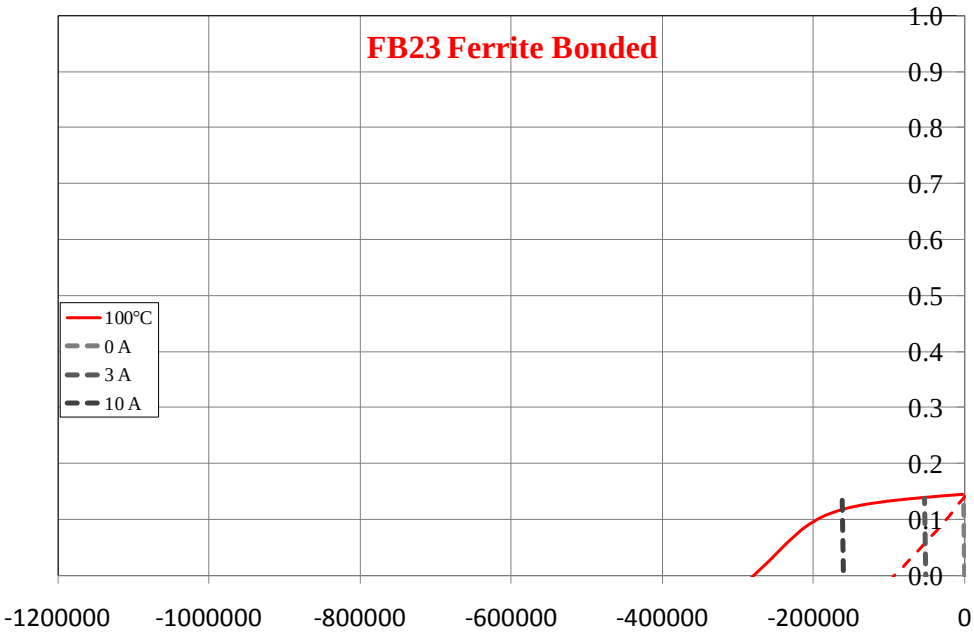

Fig. 131 - Interception between the demagnetization curve and load lines (0, 3 and 10 A) for Ferrite Bonded magnets (commercial pellets)

Overall all prototypes show good resistance to demagnetization. Nevertheless, experimental tests have been performed. The selected prototype is that with the Ferrite Bonded magnets (commercial pellets) because it is unique that can be demagnetized due to the aforementioned considerations, and the maximum applied current (10 A).

First of all, the no-load test at 750 rpm has been carried out and the voltage waveforms are shown in Fig. 132. The next step concerns to apply the maximum available current and measured again no-load test at the same condition. In Fig. 133 it is possible to observe that a slight demagnetization has happened. The reduction is about 27%. The final test has been done in order to try the re-magnetize the magnets reversing the

maximum currents. The no-load test at the same condition has been performed and the obtained voltage waveform values are shown in Fig. 134. The result is very close to the first performed test before the demagnetization (Fig. 132). The difference is minimum, about 5%; however, the very small demagnetization persists.

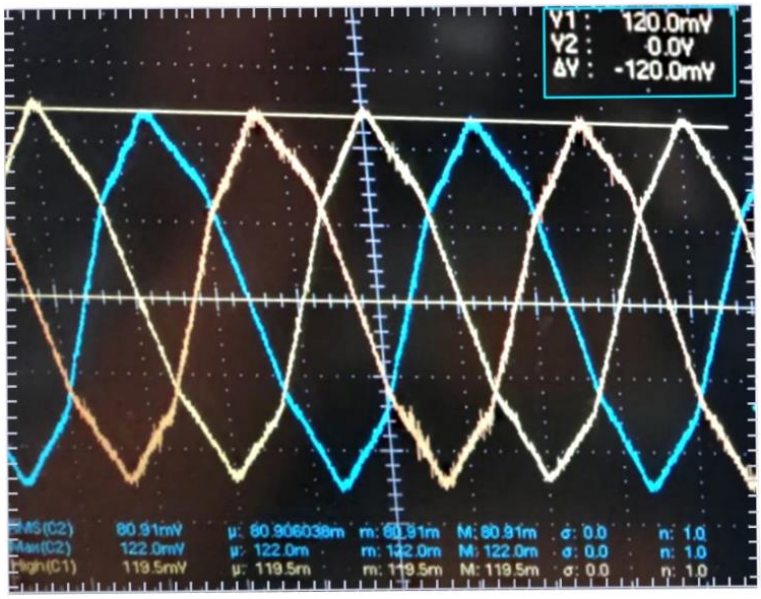

Fig. 132 – No-load test dragged at 750 rpm for the prototype with Ferrite Bonded magnets (commercial pellets)

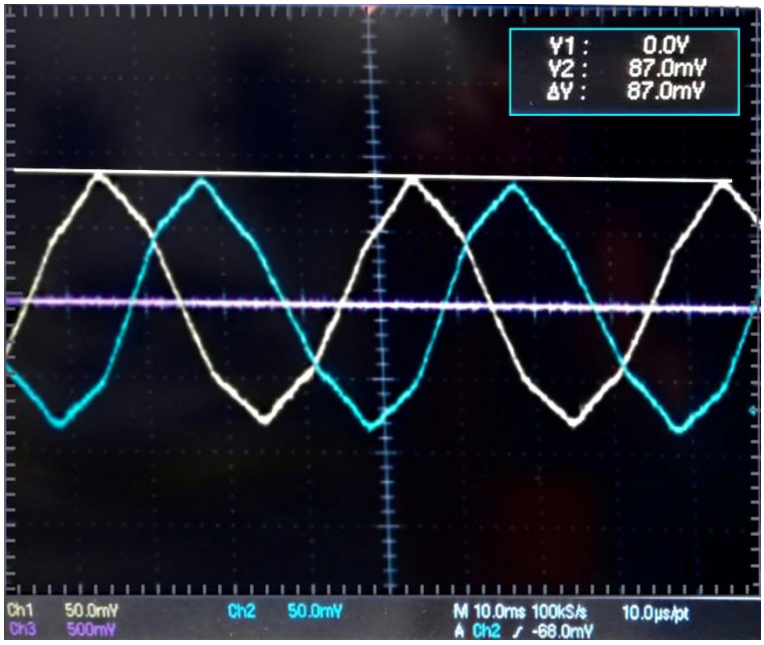

Fig. 133 – No-load test dragged at 750 rpm for the prototype with Ferrite Bonded magnets (commercial pellets) after the supply of 10 A

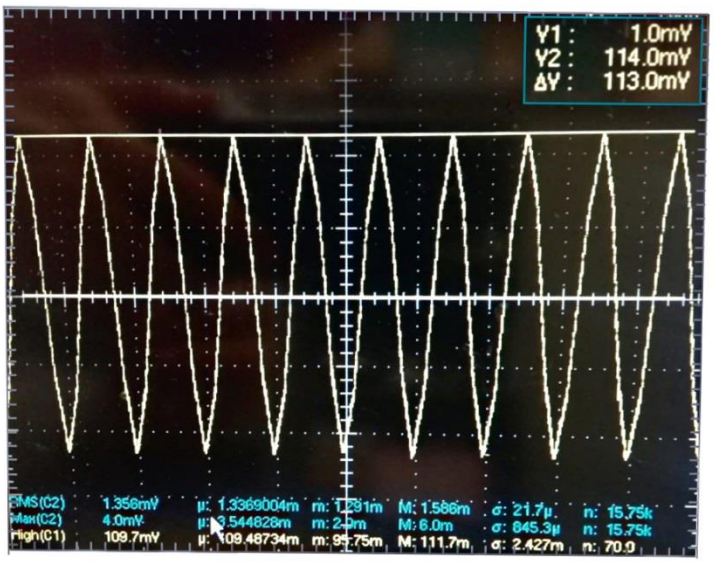

Fig. 134 – No-load test dragged at 750 rpm for the prototype with Ferrite Bonded magnets (commercial pellets) after the reversal of currents (10 A)

V.VI.VI Regular Bonded Magnets Analysis

A particular analysis, about the filling performance, has been carried out. The motor design with regular magnets has been adopted with self-prepared injection bonded magnets (PA6 Bonded 10wt%), as shown in Fig. 135. An investigation only with simulation tools has been performed. Therefore, the simulation results of the average torque values versus the current angle are reported in Fig. 136. At the rated condition the increase of torque value of 20% has been obtained with the full filling of flux barriers with respect to regular shape configuration using the same magnets typology. This result provides the success rate for filling of flux barriers with the bonded magnets.

Moreover, the demagnetization risk has been analyzed. The flux density at the supply current of 10 A has been reported in Fig. 137. The saturation distribution with the regular shape bonded magnets is less with respect to the full filling of flux barriers. Furthermore, the load lines of the regular magnets are steeper compared to bonded magnets for the full filling of flux barriers (Fig. 138). The overload capability is slightly larger with the use of regular shape configuration.

The possibility to completely fill the flux barriers in PMaSRM machine has been performed with very good results compared to traditional ones. The solution can be considered innovative and also effective in overload capability with the adoption of the NdFeB bonded magnets.

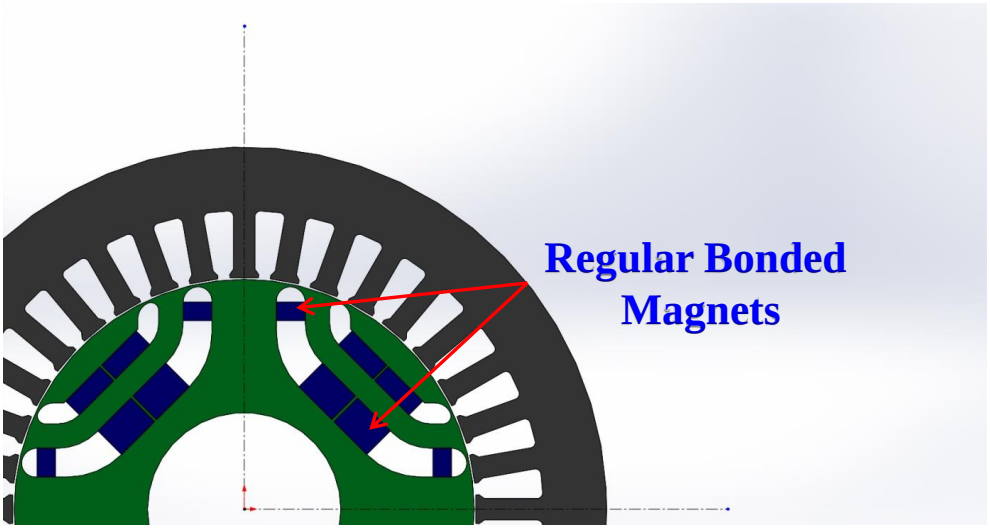

Fig. 135 – The rotor geometry with regular bonded magnets

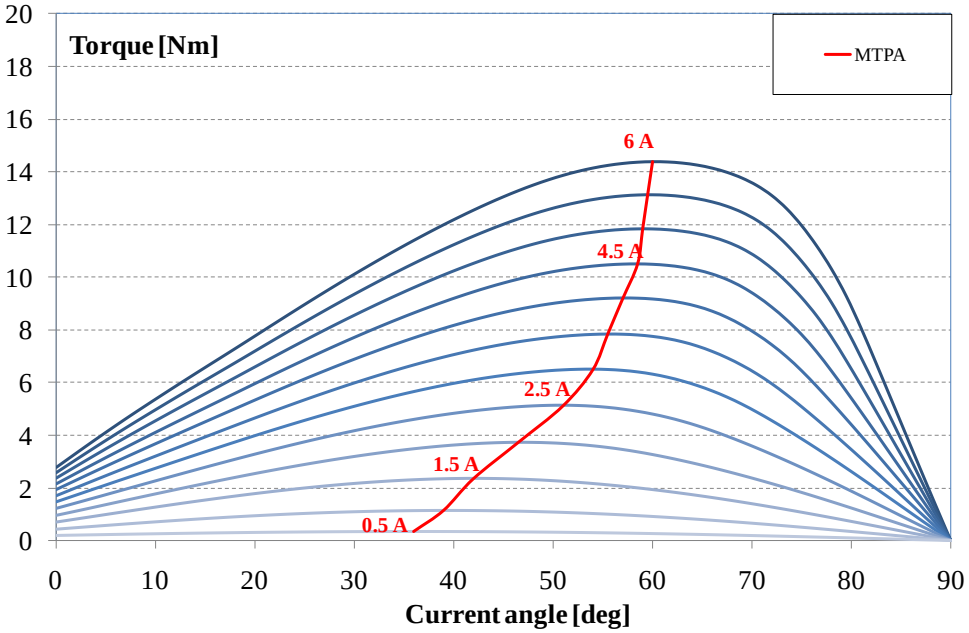

Fig. 136 – Average torque versus current angle of the PMaSRM with regular bonded magnets prepared by injection bonded magnets (PA6 Bonded 10wt%)

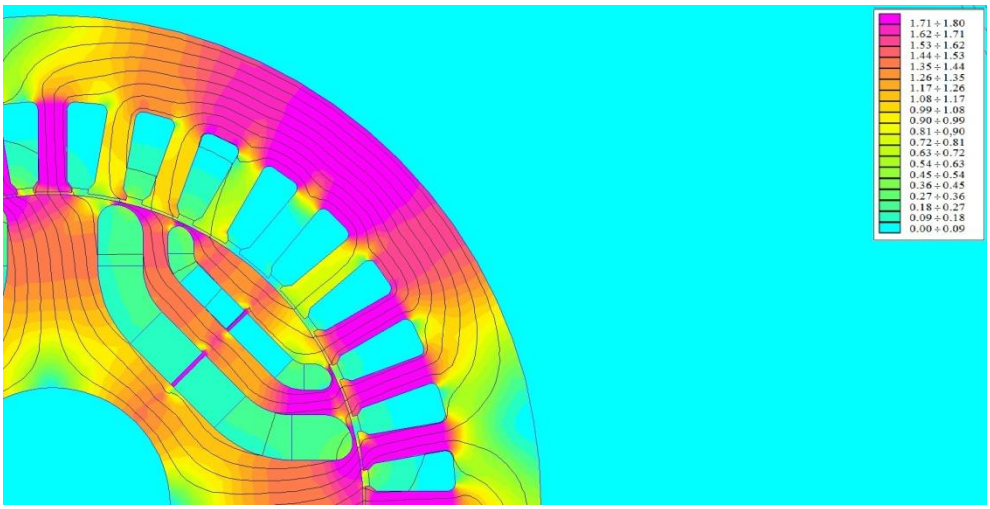

Fig. 137 - Injection self-prepared regular NdFeB bonded magnets flux density for the supply current of 10 A in MTPA loci condition

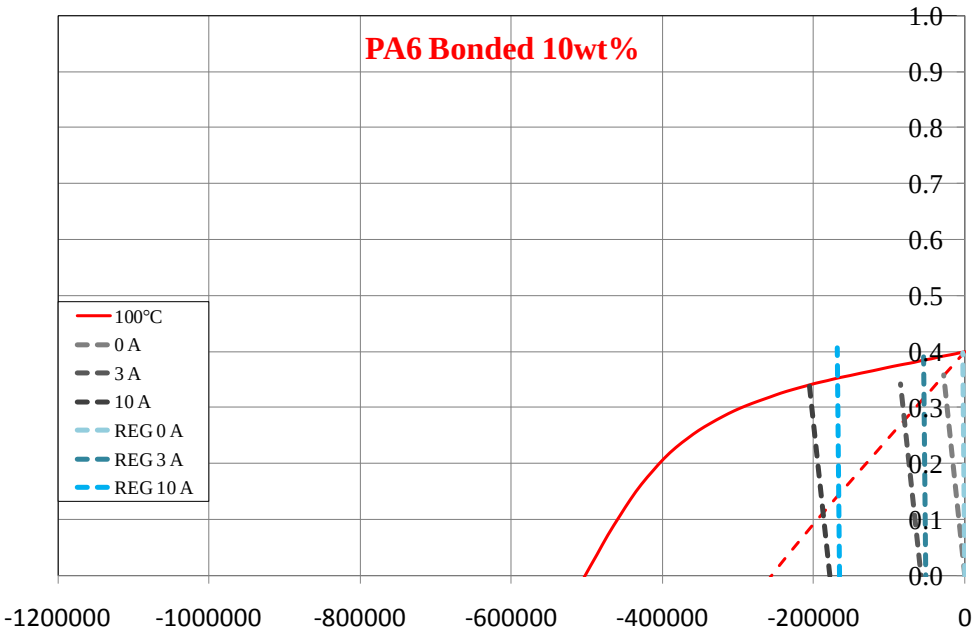

Fig. 138 – Comparison between regular and bonded magnets (PA6 NdFeB 10wt%):interception between the demagnetization curve and load lines (0, 3 and 10 A)

VI. BONDED MAGNETS APPLICATION: HALBACH MAGNETIZATION

In the case of curve magnets placed on the rotor ring, the magnetization direction assumes an important factor to affect the performances. Several magnetization types have been adopted, usually the parallel and the radial are the most applied in the radial flux machine (RFM) [97],[98]. Other options have been proposed and used [99], but in the last years the Halbach magnetization type seems to be the one presenting advantages for the maximum exploitation of the adopted magnets (Fig. 139) [100],[101]. Initially such magnetization has been introduced for linear electrical machine, to obtain a sinusoidal distribution of the magnetic induction and an increment of the rms voltage. Furthermore in this way a greater concentration of magnetic flux is obtained, resulting in a better performance with respect to the radial or parallel magnetization of the same magnets [102], [103]. Some applications already adopt this type of magnetization [104], [105-109] typically when the dimensions of the machine are big or where the magnetic ring is adopted; a special magnetization system is required and in both cases the process is expensive. For such reason in this research activity is tried to find another solution for the magnets realization.

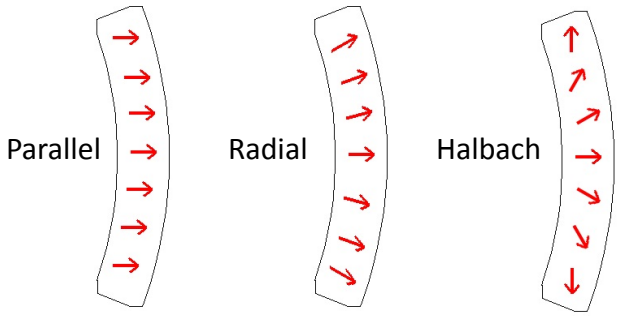

Fig. 139 – Magnetization patterns for curve shape of permanent magnets

It is necessary to dispose of a specific system to obtain the desired magnetization direction; it depends on the shape of the permanent magnets used in the electrical machine [110]. In fact, if the magnets have curve shape, there are some alternative procedures: the parallel and the radial magnetization, frequently adopted in many applications [97],[99],[111] and Halbach magnetization [112]; they provide different magnetic field distributions in the motor magnetic circuit. The process to magnetize results easier for parallel pattern than the others two, which require a special magnetic circuit.

A very special magnetization system should be necessary for the Halbach solution, very difficult to be realized and expensive too. Then the authors decided to realize the curve magnet by accosting many small elements, each presenting a magnetization with

different direction, in order to obtain an equivalent unique magnet globally presenting a Halbach magnetization. Such method may be difficult for ferrite or sintered materials, but it is relatively simple in the case of bonded magnets.

First of all the reference machine with radial magnetization has been selected. It is a Permanent Magnet Brushless DC motor (PM BLDC) with external rotor originally mounting the ferrite magnets, and adopting concentrated windings on the stator. In particular this machine had been equipped with bonded magnets [54],[55], as shown in Fig. 140, and a comparison between parallel and radial magnetization had been carried out [111],[113].

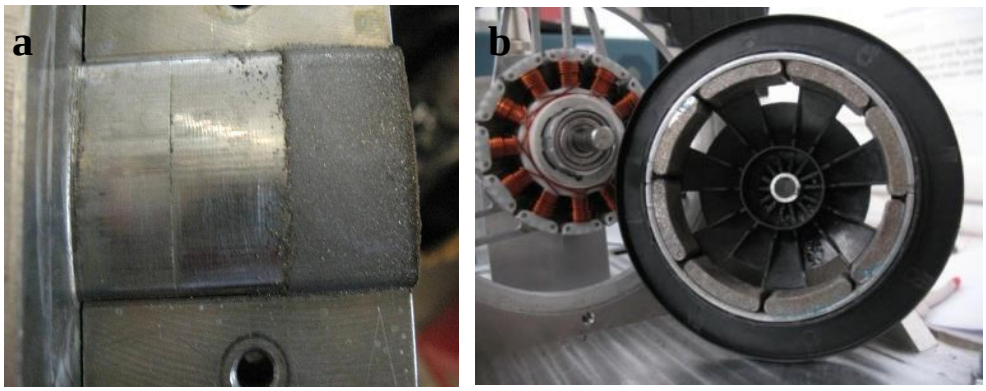

Fig. 140 - Molding of bonded magnets for reference radial flux machine: sample compaction (a) and rotor with bonded magnets (b)

The first phase of the activities is based on FEM simulations, to select for the reference motor the rotor structure with the opportune number of the elementary sectors, suitable to realize the Halbach magnetization. The choice of the appropriate number of sectors is shown in Fig. 141. In Fig. 142 the magnetic induction distribution is reported. The evaluations show an increment of the voltage of about 6% when Halbach magnetization is adopted [114].

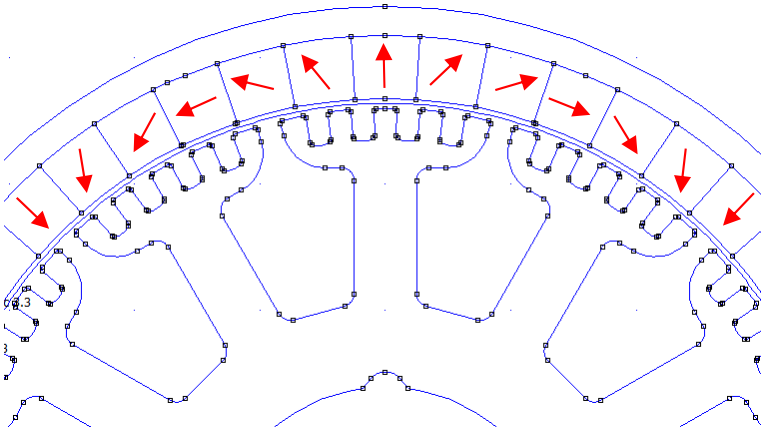

Fig. 141 - Magnetic rotor ring without bezels divided in the sectors

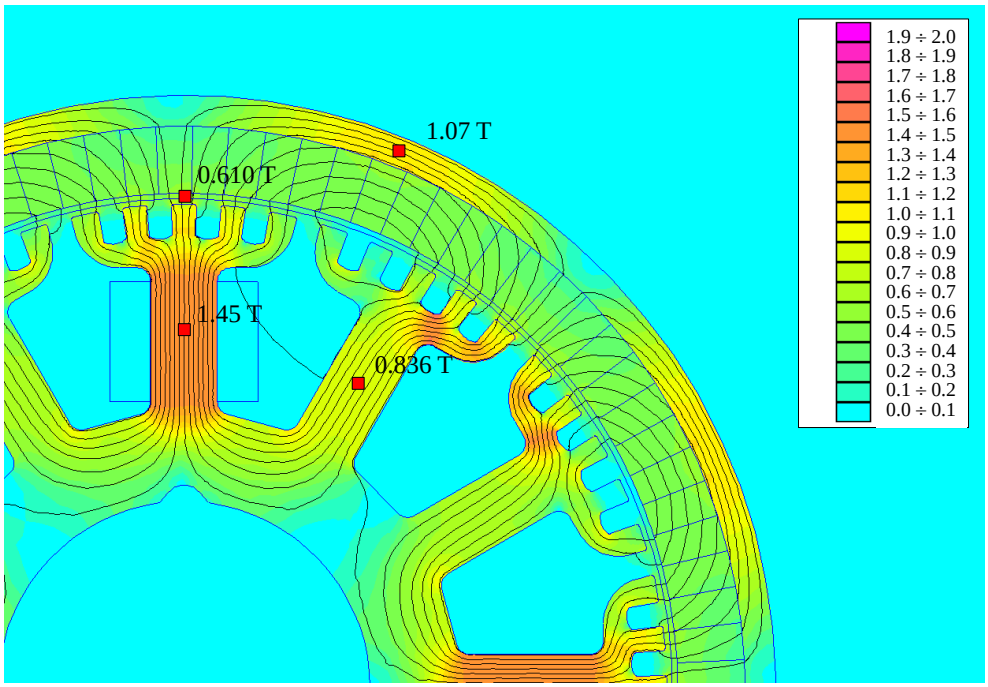

Fig. 142 – FEM simulation of the Halbach machine with 45° magnetic arc and without bezels at the extremities

Each sector is then magnetized in a particular direction approximating the Halbach pattern. The adoption of special magnetization coil is shown in Fig. 143. The expected efficiency increase has been verified starting from the original radial ferrites, to the radial bonded NdFeB, to the final sliced Halbach NdFeB, as reported in TABLE XVIII. The bonded magnets help the implementation of that high number of slices with respect to the sintered magnets, thus allowing the realization of the Halbach pattern (Fig. 144). The final rotor geometry with Halbach NdFeB Bonded magnets is reported in Fig. 145. It is important to note that Halbach and Epoxy Bonded magnets have the same magnetic characteristics; the difference is represented by the magnetization pattern.

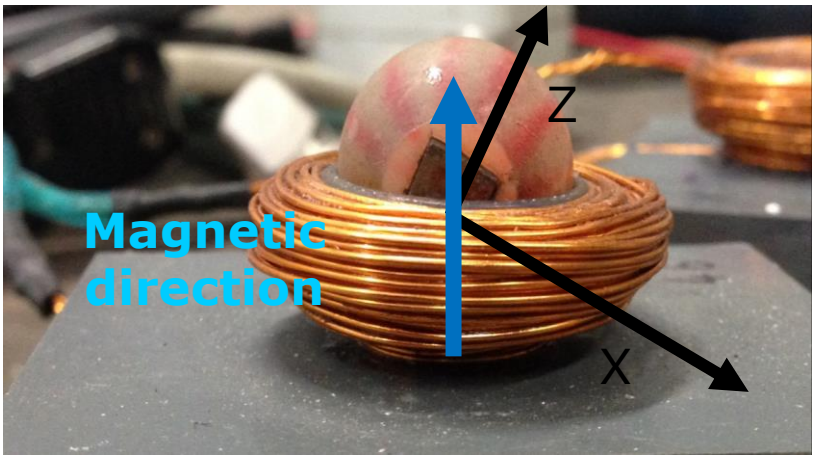

Fig. 143 – Special magnetization coil: design and procedure

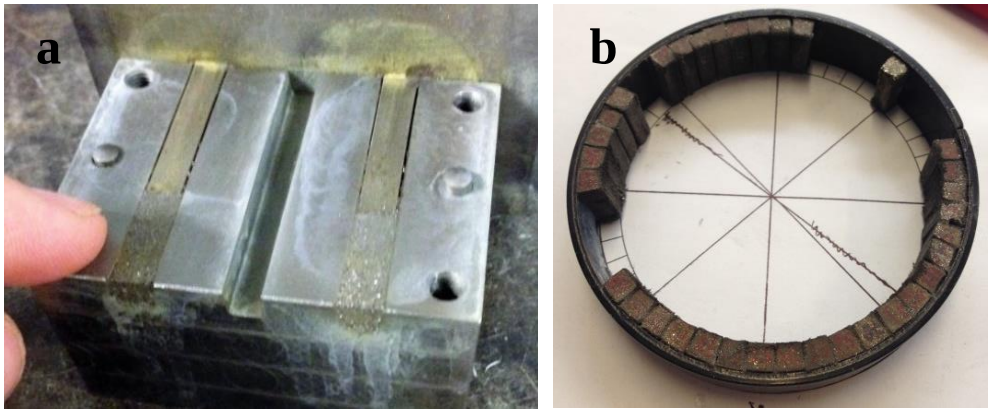

Fig. 144 - Realization of bonded magnets for Halbach pattern: moulding of magnetic sectors (a) and rotor preparation

Fig. 145 – Final rotor geometry with NdFeB Halbach Bonded magnets

TABLE XVIII – Efficiency of different magnet types and magnetization pattern

Rotor Typology	Efficiency [%]
Radial Ferrite	75.2
Radial Epoxy NdFeB	76.3
Halbach	77.2

VII. SMC MATERIALS AND APPLICATIONS

The SMCs are ferromagnetic particles covered by a layer, that can be of organic (resin) or inorganic (metallic oxide or ceramic insulation) typology. In general electrical machines are made with the SMCs adopting the production process of Powder Metallurgy; owing to such technology and SMC materials it is possible to design and realize complex structures of electrical machines, such as for example Axial Flux Machine (AFM), Transverse Flux Machine (TRM), Claw Pole Motor (CPM) and others [35],[46],[115-118]. Those typologies of electrical machines reach high efficiency and torque density.

In this research activity the SMC powders and their adoption in the realization of different electrical machines prototypes is presented. The performances of the proposed prototypes have been compared on the basis of electric and mechanical aspects.

Two SMC materials have been chosen for the aim of the work: a commercial one based on the metallic oxide layer and laboratory prepared ones using the epoxy and phenolic resins [5],[42]. The proposed epoxy resin is commonly used to glue components in electrical machines, while the phenolic resin is applied in brake applications. Both resins are normally adopted in high temperature applications; the phenolic one presents the advantage of an easier mix. The percentages in weight of polymeric binder suitable to produce the electrical machines are from 0.1 to 1%. The minor resin content guarantees the better magnetic properties but lower mechanical ones.

For the SMC materials produced in the laboratory, a specific mixing process has been conducted in order to guarantee the realization of an insulating layer. The following step consists to mold the powder in an appropriate form by means of a hydraulic press. The drawbacks in the use of hydraulic presses are represented by limited dimensions of the molded piece, especially in terms of thickness. Different compacting levels have been adopted from 400 to 800 MPa Fig. 146a); a mechanical machining process can be then necessary to get the final shape, as shown in Fig. 146b).

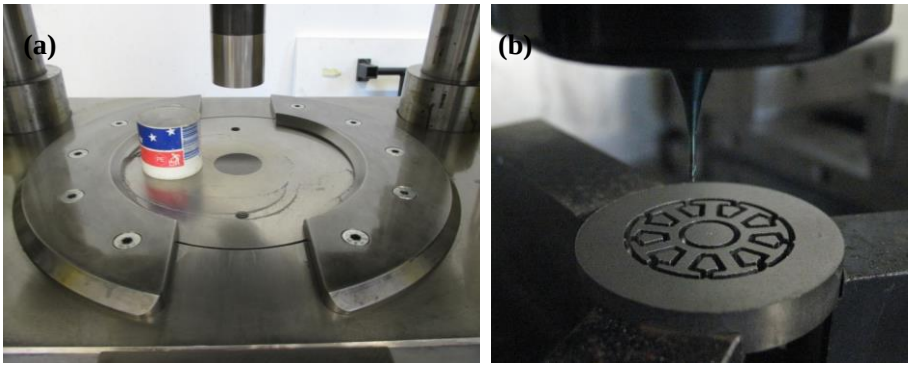

Fig. 146 – Production processes for SMC prototypes: compacting (a), and machining (b)

The final phase consists in a thermal treatment; for organic layer, the temperatures are low (100-200°C), instead for the inorganic the temperature is around 550°C.

Every SMC specimen have been classified with a letter indicating the binder type (for an instance, "P" for Phenolic and "E" for Epoxy) and indication of the binder content and the pressure level. For example "P 1-700" means Phenolic SMC with 1% of binder content pressed at 700 MPa.

Three different SMC materials have been compared in Fig. 147: a commercial one I.I.P.C (Insulated Iron Powder Compounds) and two mixtures created in the laboratories. All specimens have been compacted at 800 MPa; the SMCs developed in laboratories, Epoxy SMC and Phenolic SMC, have a binder content of 0.2% in weight. The house-created SMCs show the best results.

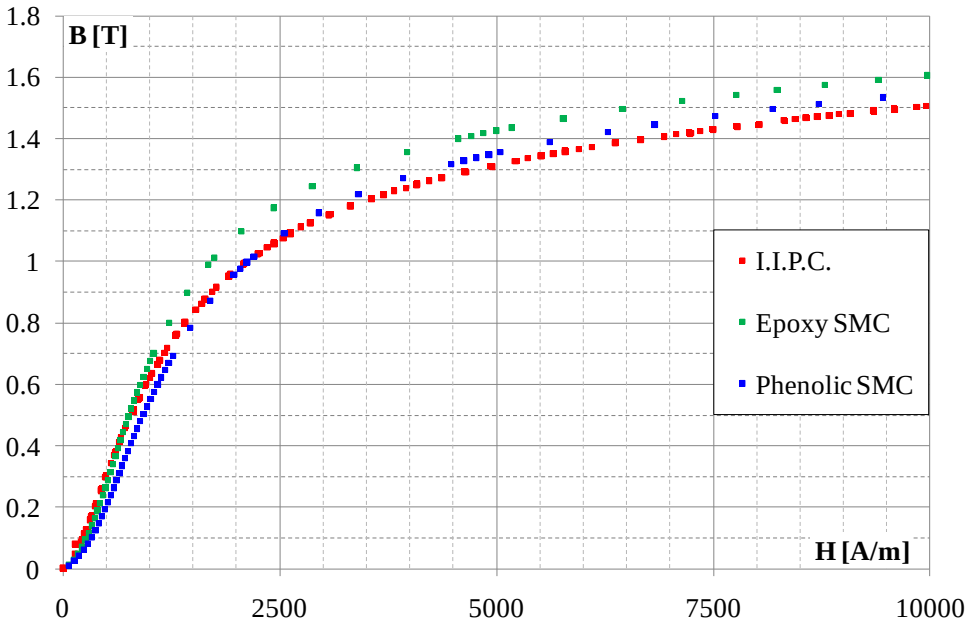

Fig. 147 - BH curves of proposed SMC

VII.I SMC Prototypes: the First Case

The prototype concerns an AFM motor with a rated torque of 2 Nm and DC link voltage of 48 V. This type of electrical motor is difficult to make in laminated steel, and it presents several advantages compared to radial flux machine: very high efficiency and reduced dimensions compared to a RFM of the same power. The SMC material is a commercial one, I.I.P.C.; the single disk has been worked (Fig. 148) and the final stator shape has been made in the laboratories (Fig. 149a). The prototype resulted very compact with a height of about 30 mm (Fig. 149b).

Fig. 148 - The machining of a single disk, the preparation of the stator slots

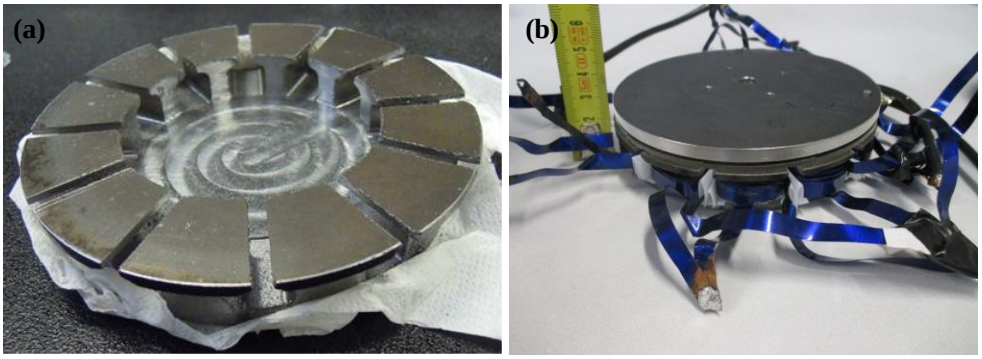

Fig. 149 - AFM stator (a) and final dimension of the prototype (b)

The torque-current characteristic has been determined by supplying the windings (two in parallel and then in series with third) with a DC current and measuring the torque by manually rotating the rotor [35]. This technique has been adopted because the driver available in the laboratory cannot work at 48 V. Nevertheless, the torque-current characteristic has been measured and has a very good comparison with analytical and simulated ones (Fig. 150). Accordingly, the experimental validation of the analytical results, makes possible to evaluate the efficiency in that way. The efficiency map has

been investigated as a function of speed and delivered torque as shown in Fig. 151; very high values have been obtained, over 90%.

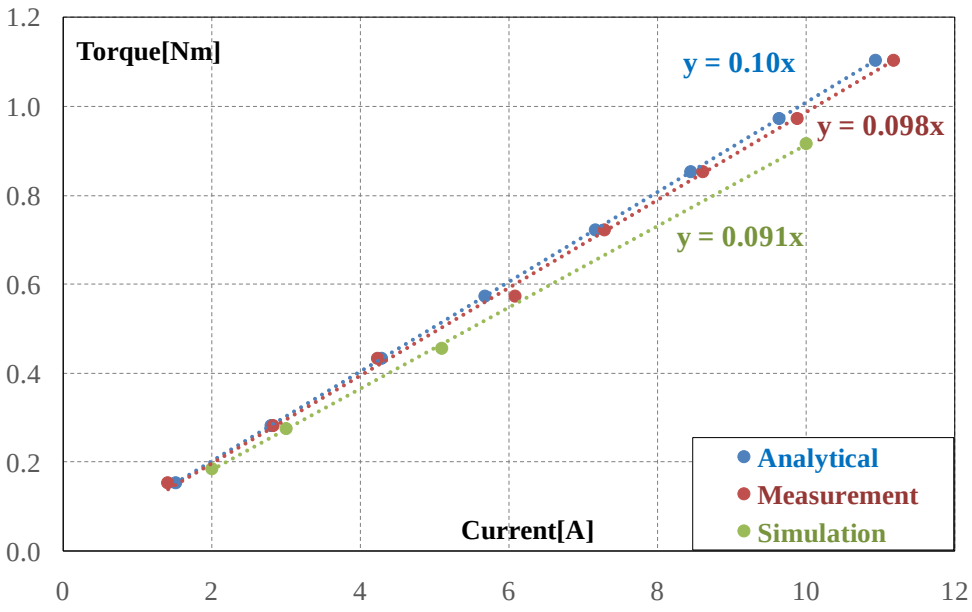

Fig. 150 - The torque-current characteristic: comparison for different methods (analytical sizing and FEM simulation) and measurement

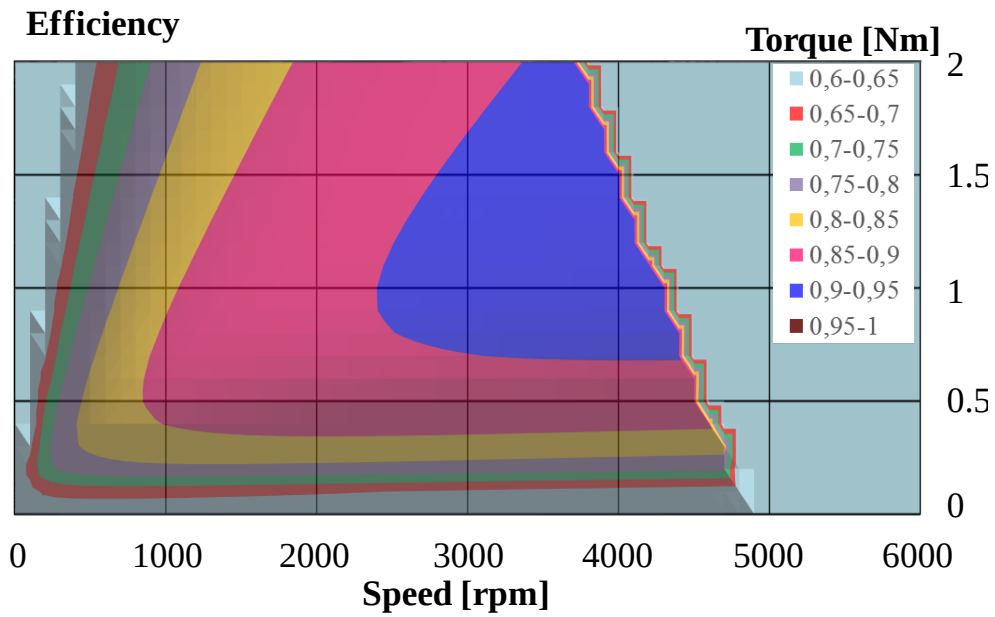

Fig. 151 - Efficiency map of proposed AFM prototype with the adoption of commercial SMC

VII.II SMC Prototypes: the Second Case

Another AFM motor, identical to the previous one, has been prepared using different SMC material. The Phenolic SMC produced in the laboratories has been adopted with a binder content of 0.2 % in weight. The AFM prototype has been prepared with a modular stator instead of a unique piece (Fig. 152), as the previous case. In this way the

process is simpler and faster compared to a unique piece; moreover, the assembly is easy. The construction of the prototype starts from the machining of a disk (40mm) until the assembly of the final stator by means of bonding the single pieces (Fig. 153).

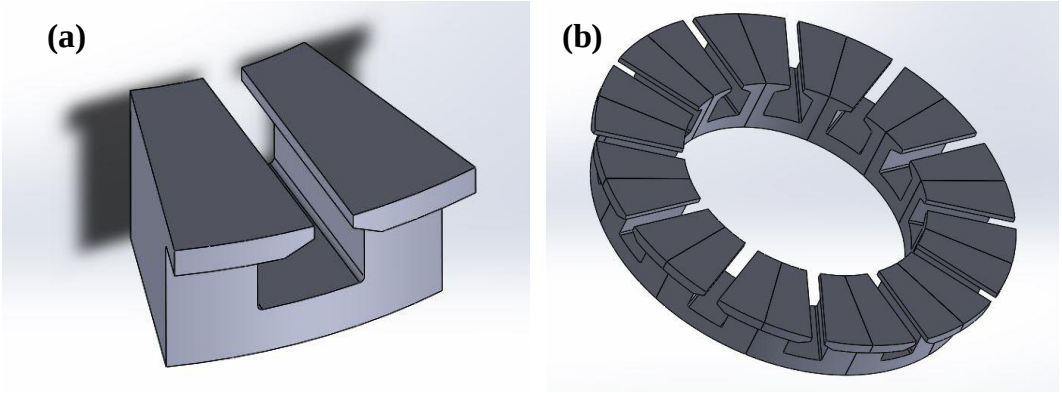

Fig. 152 - Modular stator: single machined part (a) and final stator design (b)

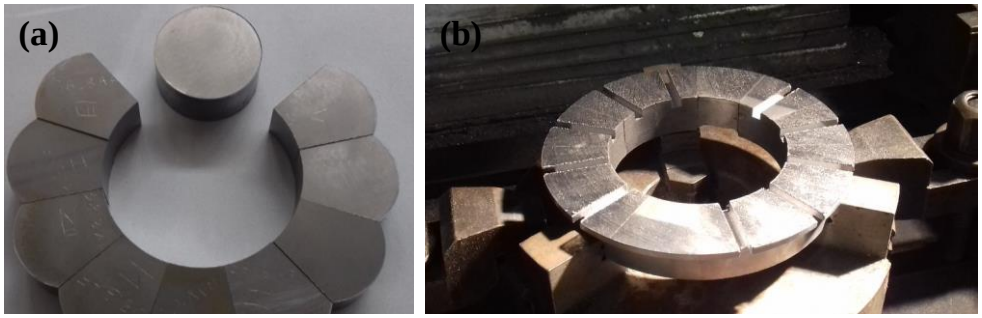

Fig. 153 - The prototype preparation: from a machined disk (a) to the assembly of modular stator (b)

Once the prototype has been completed, the torque-current characteristic has been investigated performing the same test of the previous case. The graph reported in Fig. 154 shows similar characteristics for both prototypes, even better for the machine realized with the SMC developed in the laboratory.

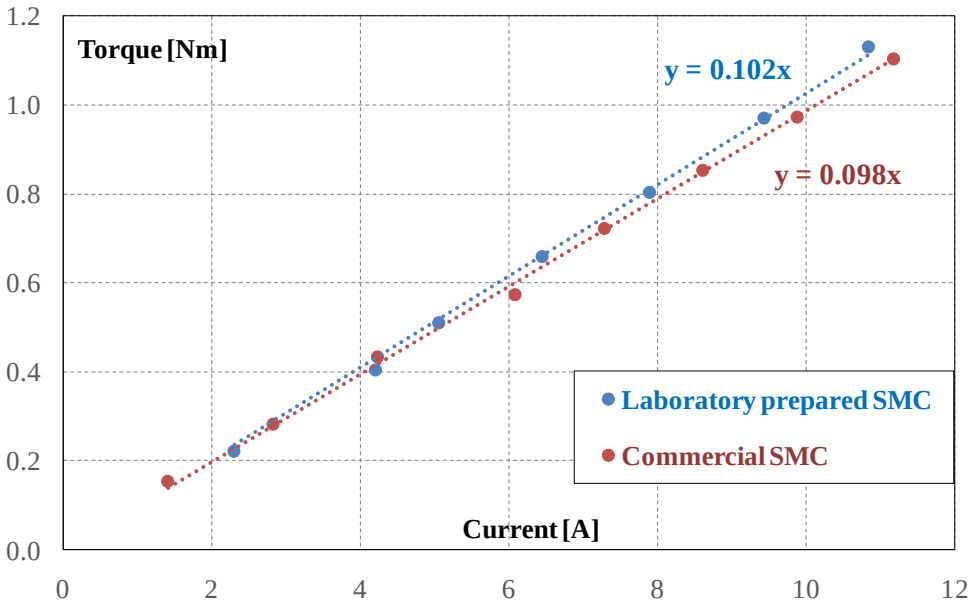

Fig. 154 - The torque-current characteristic: comparison of laboratory prepared SMC and commercial one

Moreover, as a weak point of the commercial powder is represented by the mechanical properties, a further investigation has been carried on to evaluate and compare the mechanical strengths of the commercial powder and of the ones prepared in the laboratory. Several specimens have been prepared with different pressure levels, and the mechanical properties have been evaluated and expressed through the Transverse Rupture Strength (TRS), as shown in Fig. 155, that is measured by means of the bending test and is expressed in MPa.

The TRS values of Phenolic SMC are always higher with respect to commercial one, mostly for high pressures beyond the 700 MPa where the mechanical strength remains almost constant. Furthermore, the mechanical strength of the stator prepared with Phenolic SMC is better than a commercial one; this is well evident by observing the edges Fig. 156. The SMCs prepared in the laboratory are interesting materials, allowing the same motor performance but better mechanical strength compared to the commercial one.

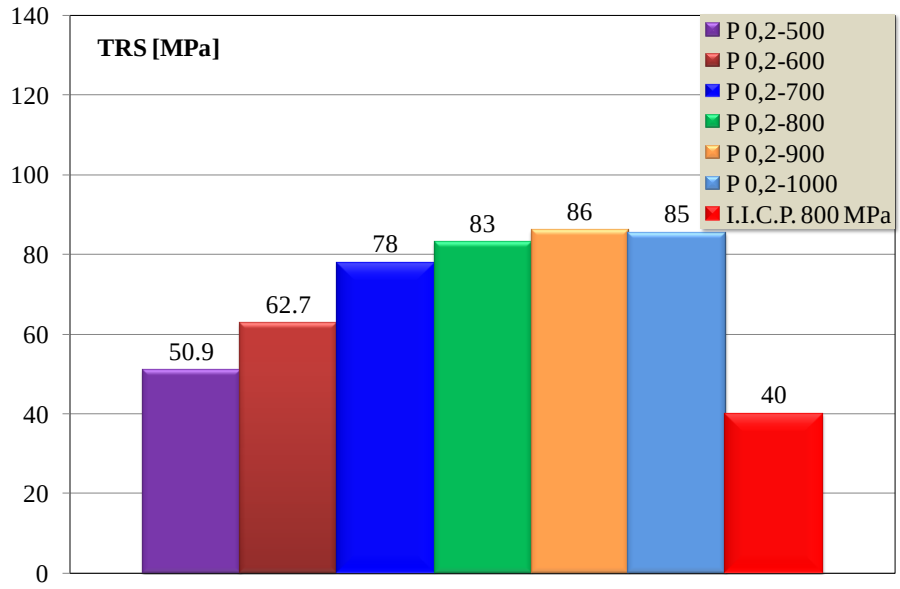

Fig. 155 - TRS values as the function of molding pressure for proposed SMC materials

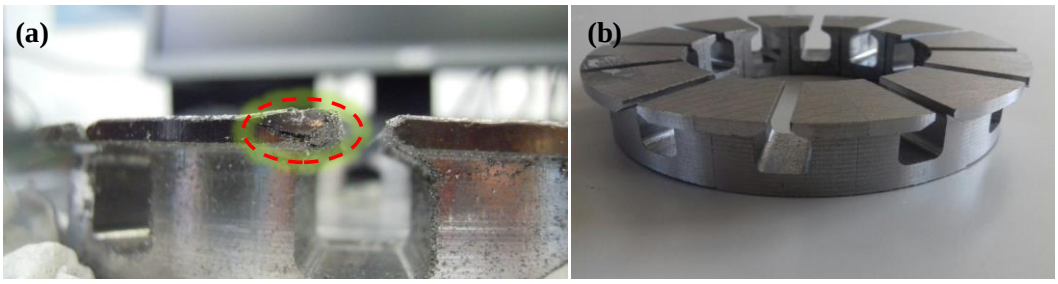

Fig. 156 - Prototype comparison between commercial and self-prepared SMC: some mechanical defects are evident with the commercial powder

VII.III SMC Prototypes: the Third Case

In the last case, the AFM prototype has been made with magnetization during the molding process [119]. The magnetization has been applied in the phase of compression of the powder (Fig. 157). This technique cannot be adopted in the case of permanent magnets for the reason of their very low relative permeability. The Phenolic SMC has been adopted and compacted at 600 MPa. The BH curve with the applied magnetic field (M) shows a higher trend with respect to the no magnetized SMC (NM), as reported in Fig. 158.

The AFM prototype of about 100 W has been realized (Fig. 159) and reached an efficiency of 81%, an interesting result for such motor power size, where typically the performances are lower. The efficiency map has been evaluated from the measurements of delivered torques for various speeds, as shown in Fig. 160. The torque values are fixed and the electric power absorption has been detected while varying the speed. Such test has been performed by means of an inverter, supplying the motor until 12 V and controlling the speed with a proper commanding law.

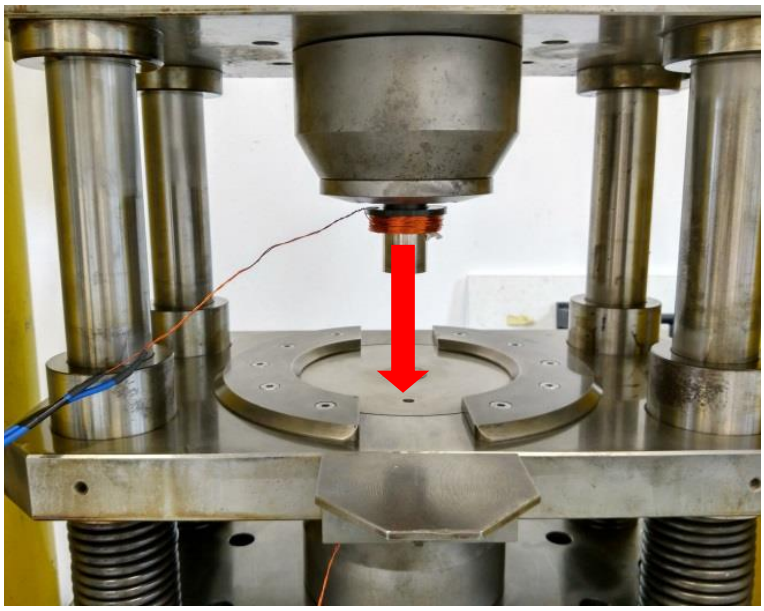

Fig. 157 - Magnetic lines directions: application of the parallel magnetic field during the compaction

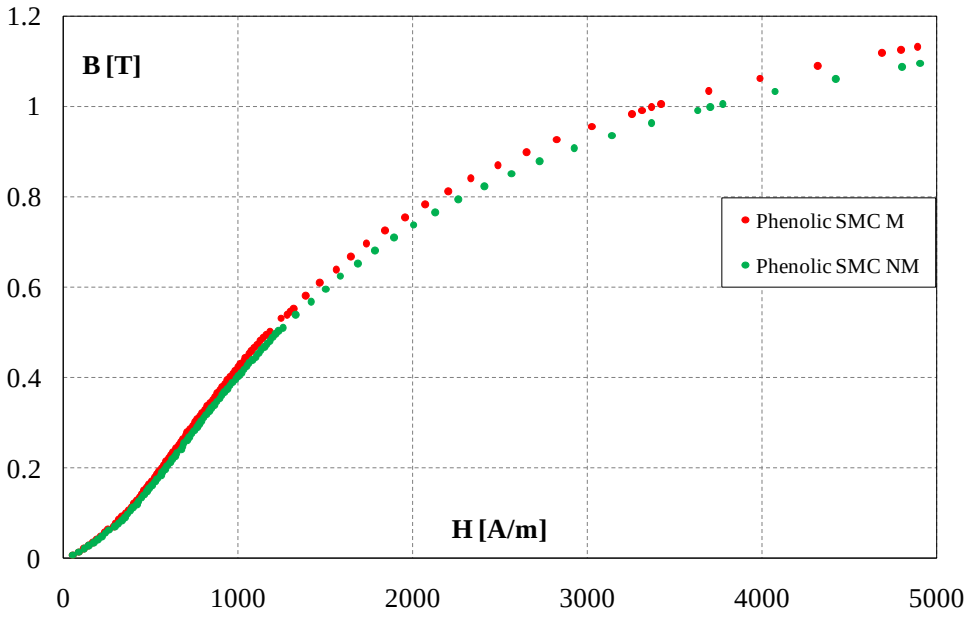

Fig. 158 – BH curves of Phenolic SMCs with (M) and without (NM) magnetization implementation

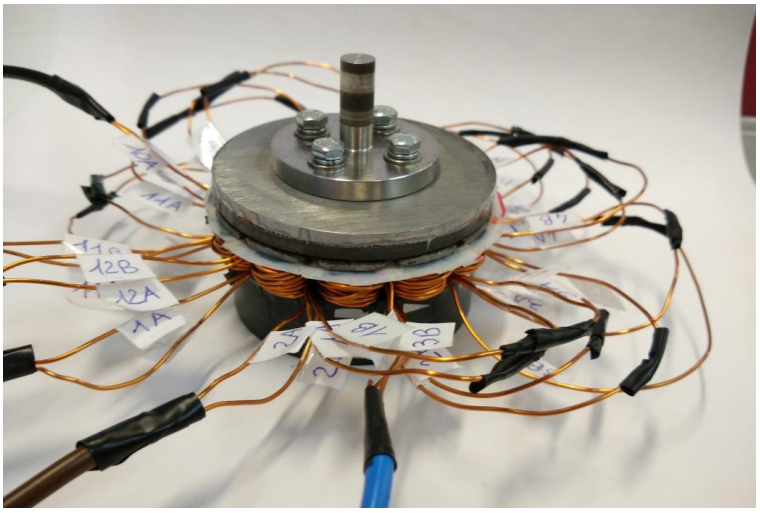

Fig. 159 - AFM prototype with production process implementation

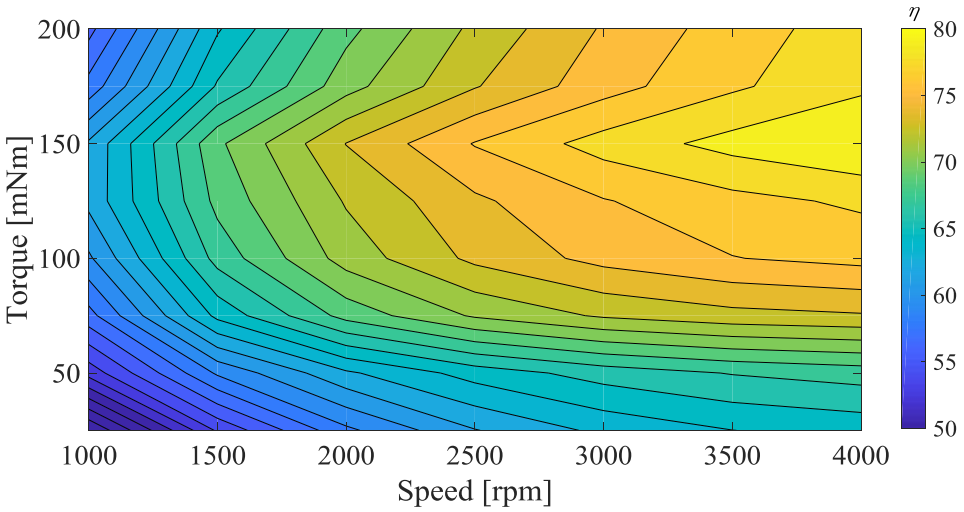

Fig. 160 - Efficiency map of AFM prototype made with the magnetization during the molding process

VIII. HMC MATERIALS AND APPLICATIONS

One of the most important properties of a material made of powder is the possibility to mix raw materials from very different fields. The idea of producing hard magnetic materials behaving like the AlNiCo alloys led to the preparation of Hybrid Magnetic Composites (HMCs). These kinds of materials, made by a part of hard magnetic powder and a part of soft magnetic powder, generally show a high remanence and a low coercive field. They are efficiently used as flux generators in magnetic sensor applications, thanks to their steep magnetic characteristic. Furthermore they can represent a specific solution for the adoption in electrical machines, as for an instance, in variable flux memory machine.

The preparation of HMCs is very similar to bonded magnets by compression moulding; the main difference consists in the use of very pure Iron powder as soft part of the proposed material. The same aforementioned hard magnetic powder has been used to prepare the mixture, with the addition of phenolic resin to improve and obtain a satisfactory mechanical resistance.

Various hybrid magnets have been made in our laboratories, and different properties have been evaluated. The proposed hybrid magnets have been classified in the following way: the first letter identifies the magnet typology (H for hybrid magnet), the second letter is referred to the type of resin (P for phenolic), the first two digits the resin content and the last two digits the Iron percentages in the weight. For example, HP 1.8 20 corresponds to a hybrid magnet with phenolic resin content at 1.8% in weight and 20% in weight of Iron.

The effect of Iron content in the material consists in a high variation of the intrinsic coercive magnetic field with a slight change in the remanence value. The proposed Iron percentages are 20, 30, 40 and 50 wt%. All samples have been compacted at 600 MPa; the resin content has been fixed at 1.8% in weight. Increasing the Iron content impacts as a reduction of the coercivity obtaining a very steep magnetic characteristic, as shown in Fig. 161. Interesting results have been obtained with 30 and 40 wt% of Iron content.

As it was already done for bonded magnets by compression and injection moulding, the binder content effect has been analyzed. The resin percentages in weight are 0.8, 1.2, 1.5 and 1.8%. The Iron content has been fixed at 30 wt% and the same compaction pressure, 600 MPa, has been applied. The results reported in Fig. 162 show a small improvement with the reduction of the resin content.

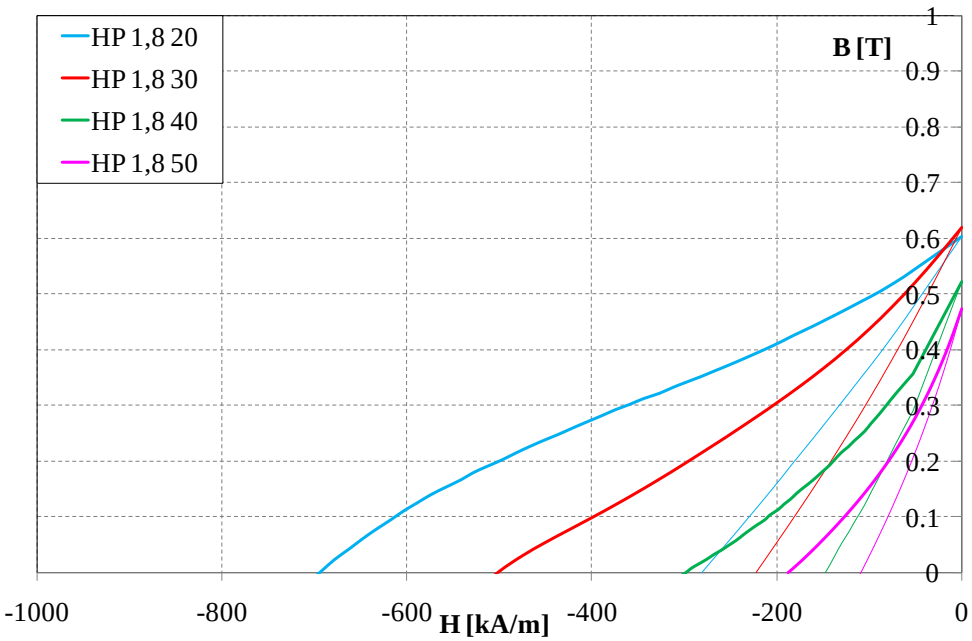

Fig. 161 – Demagnetization curves of phenolic hybrid magnets for different Iron content

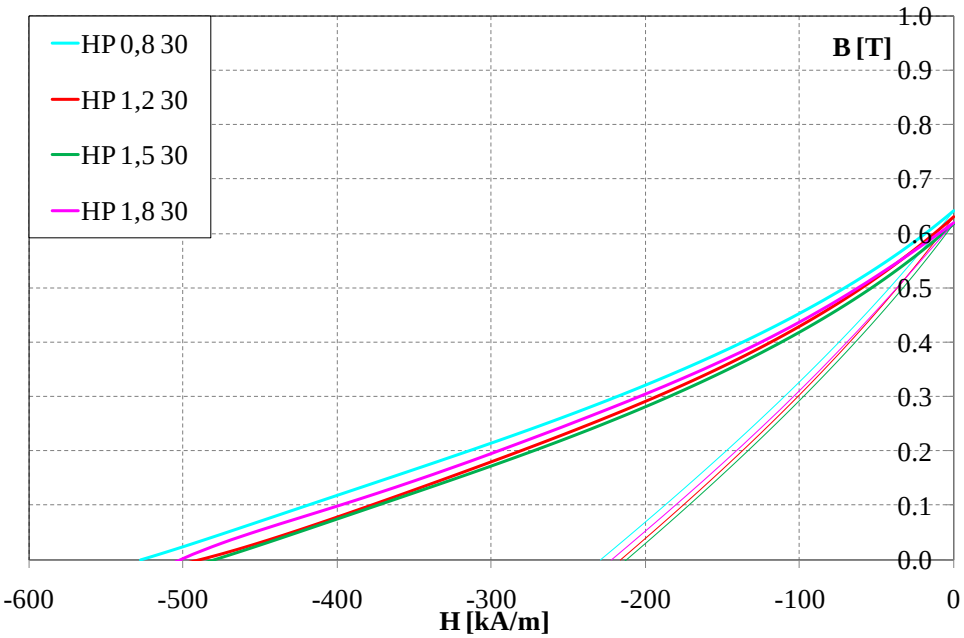

Fig. 162 - Demagnetization curves of phenolic hybrid magnets for different binder content

VIII.I HMC Applications

The materials of this family, made by a part of hard magnetic powder and a part of soft magnetic powder, can be efficiently used as flux generators in magnetic sensor applications, thanks to their steep magnetic characteristic. The preparation of HMCs is very similar to bonded magnets by compression moulding.

Hybrid magnets are particularly suited for sensor applications, like electric guitar pickups or inductive encoder transducers. Prototypes of both applications have been

realized (Fig. 163) to perform a comparison with the original systems equipped with their traditional magnets. The main HMC property, i.e. the high remanence value, induces a consistent voltage in the winding, due to the variation of the total airgap seen by the magnet.

The results obtained with the proposed hybrid materials were better than those of the traditional ferrite and AlNiCo magnets, in terms of the output voltage level (Fig. 164).

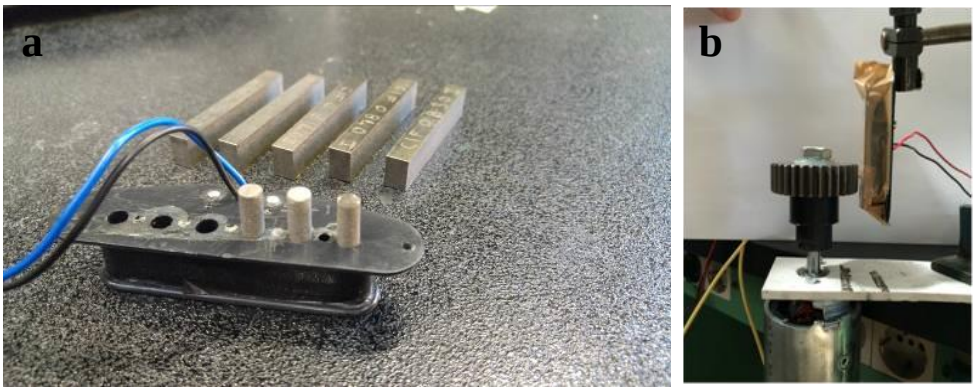

Fig. 163 – Hybrid magnets applications: guitar pickup (a) and encoder wheel (b)

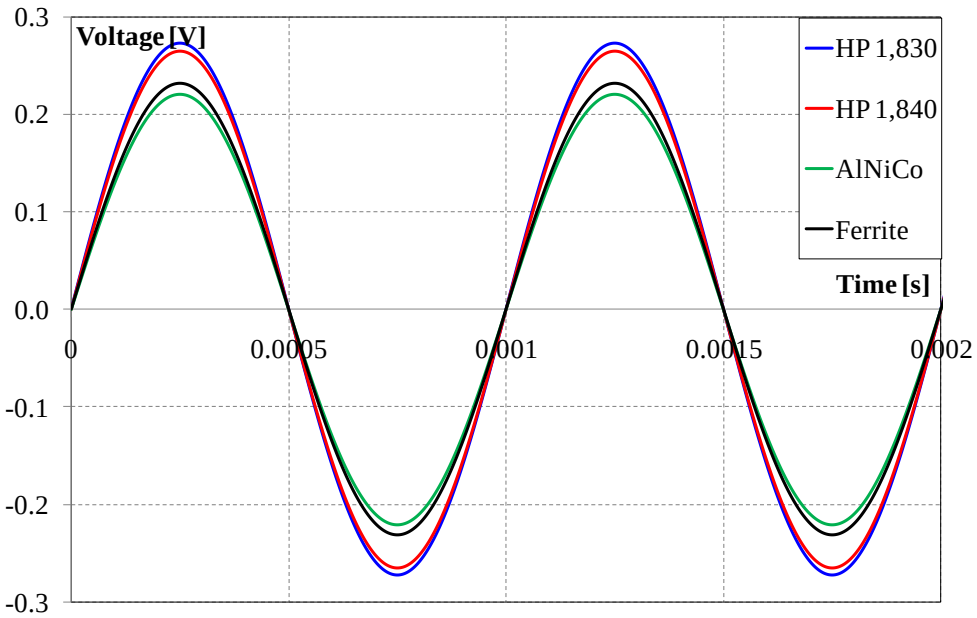

Fig. 164 - Comparison of encoder voltage values for different magnets materials: AlNiCo, Ferrite and Hybrid magnets

IX. CONCLUSIONS AND FUTURE WORK

The interesting results about the utilization of bonded magnets in PM-assisted reluctance machine have been shown. The compression technology allows to obtain better magnetic properties, while, on the other hand, the injection moulding is more suitable to an industrial process, mainly in terms of production rates.

Very promising results have been obtained concerning the torque value and the factor compared to synchronous reluctance (SRM) machine and regular anisotropic ferrite magnets assisted reluctance machine. Such as, an increment over 50% has been noted in the PMaSRM with compression moulded bonded magnets. The same prototype has a power factor of 0.96 at rated condition, much higher than SRM (0.70). Furthermore the bonded magnets permit to overload the PMaSRM motors without risk of magnets demagnetization as in the case of ferrites.

An investigation on the use of flexible bonded magnets in the flux barriers geometry has been carried out: this type of bonded magnets cannot use in the proposed rotor geometry for poor mechanics. The solution consists of other rotor geometry design with the different magnetic arc.

Different electrical motor prototypes have been examined using the SMC materials to prepare the magnetic core. For axial flux machines, the use of SMCs allows very high efficiency and the reduction of dimensions obtaining compact motors. Furthermore the possibility to make modular parts provides the assembly very easy. The application of a magnetic field during the molding process permits an improvement of magnetic properties, less iron losses of about 5% and BH curve higher compared to ones without the use of magnetization in the manufacturing process. Also, a comparison between commercial SMC materials and those developed in the laboratories has been made; a better mechanical strength has been found in self-prepared SMCs.

Different HMC materials have been produced and characterized. HMCs can be efficiently used as flux generators in magnetic sensor applications and, maybe in variable flux memory machine. However, the study of using such materials in the variable flux memory machine will be conducted in the future in other research activity.

Also, interesting novel measurement and characterization methods have been proposed and developed in the laboratory. The first, contactless thermographic method, has been adopted in the visualization of the iron losses distribution and for the defect detection in electromagnetic devices and soft magnetic materials. The novelty of the suggested method lies in the possibility to investigate devices with any shape and dimension, without the need of a special test equipment's (as for instance, vacuum chamber or

necessity to use only in the laboratory). The reliability of the presented method allows to consider its adoption also in the research activity concerning SMC materials (Fig. 165), which are becoming an important item for further developments in the electromagnetic devices production.

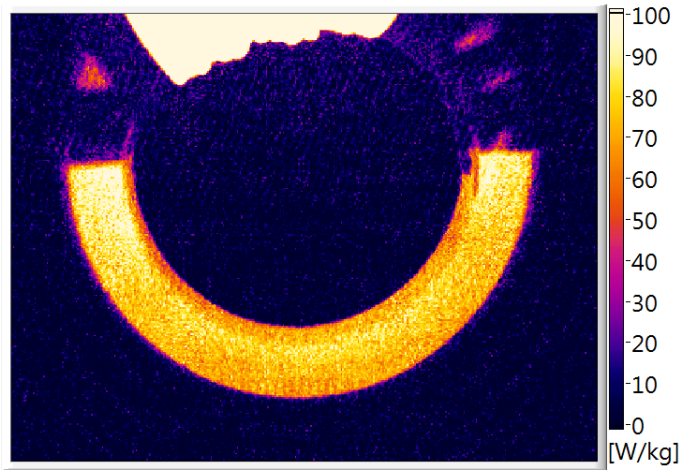

Fig. 165 – Iron losses distribution analysis of proposed SMC: 1T at 1000Hz for excitation time of 0.2 seconds

The second method consists to evaluate the cogging and hysteresis torque in radial flux machines (Fig. 166). The appropriate test bench is cheaper and does not need the use of a gearbox. The novel method is more accurate than the conventional one used to detect the cogging torque; though the measurement time is slightly longer (about 30 minutes of duration).

The further studies and optimization of these interesting measurement methodologies will be improved in the future research activities.

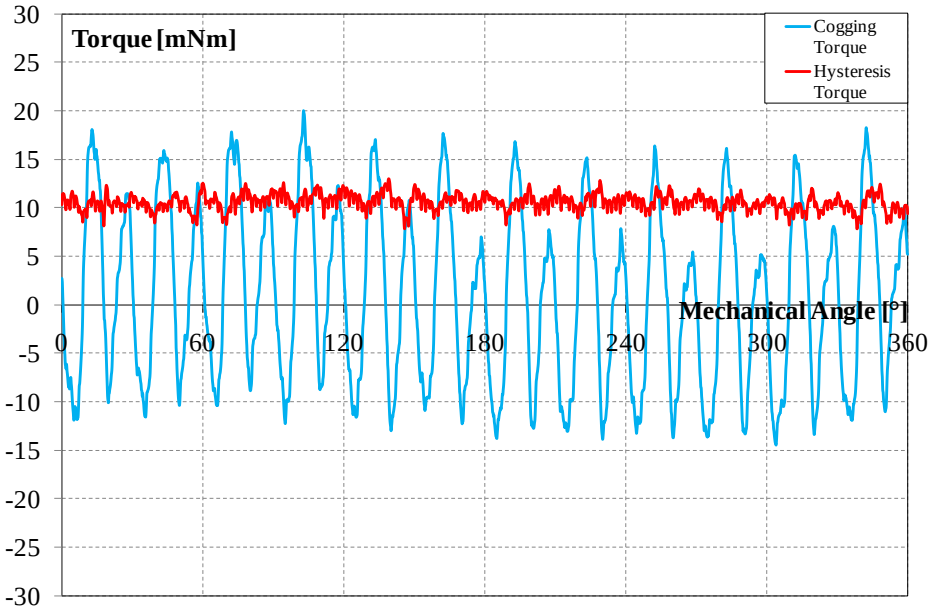

Fig. 166 - Novel method: Cogging and hysteresis torque of anisotropic ferrite with SMC core

X. REFERENCE

[1] G. V. Kurlyandskaya, S. V. Shcherbinin, S. O. Volchkov, S. M. Bhagat, E. Calle, R. Pérez, M. Vazquez, "Soft magnetic materials for sensor applications in the high frequency range". *J. of Magnetism and Magnetic Materials*, 459, 1 August 2018, pp. 154-158.

[2] H. Nakamura, "The current and future status of Rare Earth permanent magnets", *Scripta Materialia*, 154, September 2018, pp. 273-276.

[3] A. Boehm, I. Hahn, "Comparison of soft magnetic composites (SMCs) and electrical steel", *IEEE EDPC Conf*., Nuremberg (Germany), 15÷18 October 2012, Conf. Proc.

[4] A. Krings, M. Cossale, A. Tenconi, J. Soulard, A. Cavagnino, A.Boglietti, "Magnetic Materials used in electrical machines", *IEEE Industry Applications Magazine*, pp. 21–28, November/December 2017.

[5] M. Actis Grande, L. Ferraris, F. Franchini, E. Pošković, "New SMC materials for small electrical machine with very good mechanical properties", *IEEE Trans. On Ind. Appl*., Vol. 54, pp 195 – 203,January/February 2018.

[6] K. J. Sunday, M. L. Taheri, "Soft magnetic composites: recent advancements in the technology", *Metal Powder Report*, Vol. 72, pp. 425-429, November/December 2017.

[7] J. A. Bas, J. A. Calero, M. J. Dougan, "Sintered soft magnetic materials. Properties and applications", *J. Magnetism and Magnetic Materials*, 254-255, 2003, pp. 391–398.

[8] G. E. Fish, "Soft Magnetic Materials", *Proceedings of the IEEE*, 78, pp. 947 – 972, June 1990.

[9] A. Hassanpour Isfahani, S. Vaez-Zadeh, "Line start permanent magnet synchronous motors: Challenges and opportunities", *Energy*, 34, 2009, pp. 1755–1763.

[10] J. R. Riba, C. López-Torres, L. Romeral, A. Garcia, "Rare-earth-free propulsion motors for electric vehicles: A technology review", *Renewable and Sustainable Energy Reviews*, 57, 2016, pp. 367–379.

[11] J. F. Gieras, "Permanent Magnet Motor Technology: Design and Applications", Third Edition, Dordrecht, Germany: *CRC Press*, 2009.

[12] O. Gutfleisch, M. A. Willard, E. Brück, C. H. Chen, S. G. Sankar, J. P. Liu, "Magnetic Materials and Devices for the 21st Century: Stronger, Lighter, and More Energy Efficient", *Adv. Mater*., 23, 2011, pp. 821–842.

[13] H. Cai, B. Guan, L. Xu, "Low-cost ferrite PM-assisted synchronous reluctance machine for electric vehicles", *IEEE Trans. On Ind. Electron*., 61, pp. 5741-5748, October 2014.

[14] B. E. Davies, R. S. Mottram, I. R. Harris, "Recent developments in the sintering of NdFeB", *Materials Chemistry and Physics* 67, 2001, pp. 272-281.

[15] P. C. Dent "Rare Earth elements and permanent magnets", *J. of Applied Physics* 111, 2012.

[16] A. S. Rao, "Alnico permanent magnets an overview", *IEEE EEIC/ICWA Exposition*, Chicago (USA), 4÷7 October 1993, Conf. Proc. pp. 373 – 383.

[17] Q. Xing, M. K. Miller, L. Zhou, H. M. Dillon, R. W. McCallum, I. E. Anderson, S. Constantinides, M. J. Kramer, “Phase and elemental distributions in Alnico magnetic materials”, *IEEE Trans. on Magn*., 49, pp. 3314-3317, July 2013.

[18] A. Grujić, J. Stajić-Trošić, M. Stijepović, J. Stevanović, “Market and applications of bonded magnets”, *Economics Management Information Technology*, Vol. 1, 2012, pp. 151-158

[19] R. Wolf, “Recent History, Current Events and the Future of Rare Earth and ferrite magnets”, *Asian Metal Rare Earth Summit*, New York (USA), 15÷17 May 2013.

[20] W. Ervens, H.Wilmesmeier, “Magnetic Materials” in *ULLMANN'S Encyclopedia of Industrial Chemistry*, Vol. 22, Weinheim (Germany):Wiley-VCH Verlag, 2012, pp. 79-131.

[21] M. Sugimoto “The Past, Present, and Future of Ferrites”, *J. American Ceramic Society*, 82, 1999, pp. 269–280.

[22] A. Schoppa, P. Delarbre, E. Holzmann, M. Sigl, "Magnetic properties of soft magnetic powder composites at higher frequencies in comparison with electrical steels", *IEEE EDPC Conf*., Nuremberg (Germany), 29÷30 October 2013, Conf. Proc..

[23] M. Streckova, R. Bures, M. Faberova, L. Medvecky, J. Fuzer, P. Kollar, “A comparison of soft magnetic composites designed from different ferromagnetic powders and phenolic resins”, *Chinese J. of Chemical Engineering*, 23, 2015, pp. 736-743.

[24] L. Ferraris, E. Pošković, F. Franchini, "New soft magnetic composites for electromagnetic applications with improved mechanical properties", *AIP Advances* 6 (2016).

[25] E. A. Perigo, S. Nakahara, Y. Pittini-Yamada, Y. de Hazan, T. Graule, “Magnetic properties of soft magnetic composites prepared with crystalline and amorphous powders” *J. Magnetism and Magnetic Materials*, 323, 2011, pp. 1938-1944.

[26] S. Wu, A. Sun, W. Xu, Q. Zhang, F. Zhai, P. Logan, A. A.Volinsky, “Iron-based soft magnetic composites with Mn–Zn ferrite nanoparticles coating obtained by sol–gel method*”, J. Magnetism and Magnetic Materials*, 324, 2012, pp. 3899-3905.

[27] Y. Peng, Y. Yi, L. Li, J. Yi, J. Nie, C. Bao, “Iron-based soft magnetic composites with Al2O3 insulation coating produced using sol–gel method”, *Materials and Design*, 109, ,2016, pp. 390-395.

[28] Y. Peng, Y. Yi, L. Li, H. Ai, X. Wang, Lulu Chen “Fe-based soft magnetic composites coated with NiZn ferrite prepared by a co-precipitation method”, *J. Magnetism and Magnetic Materials*, 428, 2017, pp. 148-153.

[29] E. K. Papynov, O. O. Shichalin, A. A. Belov, A. S. Portnyagin, V. Yu. Mayorov, E. A. Gridasova, A. V. Golub, A. S. Nepomnyashii, I. G. Tananaev, V. A. Avramenko, “Synthesis of nanostructured Iron oxides and new magnetic ceramics using sol-gel and SPS techniques”, *AIP Conference Proceedings*, 1809, 2017, pp. 020043-1-020043-14.

[30] T. Schäfter, J. Burghaus, W. Pieper, F. Petzoldt, M. Busse, “New concept of Si–Fe based sintered soft magnetic composite”, *Powder Metallurgy*, 58, 2015, pp. 106-111.

[31] Y. Peng, J. Nie, W. Zhang, C. Bao, J. Ma, Y. Cao, “Preparation of soft magnetic composites for Fe particles coated with (NiZn)Fe2O4 via microwave treatment*”, J. of Magnetism and Magnetic Materials*, 395, 2015, pp. 245-250.

[32] R. Bureš, M. Strečkova, M. Faberova, P. Kollar, J. Fuzer, “Advances in powder metallurgy soft magnetic composite materials”, *Arch. of Metallurgy and Materials*, 62, 2017, pp. 1149-1154.

[33] G. Zhao, C. Wu, M. Yan, “Enhanced magnetic properties of Fe soft magnetic composites by surface oxidation”, *J. Magnetism and Magnetic Materials*, 399, 2016, pp. 51-57.

[34] W. Ding, L. Jiang, Y. Liao, J. Song, B. Li, G. Wu, “Effect of Iron particle size and volume fraction on the magnetic properties of Fe/silicate glass soft magnetic composites”, *J. Magnetism and Magnetic Materials*, 378, 2015, pp. 232-238.

[35] F. Franchini, E. Pošković, L. Ferraris, A. Cavagnino, G. Bramerdorfer, “Application of new magnetic materials for axial flux machine prototypes”, *IEEE IEMDC Conf*., Miami (USA), 21÷24 May 2017, Conf. Proc. pp..

[36] E. Poskovic, L. Ferraris, F. Franchini, M. Actis Grande, "The effect of particle size on the core losses of soft magnetic composites", *AIP Advances*, vol. 9, March 2019.

[37] L. Ferraris, E. Posković, F. Franchini, M. Actis Grande, “Magnetic performance dependence by grain sizes for SMC materials”, *EPMA EURO PM2018*, Bilbao (Spain), 14÷18 October 2018, Conf. Proc..

[38] H. Shokrollahi, K. Janghorban, “The effect of compaction parameters and particle size on magnetic properties of Iron-based alloys used in soft magnetic composites”, *Materials Science and Engineering B*, 134, 2006, pp. 41-43.

[40] M. Anhalt,“Systematic investigation of particle size dependence of magnetic properties in soft magnetic composites”, *J. Magnetism and Magnetic Materials*, 320, 2008, pp. e366-e369.

[41] A. H. Taghvaei, H. Shokrollahi, M. Ghaffari, K. Janghorban, “Influence of particle size and compaction pressure on the magnetic properties of Iron-phenolic soft magnetic composites”, *J. of Physics and Chemistry of Solids*, 71, 2010, pp. 7-11.

[42] L. Ferraris, E. Posković, F. Franchini, M. Actis Grande, R. Bidulský, “Effect of granulometry and Oxygen content on SMC magnetic properties”, *Acta Metallurgica Slovaca*, Vol 23, 2017,pp. 356-362.

[43] Y. J. Oh, I. B. Shim, H. J. Jung, J. Y. Park, S. I. Park, Y. R. Um, Y. J. Lee, S. W. Lee, C. S. Kim, “Effects of additives on magnetic properties of sheet Sr-Ba ferrite magnets”, J. *of Applied Physics* 76, November 1994, pp. 6877-6879.

[44] J. Wernick, “Magnetic Materials, Bulk” in *Kirk-Othmer Encyclopedia of Chemical Technology*, Vol. 15, John Wiley & Sons, 2000, pp. 1-53.

[45] M. Zeraoulia, M. El Hachemi Benbouzid, D. Diallo, “Electric motor drive selection issues for HEV propulsion systems: A comparative study”, *IEEE Trans.Veh. Technol*., 55, pp. 1756–1764, November 2006.

[46] B. Zhang, T. Epskamp, M. Doppelbauer, M. Gregor, " A comparison of the transverse, axial and radial flux PM synchronous motors for electric vehicle", *IEEE IEVC Conf.*, Florence (Italy), 17÷19 December 2014, Conf. Proc..

[47] G. Pellegrino, A. Vagati, P. Guglielmi, B. Boazzo, "Performance Comparison Between Surface-Mounted and Interior PM Motor Drives for Electric Vehicle Application", *IEEE Trans. On Ind. Electron.*, 59(2), pp. 803 - 811, February 2012

[48] P. Guglielmi, M. Pastorelli, A. Carrer, A. Beato, D. D'Antonio, L. Fagnano, "An IPM-PMASR motor for home appliance washing machines", *IEEE IECON Conf.*, Vienna (Austria), 10÷13 November 2013, Conf. Proc. pp. 2608-2613.

[49] M. Cheng, W. Hua, J. Zhang, W. Zhao, "Overview of Stator-Permanent Magnet Brushless Machines", *IEEE Trans. On Ind. Electron*, vol. 58(11), pp. 5087-5101, November 2011.

[50] F. Marignetti, M. A. Darmani, S. M. Mirimani, "Electromagnetic sizing of axial-field flux switching permanent magnet machine", *IEEE IECON Conf.*, Florence (Italy), 23÷26 October 2016, Conf. Proc. pp. 1624-1628.

[51] C. Wang, S. A. Nasar, I. Boldea, "Three-phase flux reversal machine (FRM)", *IEE Proceedings - Electric Power Applications*, vol. 146(2), pp. 139-146, March 1999.

[52] W. Hao, Y. Wang, "Analysis of double-sided sandwiched linear flux-switching permanent-magnet machines with staggered stator teeth for urban rail transit", *IET Electrical Systems in Transportation*, vol. 8(3), pp. 175-181, September 2018.

[53] R. Cao, M. Lu, N. Jiang, M. Cheng, "Comparison Between Linear Induction Motor and Linear Flux-switching Permanent-Magnet Motor for Railway Transportation", *IEEE Trans. On Ind. Electron.*, 66(12), pp. 9394 - 9405, December 2019.

[54] L. Ferraris, P. Ferraris, E. Pošković, A. Tenconi, "Theoretic and experimental approach to the adoption of bonded magnets in fractional machines for automotive applications", *IEEE Trans. On Ind. Electron.*, 59, pp. 2309-2318, May 2012.

[55] L. Ferraris, E. Pošković, "Bonded magnets for brushless fractional machines: Process parameters effects evaluation", *IEEE IECON Conf.*, Vienna (Austria), 10÷13 November 2013, Conf. Proc. pp. 2632-2637.

[56] K. Elian, H. Theuss, "Integration of polymer bonded magnets into magnetic sensors", *IEEE ESTC Conf.*, Helsinki (Finland), 16÷18 September 2014, Conf. Proc.

[57] L. Ferraris, F. Franchini, D. La Cascia, E. Pošković, "Adoption of bonded magnets in place of sintered NdFeB: performance and economic considerations on a small power generator", *IEEE EPE ECCE Europe Conf.*, Geneva (Switzerland), 8÷10 September 2015, Conf. Proc.

[58] S. Massari, M Ruberti, "Rare Earth elements as critical raw materials: Focus on international markets and future strategies", *Resources Policy* 38, 2013, pp. 36-43.

[59] L. Baldi, M. Peri, D. Vandone, "Clean energy industries and Rare Earth materials: Economic and financial issues", *Energy Policy* 66, 2014, pp. 53–61.

[60] R. Lacal-Arantegui, “Materials use in electricity generators in wind turbines e state-of-the-art and future specifications”, *J. of Cleaner Production* 87, 2015, pp. 275-283

[61] K. Binnemans, P. T. Jones, B. Blanpain, T. Van Gerven, Y. Yang, A. Walton, M. Buchert, “Recycling of Rare Earths: A critical review”, *Journal of Cleaner Production*, 51, 2013, pp. 1–22.

[62] R. Liu, M. Buchert, S. Dittrich, A. Manhart, C. Merz, D. Schüler, “Application of Rare Earths in consumer electronics and challenges for recycling”, *IEEE ICCE Conf*., Berlin (Germany), 6÷8 September 2011, Conf. Proc. pp. 286-290.

[63] R. Schulze, M. Buchert, “Estimates of global REE recycling potentials from NdFeB magnet material”, *Resources, Conservation and Recycling*, 113, 2016, pp. 12–27.

[64] M. Zakotnik, I. R. Harris, A. J. Williams, “Possible methods of recycling NdFeB-type sintered magnets using the HD/degassing process”, *J. Alloys and Compounds*, 450, 2008, pp. 525–531.

[65] T. Horikawa, K. Miura, M. Itoh, K. I. Machida, “Effective recycling for Nd-Fe-B sintered magnet scraps”, *J. Alloys and Compounds*, 408–412, 2006, pp. 1386–1390.

[66] M. Zakotnik, I. R. Harris, A. J. Williams, “Multiple recycling of NdFeB-type sintered magnets”, *J. Alloys and Compounds*, 469, 2009, pp. 314–321.

[67] M. Itoh, M. Masuda, S. Suzuki, K. I. Machida, “Recycling of Rare Earth sintered magnets as isotropic bonded magnets by melt-spinning”, *J. Alloys and Compounds*, 374, 2004, pp. 393–396.

[68] X. Li, M. Yue, M. Zakotnik, W. Liu, D. Zhang, T. Zuo, “Regeneration of waste sintered Nd-Fe-B magnets to fabricate anisotropic bonded magnets”, *J. Rare Earths*, 33, 2015, pp. 736-739.

[69] E. Poskovic, L. Ferraris, F. Franchini, M. Actis Grande, E. Pallavicini, “A different approach to rare-earth magnet recycling”, *IEEE EEEIC Conf.*, Palermo (Italy), 12 – 15 June 2018, Conf. Proc..

[70] L. Ge, X. Zhu, W. Wu, F. Liu, Z. Xiang,. “Design and Comparison of Two Non-Rare- Earth Permanent Magnet Synchronous Reluctance Motors for EV Applications”, *IEEE ICEMS Conf*., Sydney (Australia), 11-14 August 2017, Conf Proc..

[71] S. S. R Bonthu, A. Arafat, S. Choi, “Comparisons of Rare-Earth and Rare-Earth-Free external rotor permanent magnet assisted synchronous reluctance motors”, *IEEE Trans. On Ind. Electron*., 64(12), pp. 9729–9738, December 2017.

[72] N. Bianchi, E. Fornasiero, M. Ferrari, M. Castiello, "Experimental comparison of PM assisted synchronous reluctance motors", *IEEE Trans. On Ind. Appl*., 52(1), pp. 163-171, January/February 2016.

[73] N. Bianchi, S. Bolognani, E. Carraro, M. Castiello, E. Fornasiero,. "Electric Vehicle Traction Based on Synchronous Reluctance Motors”, *IEEE Trans. On Ind. Appl*., 52(6), pp. 4762-4769, November/December 2016.

[74] T. Mohanarajah, M. Nagrial, J. Rizk, A. Hellany, “Permanent Magnet Optimization in PM Assisted Synchronous Reluctance Machines”, *IEEE ISIE Conf*., Cairns (Australia), 13-15 June 2018, Conf. Proc. pp. 1347 - 1351.

[75] E. Armando, P. Guglielmi, M. Pastorelli, G. Pellegrino, A. Vagati, “Performance of IPM-PMASR Motors with Ferrite Injection for Home Appliance Washing Machine”, *IEEE IAS Annual Meeting*, Edmonton (Canada), 5-9 October 2008, Conf Proc. pp. 1-6.

[76] Q. Wu, K. Lu, P. O. Rasmussen, K. F. Rasmussen, "A new application and experimental validation of moulding technology for ferrite magnet assisted synchronous reluctance machine",. *IEEE ECCE Conf*., Milwaukee (USA), 18-22 September 2016, Conf. Proc..

[77] H. Nishiura, S. Morimoto, M. Sanada, Y. Inoue, "Characteristics Comparison of PMASynRM with Bonded Rare-Earth Magnets andIPMSM with Sintered Rare-Earth Magnets", *IEEE PEDS Conf.*, Kitakyushu (Japan), 22-25 April 2013, Conf. Proc., pp. 720-725.

[78] E. Pošković, C. Babetto, N. Bianchi, L. Ferraris, “The study of permanent magnet assisted reluctance machine with the adoption of NdFeB bonded magnets”, *IEEE SPEEDAM Conf.*, Amalfi (Italy), 20÷22 June 2018, Conf. Proc. pp. 274-279.

[79] Y. Wang, G. Bacco, N. Bianchi, "Geometry Analysis and Optimization of PM-Assisted Reluctance Motors", *IEEE Trans. On Ind. Appl*.,53(5), pp. 4338-4347, September/October 2017.

[80] C. Babetto, G. Bacco, N. Bianchi, "Synchronous Reluctance Machine Optimization for High-Speed Applications", *IEEE Trans. On Energy Convers*., 33(3), pp. 1266-1273, September 2018.

[81] C. Babetto, G. Bacco, N. Bianchi, ”Design methodology for high-speed synchronous reluctance machines”, *IET Electr. Power Appl*., 12(8), pp. 1110-1116, August 2018.

[82] E. Howard, M. J. Kamper, “Weighted Factor Multiobjective Design Optimization of a Reluctance Synchronous Machine”, *IEEE Trans. On Ind. Appl*., 52(3), pp. 2269-2279, May/June 2016.

[83] E. Howard, M. J. Kamper, S. Gerber, “Asymmetric Flux Barrier and Skew Design Optimization of Reluctance Synchronous Machines”, *IEEE Trans. On Ind. Appl*., 51(5), pp. 3751-3760, September/October 2015.

[84] T. Matsuo, T. A. Lipo, "Rotor design optimization of synchronous reluctance machine", IEEE Trans. on Energy Convers, 9(2), pp. 359-365, June 1994.

[85] A. Vagati, M. Pastorelli, G. Franceschini, C. Petrache, “Design of Low-Torque-Ripple Synchronous Reluctance Motors”, IEEE IAS Annual Meeting, New Orleans (USA), 5-9 October 1997, Conf Proc. pp. 286-293.

[86] Y. Wang, N. Bianchi, S. Bolognani, L. Alberti, L. "Synchronous Motors for Traction Applications", IEEE Automotive Conf., 15-16 June 2017, Torino (Italy), Conf. Proc..

[87] A. Boglietti, A. Cavagnino, M. Pastorelli, A. Vagati, "Experimental Comparison of Induction and Synchronous Reluctance Motors Performance". IEEE IAS Annual Meeting, Kowloon (China), 2-6 October 2005, Conf Proc., pp. 474-479.

[88] H. Kärkkäinen, L. Aarniovuori, M. Niemelä, J. Pyrhönen, J. Kolehmainen, "Technology Comparison of Induction Motor and Synchronous Reluctance Motor", IEEE IECON Conf., Beijing (China), 29 October-1 November 2017, Conf. Proc., pp. 2207-2212.

[89] G. Bacco, N. Bianchi, "Design Criteria of Flux-Barriers in Synchronous Reluctance Machines", *IEEE Trans. On Ind. Appl.*, 55(3), pp. 2490-2498, May-June 2019.

[90] W. L. Soong, N. Ertugrul, "Field-weakening performance of interior permanent-magnet motors", *IEEE Trans. On Ind. Appl.*, 38(5), pp. 1251–1258, October 2002.

[91] W. L. Soong, T. J. E. Miller, "Field-weakening performance of the five classes of brushless synchronous AC motor drives" *IEE Proc.—Elect. Power Appl.*, 141(6), pp. 331–340, November 1994.

[92] A. Vagati, M. Pastorelli, F. Scapino, G. Franceschini, "Impact of Cross Saturation in Synchronous Reluctance Motors of the Transverse-Laminated Type", *IEEE Trans. On Ind. Appl.*, 36(4), pp. 1039-1046, July/August 2000.

[93] G. Pellegrino, T. M. Jahns, N. Bianchi, W. L. Soong, F. Cupertino, "The Rediscovery of Synchronous Relutance and Ferrite Permanent Magnet Motors", *SpringerBriefs in Electrical and Computer Engineering*, Springer, 2016, pp. 1-136.

[94] G. Bacco, N. Bianchi," Choice of flux-barriers position in synchronous reluctance machines", *IEEE ECCE Conf.*, Cincinnati (USA), 1-5 October 2017, Conf. Proc., pp. 1872–1879.

[95] C. Babetto, G. Bacco, G. Berardi, N. Bianchi, "High Speed Motors : a Comparison between Synchronous PM and Reluctance Machines", *IEEE ECCE Conf.*, Cincinnati (USA), 1-5 October 2017, Conf. Proc., pp. 3927–3934.

[96] E. Poskovic, C. Babetto, N. Bianchi, L. Ferraris, "Bonded Magnets in PM-assisted Synchronous Reluctance Machines: Performance Dependence on the Production Technology", *IEEE IEMDC Conf.*, San Diego (USA), 12 ÷ 15 May 2019, pp. 442-448.

[97] D. Zhu, C. Zhao, Y. Yan, "Research on two manners of magnetization in surface-mounted permanent magnet machine", *IEEE ICEMS Conf.*, Nanjing (China), 27÷29 September 2005, Conf. Proc. pp. 460-463.

[98] S. P. Hong, H. S. Cho, H. S. Lee, H. R. Cho, H. Y. Lee, "Effect of the magnetization direction in permanent magnet on motor characteristics", *IEEE Trans. On Magn.*, 35, pp. 1231-1234, May 1999.

[99] H. N. Phyu, C. Bi and Q. Jing, "Effect of magnetization on torque pulsation of the PM BLDC Motor", *IEEE ICEMS Conf.*, Wuhan (China), 17÷20 October 2008, Conf. Proc. pp. 3685-3690.

[100] Z. Q. Zhu, D. Howe, "Halbach permanent magnet machines and applications: a review", *IEE Proceedings - Electric Power Applications*, 148, 2001, pp. 299–308.

[101] C. K. Chandrana, J. A. Neal, D. Platts, B. Morgan, P. Nath, "Automatic alignment of multiple magnets into Halbach cylinders", *J. Magnetism and Magnetic Materials* 381, 2015, pp. 396–400.

[102] S. M. Jang, H. W. Cho, S. H. Lee, H. S. Yang, Y. H. Jeong, "The influence of magnetization pattern on the rotor losses of permanent magnet high-speed machines", *IEEE Trans. On Magn.*, 40, pp. 2062–2064, July 2004.

[103] Z. Q. Zhu, Z. P. Xia, D. Howe, "Comparative study of electromagnetic performance of alternative Halbach and conventional radially magnetized permanent magnet brushless motors", *IEEE ICEMS Conf.*, Wuhan (China), 17÷20 October 2008, Conf. Proc. pp. 2778–2783.

[104] M. Andriollo, G. Bettanini, A. Tortella, "Design procedure of a small-size axial flux motor with Halbach-type permanent magnet rotor and SMC cores", *IEEE IEMDC Conf.*, Chicago (USA). 12÷15 May 2013, pp. 775–780.

[105] Z. Q. Zhu, "Recent development of Halbach permanent magnet machines and applications", *IEEE PCC Conf.*, Nagoya (Japan), 2÷5 April 2007, Conf. Proc. pp. K-9-K-16.

[106] H. Li, C. Xia, "Halbach array magnet and its application to PM spherical motor", *IEEE ICEMS Conf.*, Wuhan (China), 17÷20 October 2008, Conf. Proc. pp. 3064-3069.

[107] D. S. Arnold, A. Tura, A. Ruebsaat-Trott, A. Rowe, "Design improvements of a permanent magnet active magnetic refrigerator", *J. Refrigeration* 37, 2014, pp. 99–105.

[108] C. S. Toh, S. L. Chen, "Design and control of a ring-type flywheel battery system with hybrid Halbach magnetic bearings", *IEEE/ASME AIM Conf.*, Besançon (France), 8÷11 July 2014, Conf. Proc. pp. 1558–1562.

[109] P. V. Trevizoli, J. A. Lozano, G. F. Peixer, J. R. Barbosa Jr., "Design of nested Halbach cylinder arrays for magnetic refrigeration applications", *J. Magnetism and Magnetic Materials* 395, 2015, pp. 109–122.

[110] F. Güler, L. T. Ergene, C. Ekin, "Halbach array variations on BLDC motor under magnet constraint", *IEEE POWERENG Conf.*, Istanbul (Turkey), 13÷17 May 2013, Conf. Proc. pp. 1509-1513

[111] L. Ferraris, P. Ferraris, E. Pošković, A. Tenconi, "Comparison between parallel and radial magnetization in PM fractional machines", *IEEE IECON Conf.*, Melbourne (Australia), 7÷10 November 2011, Conf. Proc. pp. 1776-1782.

[112] Y. Shen, G. Y. Liu, Z. P. Xia, Z. Q. Zhu, "Determination of maximum electromagnetic torque in PM brushless machines having two-segment Halbach array", *IEEE Trans. On Ind. Electron.*, 61, pp. 718-729, February 2014.

[113] L. Ferraris, P. Ferraris, E. Pošković, A. Tenconi, "PM fractional machines adopting bonded magnets: Effect of different magnetizations on the energetic performance", *IEEE ENERGYCON Conf.*, Florence (Italy), 9÷12 September 2012, Conf. Proc. pp. 113-120.

[114] L. Ferraris; F. Franchini, E. Poskovic, "Study of the Halbach magnetization in small PM electrical machines adopting the bonded magnets", *IEEE ISIE Conf.*, Edinburgh (UK), 19-21 June 2017. Conf. Proc. pp. 374-380

[115] F. Giulii Capponi, G. De Donato, F. Caricchi, "Recent advances in Axial-Flux Permanent-Magnet machine technology", *IEEE Trans. On Ind. Appl.*, Vol. 48, pp 2190 – 2205, November/December 2012.

[116] S. Kahourzade, N. Ertugrul, W. L. Soong, "Investigation of emerging magnetic materials for application in axial-flux PM machines", *IEEE ECCE Conf.*, Milwaukee (USA), 18÷22 September 2016, Conf. Proc..

[117] Y. Dou, Y. Guo, J. Zhu, "Investigation of motor topologies for SMC application", *IEEE ICEMS Conf.*, Seoul (South Korea), 8÷11 October 2007, Conf. Proc. pp. 695 - 698.

[118] R. P. Deodhar, A. Pride, J. J. Bremner, "Design method and experimental verification of a novel technique for torque ripple reduction in stator claw-pole PM machines", *IEEE Trans. on Ind. Appl.*, 51, pp. 3743-3750, September/October 2015.

[119] E. Poskovic, L. Ferraris, E. Pallavicini,, A. Cavagnino, "Compaction of SMC Materials by Applying External Magnetic Fields to the Mold", *IEEE ECCE Conf.*, Portland (USA), 23 ÷ 27 September 2018, Conf. Proc. pp. 5379-5386.

[120] L. Ferraris, F. Franchini, E. Poskovic, "A novel thermographic method and its improvement to evaluate defects in laminated and Soft Magnetic Composites devices", *IEEE Trans. On Ind. Appl.*, in press, 2019.

[121] E. Poskovic, L. Ferraris, G. Bramerdorfer, M. Cossale, "A Thermographic Method to Evaluate Different Processes Effects on Magnetic Steels", *IEEE SDEMPED Conf.*, Toulouse (France), 27 ÷ 30 August 2019, Conf. Proc.

[122] L. Ferraris, F. Franchini, E. Poskovic, "Improvements in the hysteresis and cogging evaluation with an Innovative methodology", *IEEE ICEM Conf.*, Alexandroupoli (Greece), 3 ÷ 6 September 2018, Conf. Proc. pp. 250-256.

[123] L. Ferraris; F. Franchini, E. Poskovic, "The cogging torque measurement through a new validated methodology", *IEEE CPE-POWERENG Conf.*, Spain (Cadiz), 4-6 April 2017, Conf. Proc. pp. 398-403.